Chapter 4
Weathering and Deterioration

Michael Steiger, A. Elena Charola and Katja Sterflinger

Abstract It is generally assumed that stone is one of the most durable materials because it is compared to weaker building materials, such as wood or mud. But stone can deteriorate, and many factors will affect it. The nature of the stone is critical in determining its resistance to the various deterioration factors. The most important one, salt, was identified by Herodotus, nearly two and a half millennia ago. However, salt by itself is not damaging; it requires the presence of water for its aggressiveness to become evident. And water is needed for biocolonization to occur, for freeze–thaw phenomena, and for wet-dry expansion. Control of this single factor can decrease the deterioration potential of a stone and any structure built from it significantly. This chapter aims to present a review of the most important deterioration processes and their effect on the various types of stones and rocks used by man. Among them are thermal effects, the influence of moisture, both as water vapor and in liquid state, the presence of salts, and the damages that can be expected from biocolonization. This chapter also aims at identifying the areas where more research is needed to understand the actual deterioration mechanism of the various factors.

M. Steiger (✉)
Department of Chemistry, Inorganic and Applied Chemistry, University of Hamburg, Martin-Luther-King-Platz 6 20146 Hamburg, Germany
e-mail: michael.steiger@chemie.uni-hamburg.de

A. E. Charola
Museum Conservation Institute, Smithsonian Institution, Washington, DC, USA
e-mail: charola_ae@yahoo.com

K. Sterflinger
Institut für Angewandte Mikrobiologie, Universität für Bodenkultur, Muthgasse 18, 1190 Wien, Austria

S. Siegesmund and R. Snethlage (eds.), *Stone in Architecture*,
DOI: 10.1007/978-3-642-45155-3_4,

4.1 Introduction

Stone is generally considered one of the most resistant materials, and so it is when compared to other construction materials such as adobe or wood. Nonetheless, it is also susceptible to deterioration. Herodotus mentioned in his *The History* that the stones of the pyramids in Egypt were already deteriorating when he saw them in the 5th century BC.

Deterioration is a complex process, and, therefore, there are many words that are used to describe it. For example, "weathering" is used for the natural process of rock disintegration by external factors, while "deterioration" implies the impairment of value and use. Thus, rocks weather while stones deteriorate. The difference is that man has intervened in producing and using the stones. Therefore, these two terms are not really equivalent.

On the other hand, "alteration" is defined as a modification of the material; for example, geologists use it to refer to the change in mineral composition of a rock, such as occurs in volcanic rocks. The word does not imply a worsening of its characteristics from a conservation point of view (Grimmer 1984; UNI 11182 2006).

Two other words tend to be used interchangeably with the previously mentioned ones. These are "degradation" and "decay". Both imply a change for the worse; the former implies disintegration and has specific meanings for chemists, physicists, and geologists. Biologists simply turned it into biodegradation, thus avoiding misunderstandings. On the other hand, decay has the connotation of rotting or decomposition, as reflected in tooth decay. Only some years ago, an online dictionary further described "decay" as "the result of being destroyed… by not being cared for", a point that always should be kept in mind when considering the conservation of buildings and monuments.

Finally, the last word that needs to be mentioned is "damage". This is the most general term and needs to be accompanied by a qualifying term, as in "mechanical damage".

There are many types of damages that stones can undergo (Charola 2004). These may produce particular deterioration patterns that are then described by specific terms. Given the high number of these patterns, and the fact that this problem is being addressed around the world in different languages, it is important to try to come to a consensus about their use (see Chap. 6).

It is important to point out that the same pattern may result from different deterioration mechanisms, while any one specific mechanism may result in different types of patterns, depending on the substrate in question. For example, granular disintegration can be the result of chemical attack, frost damage, or other processes. Hence, in practice, it is generally impossible to deduce the major causes of damage simply by observing the deterioration pattern. Visual observation and documentation serve mainly to attain an overall estimate of the amount and type of damage present. Determining the origin of the damage requires one or more analyses to interpret the observed pattern. In order to assess the relative importance

of different degradation processes and their rates, a detailed understanding of the underlying mechanisms is indispensable.

This chapter describes the various types of damages that can occur as a function of the main process underlying them, such as mechanical, chemical, or biochemical. Specific emphasis is placed on problems introduced by the presence of salts because this is probably the single most relevant deterioration mechanism for building materials.

4.2 Deterioration by Mechanical Processes

Mechanical damage results when stone is subjected to a load or a stress that is above the mechanical resistance it has. Many cases of mechanical damage result from poor design of the buildings. For example, the cracks that form around window and door openings are very likely the result of unsymmetrical loads or side thrusts. Other times, differential soil settlement may be the cause of the cracks in structures, while catastrophic events such as earthquakes are responsible for heavy damages in buildings. Binda and Anzani (1997) give a good introduction to this topic that is beyond the scope of this chapter.

The growth of vegetation, starting with grasses and ferns that tend to grow in the mortar joints of masonry, deteriorate the mortar with the mechanical stresses induced by their roots. If maintenance is not regularly performed, this damage will increase with the development of higher vegetation, bushes and even large trees, resulting in the breaking up of the stone masonry itself, as frequently seen in archaeological sites.

Fire is yet another catastrophic event. This can induce stresses because stone is not a good thermal conductor, and, therefore, the surface temperature will be significantly different from that in the underlying stone. The mechanism of this deterioration is described in detail in the previous chapter (Sect. 3.4.2). The expansion suffered during heating to high temperatures will result in the literal shattering of the external layers of the stone blocks, leaving a typical rounded surface behind, known as a conchoidal fracture (Fig. 4.1).

Apart from fissuring, fracturing and spalling, fires may induce discoloration and mineralogical changes in some of the stones' components, modifying their physical properties. For example, the oxidation of iron minerals with the formation of hematite (Dionisio and Aires Barros 2004; Dionisio et al. 2005; Hajpál and Török 2004; Török and Hajpál 2005), the dehydration of clays, the decomposition of calcite or dolomite, the sudden contraction of quartz during transformation of α to β variety when temperatures increase above 573 °C, and occurrences of partial melting and sintering have also been observed (Kleber 1959; Matthes 1987; Sippel et al. 2007). All of these changes mostly result in an increase of the susceptibility of the material to deterioration. Finally, the damage may be increased by the thermal shock induced during attempts to extinguish the fire with water that rapidly will cool the heated stone surface causing further spalling.

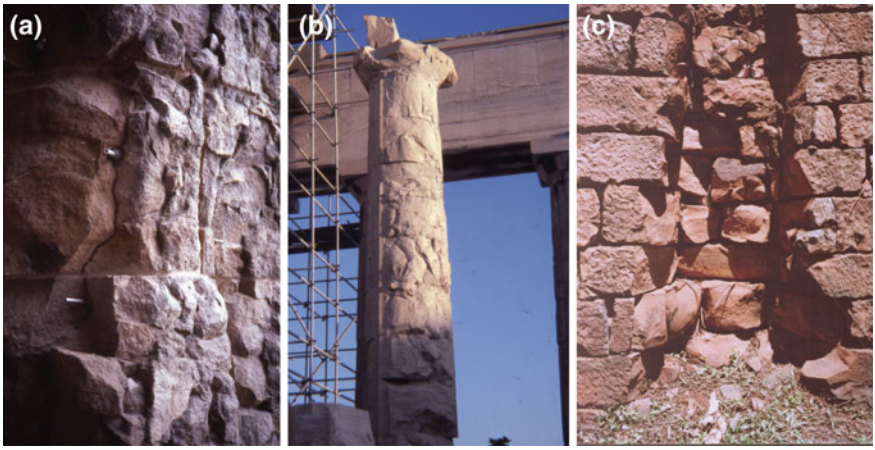

Fig. 4.1 Detail of the conchoidal fractures resulting from historical fires: **a** Granite pillars in the former custom building, now a market, in Salvador, Bahia, Brazil; **b** Marble columns of the Parthenon, Athens, Greece; **c** Niche for a wooden column in the church wall constructed with argillaceous sandstone in the Jesuit Guaraní Mission of Santa Ana, Misiones, Argentina

Ironically, fire is used to finish some stones, such as the flame-finished granite, which became popular in the 1970s because of its rustic appearance. The applied heat spalls off small scales from the surface and, in this process, opens up many fissures in the stone. As a result, far more moisture is absorbed by the stone than if the surface was just sawn (Grissom et al. 2000). Also, traditional decorative stone finishes used in the past have induced damage to the stone surface, resulting in a deterioration increase (Cecchi et al. 1978; Alessandrini et al. 1979).

Finally, vibrations caused by traffic, including trains and airplanes, and machinery, e.g. air-conditioners, can induce alternating tensile and compressive stresses in building structures. Stone elements may be affected, especially if they are cracked or small and not well connected to the rest of the structure, as smaller elements have higher resonance frequency. Therefore, ceilings, floors, and windows are more likely to suffer from resonance amplification than the building itself. While, in general, vibration may not cause direct damage, it certainly may accelerate the overall deterioration rate, for example, from dust settling into existing open cracks that subsequently cannot return to their previous state.

4.2.1 Thermal Cycling

Another source for mechanical damage is the dimensional change that stone and other building materials undergo induced by thermal cycling. As discussed in detail in Chap. 3 (Sect. 3.4.2), changes in temperature, either increases or decreases, will result respectively in volume expansion or contraction of stone.

Table 4.1 Thermal expansion coefficients for magmatic, metamorphic, and sedimentary rocks

Rock class	Rock types	Linear expansion coefficient ($10^{-6} \times K^{-1}$)		
		Average	Max	Min
Magmatic	8 rock types	7.4	10	5
Metamorphic	5 marbles	11	15	8
	1 gneiss, 1schist	7.9	9	6
	2 quartzitic rocks	12.5	14	11
Sedimentary	2 calcareous sandstones	7.5	8	7
	2 limestones	4	6	2
	1 travertine	5	6	4
	5 sandstones	10.8	12	9.5

The data correspond to eight magmatic rock types (granodiorite, granite, gabbro-norite, metagabbro, peridotite, 2 quartz porphyries, and tuff); 12 metamorphic rocks, 5 marbles, and 7 siliceous rocks (slate, serpentinite, 2 paragneiss, orthogneiss, quartzite, and quartz mylonite); 10 sedimentary rocks (2 calcareous sandstones, 2 limestones, travertine, and 5 sandstones)

In general, the volume expansion coefficient for rock varies between 15 and 33×10^{-6} K^{-1}. For isotropic rocks, it can be estimated as three times their linear expansion coefficient. It is to be highlighted that expansion coefficients vary with temperature and that the correlation is not necessarily linear. Table 4.1 lists the linear thermal expansion coefficients for some types of rocks (see also Table 3.7).

It should be remembered that, particularly for coarse grained stones, such as granites and marbles, there may be significant differences in the expansion between different varieties of the same rock type. This is a consequence of the various rock textures, e.g. size and orientation of the crystals as well as the type of boundaries between them.

Even if the temperature changes are not particularly large, the repeated heating and cooling of the stone will eventually lead to its deterioration over time. Apart from the expansion that may result from heating, the residual stress that may remain in the stone once it returns to the "normal" temperature, i.e. average temperature, is important since it will accumulate over time.

The expansion coefficients of rocks result from those of the minerals present in them. Thus, granite and sandstone have high expansion values because of the presence of quartz, while marble and limestone reflect that of calcite or dolomite, and slates that of clays and micas, since they are metamorphosed argillaceous rocks such as mudstone. Table 4.2 gives the linear expansion coefficient for some of these minerals, while Fig. 4.2 shows the linear expansion changes they undergo with temperature.

In general, thermal cycling between 20 and 90 °C induces more or less deterioration to most of the stones. However, an equivalent decrease in temperature, down to −40 °C, does not induce damage as long as the sample is dry (Weiss et al. 2004b). Marbles are more susceptible than other stones and are discussed in more detail below.

As can be seen from Table 4.2, calcite is the only mineral that, upon heating, expands in one direction while contracting in the other (Figs. 4.2 and 4.3); upon

Table 4.2 Linear expansion coefficient α for some minerals

Mineral	Linear thermal expansion coefficient (K^{-1})		Temp range (°C)
	Parallel to c-axis	Perpendicular to c-axis	
Calcite[a]	25.1×10^{-6}	-5.6×10^{-6}	0–85
Dolomite[b]	25.8×10^{-6}	6.2×10^{-6}	24–700
Quartz[a]	7.7×10^{-6}	13.3×10^{-6}	0–80
Albite[c]	10.5×10^{-6}	5.6×10^{-6}	25–970
Gypsum[d]	54×10^{-6}	*7–117 $\times 10^{-6}$	**25–42
Micas[e]	8.7×10^{-6}	17.8×10^{-6}	
Clays[f]	6×10^{-6}	15×10^{-6}	25–350

Values from
[a] Hodgman et al. (1963)
[b] Reeder and Markgraf (1986)
[c] Average of high and low albite (Kleber 1959)
[d] * or a–b axis, respectively, ** calculated average for temperature range (Ballirano and Melis 2009)
[e] Average for muscovite and phlogopite (McKinstry 1965)
[f] Average for kaolinite, dickite, and halloysite (McKinstry 1965)

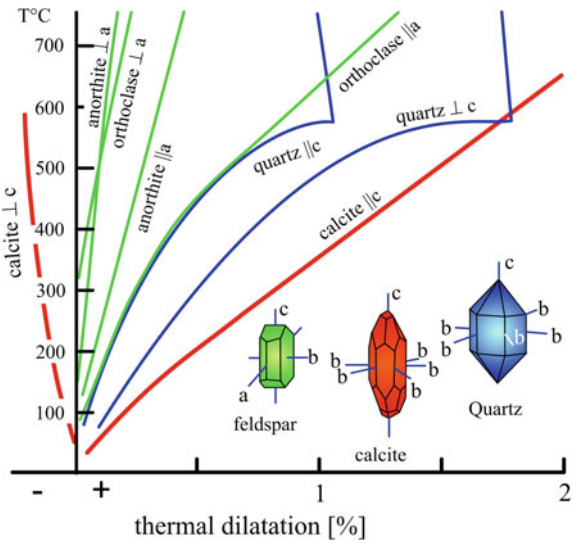

Fig. 4.2 Linear expansion for some minerals as a function of temperature. Adapted from Winkler (1994)

cooling, it will contract along the c axis while expanding along the other ones. Therefore, calcite marbles are the most susceptible to thermal cycling that leads to granular decohesion of the stone matrix, i.e. the so-called "sugaring" deterioration pattern that has been long known (Kessler 1919; Franzini et al. 1983). This is mostly the result of the thermal stress induced along grain boundaries that leads to their failure and even to grain fissuring (Fig. 4.3).

From the above, it follows that, in principle, dolomite marbles should be more resistant to this deterioration, because their crystals only expand, while calcite

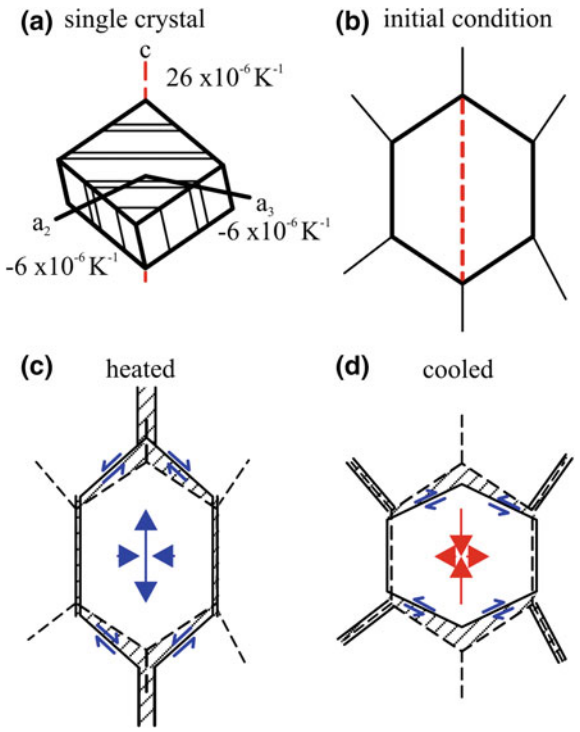

Fig. 4.3 Diagram illustrating the deterioration mechanism for calcite due to thermal cycling. **a** Anisotropy of individual calcite crystal upon heating, **b** Calcite crystal within an idealized marble matrix, **c** Expansion and contraction suffered upon heating, and **d** Contraction and expansion suffered upon cooling. Adapted from Siegesmund et al. (2004)

expands in one direction and contracts in the other. Mathematical modeling of the thermal expansion behavior of marbles via microstructure-based finite element simulations have been shown to provide good correspondence to real experiments (Weiss et al. 2002b, 2003; Shushakova et al. 2011). Onset and magnitude of thermal microcracking vary for calcite- and dolomite-bearing marbles even when assumed to have exactly the same microstructure and texture; the onset being earlier, and the microcraking greater, for the calcite marbles. Thus, finite element modeling indicates that dolomite marbles may be more resistant against thermal weathering than calcite marbles. Variations in the texture may significantly affect the distribution of thermal stresses within the marble. There is a strong inverse correlation between thermal stresses and degree of texture, i.e. lattice preferred orientation of the minerals, since higher elastic strain energies are associated with weakly textured marbles, and vice versa.

This is the case in general, though specific dolomite marbles may be more susceptible to thermal cycling than specific calcite ones due to their texture and the nature of the residual strain, as exemplified by the Greek Arabella dolomite marble, which is more susceptible to this deterioration than the Portuguese Rosa Estremoz marble (Zeisig et al. 2002).

For the case of marbles, the stress induced by heating leads to fissuring and, eventually, fracturing and results in an increase in porosity (Malaga-Starzec et al. 2002). This may already occur at temperatures around 40–50 °C, a value that is

easily reached by a stone surface on summer days, even in northern countries. But then, the cooling cycles that occur in winter in these countries will also contribute to grain decohesion. This phenomenon has also been observed in marble quarries, and the deteriorated marble is referred to as "marmo cotto" (Bertagnagi et al. 1983).

Although marble weathering by thermal cycling has been studied extensively, the key factors triggering this deterioration have not as yet been quantified (Widhalm et al. 1996; Winkler 1996; Weiss et al. 1999; Ruedrich et al. 2002; Weiss et al. 2002a, b; Zeisig et al. 2002). The deterioration starts with an initial stage of insolation that leads to the progressive loss of cohesion along grain boundaries (Siegesmund et al. 1999, 2000) caused by the different thermal expansion coefficients of the rock-forming minerals during either heating or cooling (Fredrich and Wong 1986). The resulting induced tensile, compressive, or shear stresses along the grain boundaries may be large enough to cause failure along microstructural precursors, such as cracks and cleavage planes (Sage 1988). The grain to grain orientation relationship, frequently called misorientation, and its distribution within the stone is also an important parameter. The magnitude of residual strain may be associated with the grain size, grain shape, and lattice preferred orientation in the marbles (Royer-Carfagni 1999; Weiss et al. 2002a, 2003; Zeisig et al. 2002; Siegesmund et al. 2008b). This suggests a fabric dependence of residual strain after thermal treatment and, consequently, of thermal degradation. Thermally induced microcracks lead to a residual strain after heat treatment and, thus, to the progressive deterioration. However, some authors (e.g. Sage 1988; Koch and Siegesmund 2004) have shown that, after a few heating cycles, there is no further increase of the residual strain as long as moisture is absent.

While marbles show a positive residual strain, rocks containing clays that can dehydrate, such as tuffs, show a significant negative residual strain only during the first cycling that is associated with the shrinking due to dehydration (Weiss et al. 2004b). Some siliceous rocks may also show a directional dependence of the thermal expansion coefficient as a consequence of texture (e.g. quartzites); this observation is rather the exception than the rule and by far not as pronounced as in marbles. The deterioration induced by thermal cycling in granite results in the "sanding disintegration" and is mostly found on weathered granites (Delgado Rodrigues 1996).

In stones, such as granite, that are constituted by different colored minerals, the variations in light absorption or reflection, the latter called albedo, can result in localized deterioration because of temperature differences between lighter and darker colored areas of the same stone. An interesting example has been described by Gómez-Heras et al. (2008) for a 60 year old granite building. The granite was rich in micro-granular (tonalite) enclaves that were darker in comparison to the rest of the stone (monzogranite). These darker areas, with different albedo and thermal conductivity properties compared to the host stone, tended to spall. The study found that the driving factor was the difference in thermal response to insolation and the short term variations in surface temperatures between them.

Another deterioration pattern that can be attributed to thermal cycling is the deformation, i.e. bowing, of stone slabs. In particular, marble slabs suffer it, though granite ones are also prone to this deterioration (Siegesmund et al. 2008a). This has

been a phenomenon long observed on marble tombstones and described in the early literature (Kessler 1919; Fritz 1922), but has become increasingly more evident with new construction technology that uses stone cladding. With improved cutting technology, the thickness of these slabs has decreased from ca. 90 mm down to 20 mm, and, consequently, the bowing of marble has become a growing concern during the past 30 years. As mentioned in the preceding chapter (Sect. 3.4), there is an extensive number of publications dealing with this topic. The deformation of marble panels is a consequence of fissures resulting from thermal expansion. Consequently, porosity increases, and so does the bowing. Therefore, the more bowed the marble, the higher its porosity. However, some studies carried out monitoring this phenomenon have shown that the bowing rate is higher in the first years and decreases in the subsequent ones from ca. 0.5 mm m^{-1} per year for the first 9 years to 0.38 mm m^{-1} for the subsequent 3 years (Siegesmund et al. 2008b).

However, it should be pointed out that thermal cycling rarely occurs by itself in nature. Even in desert climates, some moisture resulting from condensation is present, especially if temperature differences are high, such as 40 °C, and the change occurs rapidly. Thus, the presence of moisture enhances the deterioration suffered by thermal cycling (Koch and Siegesmund 2004).

Rocks that contain hydrated minerals are also susceptible to thermal cycling because of the loss of the hydration water in these minerals. For example, alabaster, the massive variety of gypsum, was used in historical times for window panes before thin glass sheets became industrially available. These window panes also show deformation that can be attributed to the anisotropic thermal expansion of the constituting gypsum mineral ($CaSO_4 \cdot 2H_2O$) over years of thermal cycling.

Other important hydrated minerals are clays, and many rocks contain them, ranging from marls to sandstones to volcanic tuffs. Heating these rocks results in the dehydration of these minerals and their consequent shrinking. However, this is not the main deterioration problem for these rocks, because clays are far more susceptible to the presence of water, as discussed in the following section.

4.2.2 Hygric and Hydric Swelling

All porous materials will adsorb water vapor from the atmosphere and expand. Although stone does not suffer this hygric expansion to the degree that wood does, it will still be affected by the inevitable cycling that it is subjected to by the normal changes in relative humidity in the air. Most affected by this process are the stones that contain clays, because their platy structure makes them particularly susceptible to retaining moisture between them.

Water vapor will diffuse into a porous material and be adsorbed onto the pore surface. Initially, a monomolecular water layer will develop that, because of its affinity to the mineral surface, does not behave as “normal” water, generally referred to as “bulk” water. If more water vapor is available, a second layer will form and then a third one. If the pores are very small, they may be totally filled

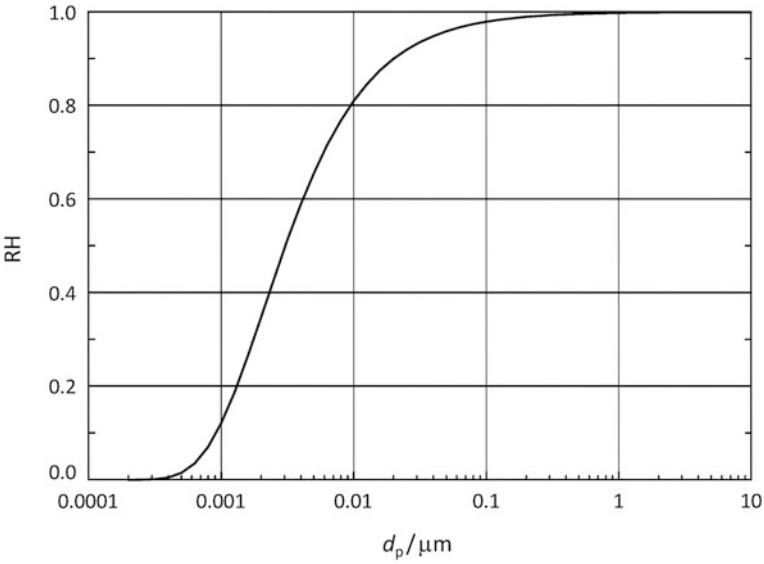

Fig. 4.4 Capillary condensation for pores with various diameters d_p as calculated with the Kelvin-Thomson equation

with water by capillary condensation. The Kelvin-Thomson equation gives the relation between RH and the capillary radius and, plotted for cylindrical pores, gives the graph shown in Fig. 4.4.

It can be seen that capillary condensation can occur at 10 % RH for pores of 1 nm diameter—for reference, the diameter of a water molecule is about 0.3 nm—while at 80 % RH, condensation occurs in pores one order of magnitude larger, i.e. 0.01 µm. It is in about this range of RH that hygric expansion increases significantly, as illustrated in Fig. 3.47 for the Schöttmarer sandstone (Sect. 3.5). It is important to remember that, in pores >0.1 µm, water will already behave as bulk water (Stockhausen 1981), and capillary condensation will occur in these pores at 95 % RH. Therefore, hygric expansion will be of practical concern only when water starts to behave as normal water, i.e. bulk water, not adsorbed water.

Figure 4.4 shows a theoretical situation, and it should be remembered that pores in stone have many shapes (Fig. 4.5), and these will influence the behavior of the water in them (Bourgès et al. 2008).

Particularly in flat pores, for example at the boundary between two flat crystal surfaces and especially between thin, platy minerals such as micas, clays, and chlorites, capillary condensation is important. This explains the deterioration suffered by clay bearing stones, either sandstones or limestones, where spalling and delamination parallel to the bedding layer are the characteristic deterioration patterns (Rodriguez-Navarro et al. 1997; Sebastián et al. 2008).

For materials that do not contain clays or other phyllosilicates, the hygric expansion has been attributed to the disjoining pressure and corresponds to the

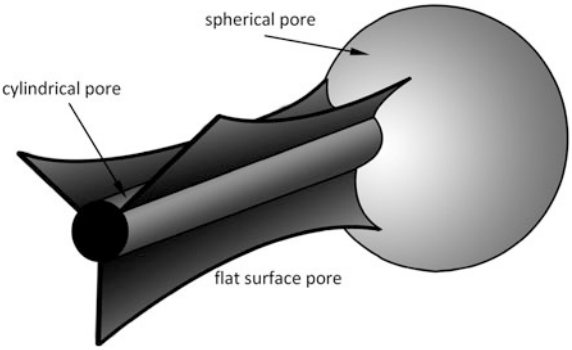

Fig. 4.5 Diagram representing basic pore geometries, particularly for sandstones. Adapted from Bernabe (1991)

difference in pressure within a water film between two surfaces and the pressure of the bulk phase (Weimann 2001). The expansion has been attributed to the capillary condensation occurring in the micropore region; however, this is a controversial topic that has as yet not been elucidated (Ruedrich et al. 2005, 2011). The hydric behavior has been studied in detail for several German sandstones, many of them containing little or no clay, and a distinct correlation could be established between microporosity and hygric swelling. Hygric swelling increases with decreasing average pore radius and increasing microporosity. Furthermore, there is a distinct influence of the distribution of clays in the sandstones. When the clays are present in lithoclasts, they can transfer the stresses to the rock fabric. If the clays are merely coating quartz grains, their swelling will not be as critical since there is pore space to accommodate this phenomenon (Ruedrich et al. 2011).

Of the phyllosilicates that comprise micas, chlorites, and clays, the latter, because of their mineralogy, shape, and small size, tend to have cations, such as K^+ or Na^+, adsorbed onto their surfaces to balance isomorphic substitution. The kaolinite group is the least expansive one because it has minimum substitution and a strong bonding between the tetrahedral and the octahedral layers. However, for the other clay groups, the liability of these interlayer exchangeable cations increases from the illite (or hydromica) group of clays to the montmorillonite (or smectite) group, i.e. the expansive clays. Furthermore, these expansive clays can form interstratification with non-swelling clays such as kaolinite and other phyllosilicates such as micas and chlorite, thus leading to significant swelling (Bühmann et al. 1988; Senkayi et al. 1981). Micas can also show interlayer swelling when K^+ ions are replaced by Na^+ (Sánchez Pastor et al. 2010). The expansive behavior of clays can occur via two different regimes: crystalline and osmotic swelling.

Crystalline swelling can occur in all types of clay minerals when they are exposed to changes in relative humidity. It is known to take place in discrete, stepwise formation of adsorbed water layers, and the resulting spacing transitions are thermodynamically analogous to phase transitions (Anderson et al. 2010). The distinct water layers, bonded between the cations and the negative charges of the clay particle surfaces, are more ordered, denser, and viscous than bulk water, being generally referred to as “structured” water (Stockhausen 1981; Madsen and

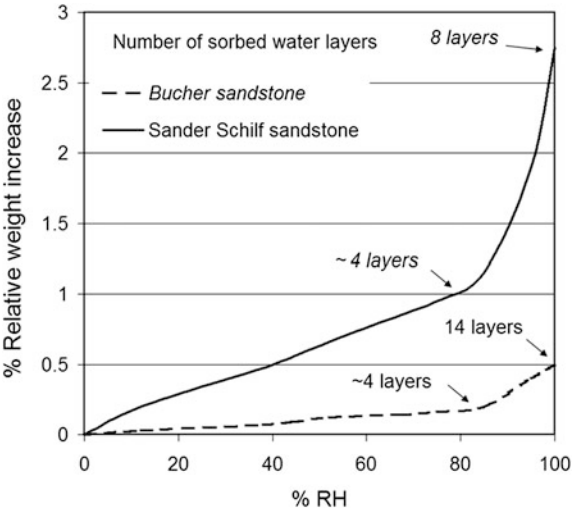

Fig. 4.6 Water sorption curves for the coarse-pore Bucher sandstone and the mixed-pore Sander Schilf sandstone which also contains more phyllosilicates. Adapted and simplified from Snethlage (1984). The number of sorbed water layers was calculated based on the amount of sorbed moisture that, in turn, reflect the specific surface area of the stones (2.63 and 14.8 m^2/g, respectively). Note that, at the inflection point of the curve (approx. 80 % RH), both stones adsorbed the same number of water layers

Müller-Vonmoos 1989). A more detailed study of the water adsorption mechanism on swelling clays has found that, below 10 % RH, only the external clay surfaces are hydrated. At RH >10 %, water enters the interlayer space, hydrating the cations while also filling the interparticular porosity that falls into the 2–50 nm range (Salles et al. 2009). At what RH the whole pore system is covered with a water layer depends on the nature of the minerals present. For example, the amount of adsorbed water will vary with the interlayer cation in the order of $Li^+ > Cs^+ > Na^+ > K^+ > Ca^{2+} > Na^+/Ca^{2+}$ and does not follow the hydration energy sequence for the cations in solution: $Li^+ > Na^+ > K^+ > Cs^+$ (Salles et al. 2009). Crystalline swelling of montmorillonite can lead to a two-fold volume increase of this expansive clay (Madsen and Müller-Vonmoos 1989).

The influence of the presence of clays and of smaller pores is immediately evident in the different hygric water adsorption of sandstones shown in Fig. 4.6. The coarse-pore (most have 100 μm radius) Bucher sandstone (95 % quartz, 5 % kaolinite) adsorbs far less moisture than the mixed-pore Sander Schilf sandstone (55 % quartz, 10 % feldspars, 5 % chlorite, illite, and muscovite, plus 35 % lithic fragments) with fine pores around 0.05 μm and coarse pores around 50 μm radius.

The inflection point of the curves falls around 80 % RH, and, at that point, both stones had only adsorbed approximately 4 water layers; this corresponds to an approximate thickness of 1 nm, indicating that pores of this size are already filled with water. It is at this point that the moisture content in the stone starts to induce hygric swelling as discussed previously for the Schöttmarer sandstone (see Fig. 3.47, Sect. 3.5).

The curves above are not representative of what actually happens in nature as it has been shown that equilibrium is rarely attained. From experiments with the calcareous Baumberger sandstone, it has been found that the stone surface–subsurface quickly changes moisture content upon RH changes (Franzen and Mirwald 2004), but an equilibrium moisture content about 8 cm in depth requires

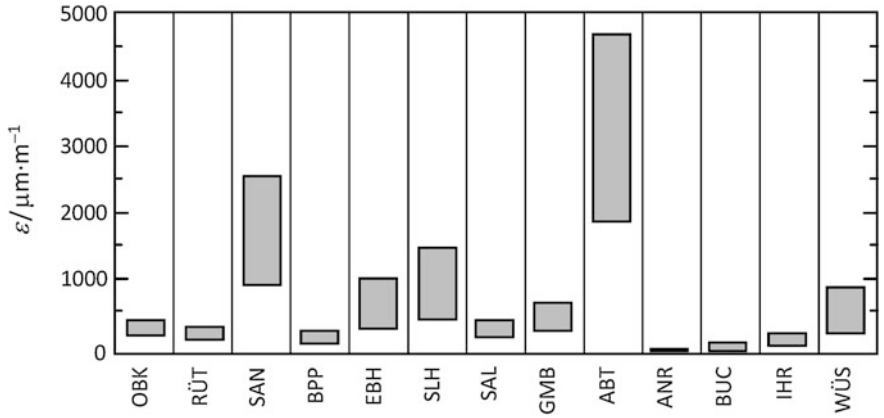

Fig. 4.7 Hydric dilation ε of various German sandstones (in parentheses, the binder type): OBK = Obernkirchener (silica); RUT = Rüthener green (clay and silica with barite); SAN = Sander Schilf (clay); BPP = Burgpreppacher (silica); EBH = Ebenheider (silica and clay); SLH = Schleerither (clay); SAL = Saaler green (calcareous); GMB = Yellow Maulbrunner (clay); ABT = Abtswinder (clay); ANR = Anröchter green (calcareous); BUC = Bucher (silica); IHR = Ihrlersteiner green (calcareous); WUS = Wüstenzeller (silica and clay). Adapted from Snethlage and Wendler (1997)

2 weeks to be achieved (Chkirda et al. 1999). Nonetheless, hygric cycling over centuries will contribute to the weakening of the stone matrix.

Osmotic swelling is based on the repulsion between electric double layers and can act over larger distances compared to the 1 nm range of crystalline swelling, and is mostly relevant when liquid water is present. As the name indicates, this process is driven by the difference in concentration of the ions electrostatically held by the clay surface and those in the pore water of the rock. Significantly larger volume increases are observed (>2 to ~13 nm). The swelling behavior of clay in rocks depends on the type and amount of clay minerals present, their surface charges, and the cations in the double layer (Madsen and Müller-Vonmoos 1989). For example, Na^+-saturated smectites will swell far more than K^+-saturated ones (Anderson et al. 2010).

The hydric swelling of various German sandstones, including the ones previously mentioned, is shown in Fig. 4.7. Most of them show an expansion of some 500 µm/m, except for the clay-bearing ones, where this value can increase tenfold, up to 5,000 µm/m (Snethlage and Wendler 1997). Further examples can be found in Chap. 3.

Based on the above, it would appear that wet-dry cycling will induce far more swelling, and, therefore, more deterioration to the stone matrix, than changes in relative humidity. Nonetheless, it has been suggested that crystalline swelling could, for some clay-bearing sandstones such as the Portland brownstone of the northeast US, known for its use in the construction of the typical row-houses in New York City, be the main mechanism for its deterioration (Wangler and Scherer 2008). This sandstone has long been known for its poor performance (Julien 1883)

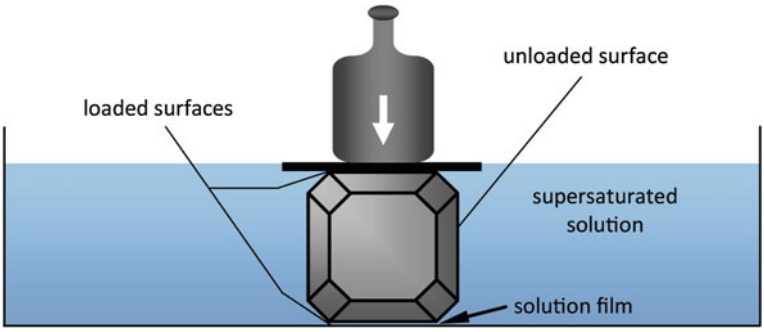

Fig. 4.8 Growth of a loaded salt crystal

and has a hydric dilation, i.e. strain, perpendicular to its bedding of 1,000 μm m^{-1} (Wangler and Scherer 2008). This result would appear to confirm the statement that the swelling stress from the crystalline process is far higher (ranging from 400 N mm^{-2} for the first to about 30 N mm^{-2} for the fourth adsorbed water layer) than the osmotic swelling (about 2 N mm^{-2}) for montmorillonite clay (Madsen and Müller-Vonmoos 1989).

4.2.3 Crystal Growth

In the case of thermal and moisture cycling, stresses in the stone fabric are induced by expansion of the matrix constituents themselves. In this section, stresses that are induced by the formation and confined growth of new phases within void spaces in the fabric of building stones are considered. The pressure generated by growing crystals is called "crystallization pressure". Apart from the crystallization of salts, such processes also include the growth of ice crystals upon the freezing of a pore solution.

It is generally accepted that the crystallization of salts is a major damage mechanism in stone. Although experimental evidence that growing crystals can exert pressure in porous materials was provided more than a century ago, until recently, there was no agreement among researchers regarding the nature of the process responsible for the generation of stress (e.g. see reviews of Evans 1970; Ginell 1994). However, in recent years, there has been substantial progress in understanding the thermodynamics of confined crystal growth and the generation of crystallization pressure (e.g. Scherer 1999, 2004; Flatt 2002; Steiger 2005a, b). The following paragraphs present a brief summary of the current state of knowledge.

Evidence that growing crystals can exert pressure was provided by the pioneering experiments of Becker and Day (1905, 1916); Taber (1916) and Correns and Steinborn (1939). The practical setup in these early experiments is illustrated in Fig. 4.8. It was observed that crystals submerged in their solutions and loaded

with additional weights continued to grow against the constraint. Thus, the confined crystals were able to generate stress. Important conclusions were drawn from these experiments. First, in order for a crystal to continue growing on its loaded surface, a solution film must exist, separating the loaded face from its constraint. Otherwise, deposition of matter and growth in this contact region is impossible. The solution film, originating from repulsive forces between the crystal and its constraint, acts as a diffusion path, allowing the exchange of ions between the solution and the crystal (Correns and Steinborn 1939; Scherer 1999).

The second important conclusion drawn from the early experiments was that growth upon the loaded face of a crystal can only exert pressure if this face is in contact (via the solution film) with a supersaturated solution. The degree of supersaturation required for growth to occur increases with increasing load (Correns and Steinborn 1939). A thermodynamic treatment of the situation of a growing crystal that is subject to non-hydrostatic, anisotropic stress yields an equation for the pressure that is generated by a crystal confined in void spaces of a rock or any other porous material:

$$\Delta p = \frac{RT}{V_\mathrm{m}} \ln S \tag{4.1}$$

Here, the crystallization pressure is defined as the difference between the pressure p_c upon the loaded face of a confined growing crystal and the liquid phase pressure p_l, i.e. $\Delta p = p_\mathrm{c} - p_\mathrm{l}$. R is the gas constant, T is the absolute temperature, V_m is the molar volume of the crystalline solid, and S is the degree of supersaturation in the liquid phase. Equation (4.1) is the most general equation for crystallization pressure. Its application requires an appropriate expression for the degree of supersaturation. For this purpose, the simple situation of a large crystal growing in a large pore where the liquid phase pressure equals the ambient pressure is considered. In this case, the supersaturation $S = a/a_0$ is defined as the ratio of the activity a of the dissolved species in the supersaturated solution and the activity a_0 of the saturated solution, thus yielding:

$$\Delta p = \frac{RT}{V_\mathrm{m}} \ln(a/a_0) \tag{4.2}$$

For a dissociating solid of general composition

$$\mathrm{M}_{\nu_\mathrm{M}}\mathrm{X}_{\nu_\mathrm{X}} \cdot n\mathrm{H_2O} \rightleftharpoons \nu_\mathrm{M}\mathrm{M}^{z+} + \nu_\mathrm{X}\mathrm{X}^{z-} + n\mathrm{H_2O} \tag{4.3}$$

consisting of ν_M positive ions M of charge z_M, ν_X negative ions X of charge z_X, and n molecules of water, the activity of the solid in an aqueous solution is given by the ion activity product:

$$a = a_\mathrm{M}^{\nu_\mathrm{M}} a_\mathrm{X}^{\nu_\mathrm{X}} a_\mathrm{w}^{n} \tag{4.4}$$

where a_M and a_X are the activities of the cation and the anion, respectively, and a_w is the water activity. It should be noted that a_0, the activity of the saturated solution, is equal to the thermodynamic solubility product of the respective salt. Several

authors have used Eq. (4.2) to calculate crystallization pressures for different salts. However, many of these calculations contain errors that require further comments to avoid confusion. For example Correns and Steinborn (1939) were the first who recommended the use of Eq. (4.2) for the calculation of crystallization pressure. However, in their own calculations, they replaced activities in Eq. (4.2) with molar concentrations, overlooking the fact that salts are dissociating species and that, in concentrated solutions, molar concentrations differ significantly from the ion activities. This resulted in quite substantial errors (Steiger 2005a, 2006a; Flatt et al. 2007). For example, neglecting dissociation leads to an underestimation of the crystallization pressure by a factor of two in the case of 1–1 salts such as NaCl or KNO_3. For salts with more complicated stoichiometry, the error is even greater. The influence of the non-ideal behavior in crystallization pressure calculations is discussed in some detail by Steiger (2006a) and Flatt et al. (2007).

Later Winkler and Singer (1972) and Winkler (1994) presented extensive calculations of crystallization pressures for a number of different salts. However, their calculations are also erroneous for several reasons. First, in their calculations, salts were treated as non-dissociating species, and the non-ideal behavior of their concentrated solutions was neglected. Second, they extended their calculations to entirely unrealistic supersaturation. For example, they list calculated crystallization pressures for supersaturation ranging from 2 to 50 (based on concentration ratios of undissociated solids). Such high supersaturations have no practical relevance and do not even exist for most of the salts listed in their tabulation. For instance, in the case of NaCl, the supersaturation of 50 used by Winkler and Singer (1972) for their calculations refers to a "solution" consisting of about 18 g NaCl per g of water! In contrast, the maximum known concentration that was achieved by evaporation from levitated droplets (Tang 1997) was in the order of 0.8 g NaCl per g H_2O.

The unrealistic supersaturations in the calculations of Winkler and Singer (1972) caused severe criticism (Lewin 1974; Snethlage and Wendler 1997), and, subsequently, many authors preferred an apparently different damage mechanism previously suggested by Everett (1961). Based on the properties of curved interfaces between crystal and solution and assuming spherical geometry, Everett derived the following equation for the crystallization pressure:

$$\Delta p = 2\gamma_{cl}\left(\frac{1}{r_1} - \frac{1}{r_2}\right) \tag{4.5}$$

Here, $r_2 > r_1$ are the radii of two crystals in adjacent pores of different sizes (see Fig. 4.9), and γ_{cl} is the surface free energy of the crystal-liquid interface. Many researchers preferred this equation, probably because it is apparently more realistic to calculate crystallization pressures on the basis of a measurable quantity such as the pore-size distribution than to estimate the degree of supersaturation in a pore solution. Only a few authors have pointed out that both approaches are entirely equivalent (Scherer 2004; Steiger 2005b). Recently, it has been shown (Steiger 2005b. 2006a) that Eq. (4.5) can be directly derived from Eq. (4.2) by comparison of the different solubilities of crystal surfaces in large and in small

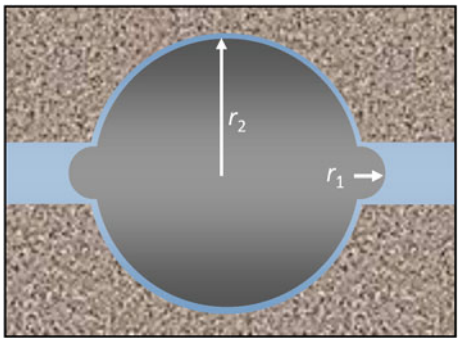

Fig. 4.9 Large crystal growing in a spherical pore (radius r_2) with small cylindrical pore entrances (radius r_1)

pores (see Fig. 4.9). It has been further shown that Eq. (4.5) is a special case of the more general Eq. (4.2), and equations were also derived for other pore geometries, e.g. cylindrical pores.

The major difference between the more general case of crystallization pressure represented by Eq. (4.2) and the situation in a large pore with small entries as shown in Fig. 4.9 is the fact that the former situation represents a non-equilibrium situation. The crystal shown in Fig. 4.8 can only generate stress as long as the solution is supersaturated. This solution is then just in equilibrium with the crystal face under pressure, but is supersaturated with respect to the unloaded faces of the crystal. Therefore, the crystal continues to grow upon its unloaded faces, and the high concentration required for stress upon the loaded crystal faces to be generated cannot be maintained. As long as unloaded crystal faces are present, the evolution of crystallization pressure in a porous material is a dynamic process that is determined by kinetic influences such as evaporation and cooling rates, the diffusion of ions in the free solution and in the liquid film, the availability of unloaded crystal surface, and the growth rates on unloaded faces. Under such conditions, it is very unlikely that crystallization pressure builds up and remains constant over long periods of time. More likely, high pressures occur as transients if high supersaturation in the pore solution evolves temporarily as a result of sharply dropping temperatures or rapid evaporation. Amplitude and duration of stress maxima are, therefore, dependent on the parameters controlling the degree of supersaturation.

In contrast, the crystal shown in Fig. 4.9 represents an equilibrium situation. Growth of the crystal into the small pore entrances requires a higher concentration of the pore solution due to the greater solubility of the small satellite crystals. At equilibrium under ambient pressure, the concentration in the surrounding solution is just equal to the solubility of the hemispherical crystal of size r_1. However, this solution is supersaturated with respect to the unloaded large crystal. Therefore, stress is generated due to growth of the confined crystal in the large pore until equilibrium is reestablished. At equilibrium, the solution is saturated with respect to both crystal faces. However, due to their different sizes, the particle in the pore entrance is under ambient pressure, while the large particle must be under enhanced pressure. This is an equilibrium situation, and the result is a static crystallization pressure. However, it should be noted that the equilibrium

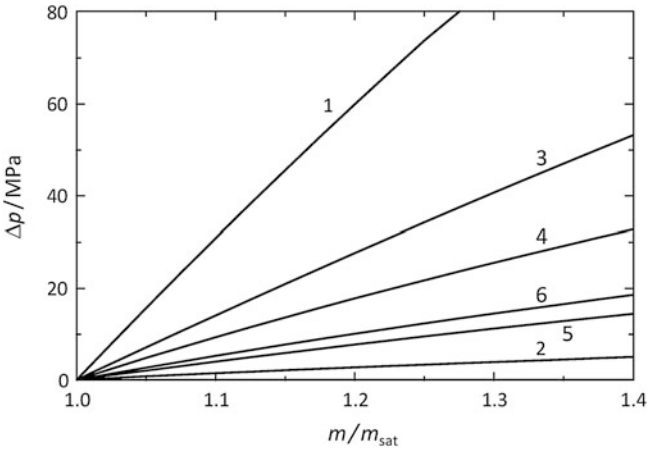

Fig. 4.10 Crystallization pressures at 25 °C in supersaturated solutions of *1* NaCl (halite), *2* $Na_2SO_4 \cdot 10H_2O$ (mirabilite), *3* Na_2SO_4 (thenardite), *4* $NaNO_3$ (nitratine), *5* $MgSO_4 \cdot 7H_2O$ (epsomite), and *6* $MgSO_4 \cdot 6H_2O$ (hexahydrite). Adapted from Steiger (2005a); supersaturation is expressed as the ratio of the molality m of the supersaturated solution and the saturation molality m_{sat} of the respective salt

crystallization pressure requires the presence of very small pores, preferably with pore radii smaller than about 50 nm.

Crystallization pressures for several salts commonly found in building stone are depicted in Fig. 4.10. They are taken from Steiger (2005a) and were calculated using Eqs. (4.2) and (4.4) together with an electrolyte solution model to account for the non-ideal behavior of highly concentrated solutions. If these pressures are generated in a porous stone, they induce tensile stress within the solid matrix that might eventually exceed the strength of the stone. As a first indicator, the crystallization pressures may be compared to the tensile strengths of natural stones that hardly exceed values of about 3–5 MPa (see Sect. 3.6). Therefore, the pressures shown in Fig. 4.10 may be sufficient to cause damage in nearly every building stone. A more sophisticated treatment is based on the theory of poromechanics (Coussy 2004; Espinosa-Marzal and Scherer 2009). Applying this theory, it has been recently shown that there is reasonable accordance between calculated crystallization pressures using Eq. (4.2) and the crystallization pressure derived from deformation measurements (Espinosa-Marzal and Scherer 2010; Espinosa-Marzal et al. 2011).

Are the high supersaturations required for crystallization stress to be induced likely to occur in the pore solutions of building stones? First of all, according to nucleation theory (Nielsen 1964), a certain degree of supersaturation is always required in order for nucleation and crystal growth to occur. In fact, very high critical supersaturations in sodium sulfate and sodium carbonate pore solutions subject to cooling were determined experimentally (Rijniers et al. 2005; Espinosa-Marzal and Scherer 2008). The observation of both stable and metastable crystalline phases in the same pores during evaporation of sodium sulfate solutions from porous stone

(Rodriguez-Navarro and Doehne 1999; Rodriguez-Navarro et al. 2000) also provides clear evidence of the presence of extremely high supersaturations.

It is also possible to design laboratory salt damage experiments in such a way that crystal growth occurs under conditions of very high supersaturation. One prominent example of this is the classical sodium sulfate durability test for building materials (e.g. RILEM PEM–25 1980) or similar tests as reviewed by Goudie and Viles (1997). Typically, in such tests, a porous material is impregnated with a sodium sulfate solution and dried at an enhanced temperature (e.g. 60–105 °C) such that anhydrous Na_2SO_4 is formed. Subsequently, after cooling to room temperature, the specimen is impregnated again with a Na_2SO_4 solution leading to the hydration of Na_2SO_4. Repeating this procedure several times, sodium sulfate has been proved to be extremely destructive, and it was observed that most of the damage occurred during the impregnation phase (Schmölzer 1936; de Quervain and Jenny 1951). It is now accepted that the destructive effect is due to the growth of mirabilite crystals from the highly supersaturated solutions originating from the dissolution of anhydrous sodium sulfate during the re-wetting phase (Chatterji and Jensen 1989; Flatt 2002). Under such conditions, a crystallization pressure of 15 MPa at 20 °C can be calculated (Steiger and Asmussen 2008), which is in good accordance with the pressure derived from deformation measurements (Espinosa-Marzal et al. 2011). The crystallization pressure calculations also confirm the strong influence of temperature in the sodium sulfate crystallization test, as observed by several investigators (Price 1978; Chatterji and Jensen 1989; Tsui et al. 2003).

The sodium sulfate crystallization test has been studied extensively to understand the reason for the amount of deterioration it induces. Among these studies, that of Angeli et al. (2008) has been able to provide a clear picture of the induced damage. Through careful analysis of the weathered samples via microscopic observation, both optical and SEM, and mercury intrusion porosimetry, MIP, it has been shown that the porosity after weathering (and after having washed out the salt) is higher than prior to it. From weathered samples that still contain the salt, it was possible to determine in which pore types the sodium sulfate would crystallize, to calculate the pore space occupied by thenardite (since the MIP operates under a vacuum), and to estimate from this the pore space that would have been occupied by mirabilite during the wetting cycle. It was further found that most of the pores were affected by the crystallization of the salt and that a crystal growing in smaller pores (up to several microns) is capable of exerting sufficient pressure to start or propagate a crack. While, in general, stones with smaller pores (up to several microns) are more susceptible to deterioration, there are exceptions when the stone has a high overall porosity, or a low pore connectivity and high tortuosity. Finally, the pre-existing cracks in the stone matrix will accelerate the deterioration if all the other parameters are equal.

Apart from the theories addressing the mechanism that underlies the observed damage in porous materials, it is of practical relevance to find a methodology to quantify and estimate the actual damage that is observed with the standard salt crystallization test using sodium sulfate. For this purpose, a study on various types

of stones was carried out, and the results obtained were carefully analyzed. Three stages were identified during the salt crystallization test: the initial weight increase because of the introduction of salt into the material, the first visual appearance of deterioration including weight variation—a stage that sometimes merges directly with the last one, wherein the weight decrease is continuous as deterioration progresses. These stages reflect the type and degree of deterioration that could be quantified by two indicators: the alteration index (AI) and the alteration velocity (AV). The former correlates the capillary and evaporation coefficient with the lowest mechanical strength, i.e. tensile strength, of the sample. The alteration velocity can be measured via the P-wave velocity, but it has to be taken into account that comparisons can only be made between stones of similar composition given the difference of the P-waves for quartz and calcite. This method allows differentiating stones that have a high AI, but those having a low AV will be more resistant in the long term than others with a low AI and a high AV. Important points to consider are the size and shape of the samples and the fact that these indicators apply only to deterioration by sodium sulfate crystallization (Angeli et al. 2007). Other critical factors in the deterioration induced in a porous material are its characteristics. To determine the most important ones, principal component analysis, PCA, was performed on various rock types, ranging from a quartz sandstone to a calcite or a dolomite sandstone to a calcite quartz conglomerate. Various parameters were measured for them, such as pore size, specific surface, connected porosity, bulk density, and real density. Additionally, mechanical properties and water transport characteristics were determined. Salt crystallization tests were included in the study as well. Through PCA, two principal components were identified that accounted for 86.5 % of the total variance. The first one was linked to mechanical properties, porosity and density, while the second one was associated with water transport and pore structure. Both of them included the dry weight loss (DWL) from standard salt crystallization tests. A multiple regression analysis showed that rock strength has a predominant statistical weight for predicting deterioration induced by salt crystallization, while water transport characteristics and pore structure parameters have a minor influence (Benavente et al. 2007).

Several common salts can exist in different hydrated forms. Hydrated salts that are commonly found in building materials include the series $Na_2SO_4{\cdot}nH_2O$, $MgSO_4{\cdot}nH_2O$, and $Na_2CO_3{\cdot}nH_2O$. The general form of a hydration reaction is given by

$$M_{\nu_M}X_{\nu_X} \cdot n_1H_2O(cr) + (n_2 - n_1)H_2O(g) \rightleftharpoons M_{\nu_M}X_{\nu_X} \cdot n_2H_2O(cr) \tag{4.6}$$

The equilibrium constant for this reaction is

$$K = \frac{p_{w,0}}{p_{w,eq}} = \frac{1}{RH_{eq}} \tag{4.7}$$

where $p_{w,eq}$ is the equilibrium water vapor partial pressure, $p_{w,0}$ is the saturation water vapor pressure, and RH_{eq} is the equilibrium relative humidity for the hydration–dehydration equilibrium of the two hydrates with n_1 and n_2 molecules of

water. If the lower hydrated form is confined to void spaces of a porous material, pressure can be generated during the hydration reaction. The maximum hydration pressure Δp_{hydr} that can be exerted by the growing hydrated crystal is given by

$$\Delta p_{\mathrm{hydr}} = \frac{\Delta nRT}{\Delta V_{\mathrm{m}}} \ln\left(\frac{\mathrm{RH}}{\mathrm{RH}_{\mathrm{eq}}}\right) \tag{4.8}$$

where ΔV_{m} is the difference in the molar volumes of the two solids, $\Delta n = n_2 - n_1$, RH is the relative humidity at which the hydration reaction proceeds, and $\mathrm{RH}_{\mathrm{eq}}$ is the equilibrium value at temperature T as defined in Eq. (4.7). The hydration pressure is the pressure that would have to be exerted on the hydrated crystal to prevent its growth. In other words, RH is the equilibrium relative humidity of the hydration–dehydration equilibrium if the vapor phase is under ambient pressure p_{a} and the solid phases are under the enhanced pressure p_{c}; thus, $\Delta p_{\mathrm{hydr}} = p_{\mathrm{c}} - p_{\mathrm{a}}$ (Steiger et al. 2008a). It is important to note that the driving force for the hydration pressure is also supersaturation. While the supersaturation of a solution is the driving force for the crystallization pressure, it is the water vapor supersaturation of the ambient air with respect to the equilibrium water vapor pressure of the hydrated salt which is responsible for the generation of hydration pressure.

Equation (4.8) was first derived by Mortensen (1933); later, it was misused by calculating very high hydration pressures at relative humidities close to 100 % (Winkler and Wilhelm 1970; Winkler 1994). In these calculations, the upper limit of the ambient RH due to the deliquescence of both the educt and the product phases, was overlooked (Steiger 2003). If a salt is subjected to a slowly increasing relative humidity, a point will be reached—the deliquescence or saturation humidity—where the solid picks up water vapor forming a saturated solution. Hence, above the deliquescence relative humidity, DRH, of the product phase, i.e. the higher hydrated form, a solid cannot exist anymore and, consequently, there is no hydration pressure at all. On the other hand, if the DRH of the educt phase is exceeded, a solution supersaturated with respect to the product phase is formed, and the hydration reaction follows a two step reaction mechanism including the dissolution of the lower hydrated form (n_1) and subsequent crystallization of the hydrate (n_2) from a supersaturated solution (Steiger 2003). In this case, the pressure generated by the hydrated crystal is a crystallization pressure, according to Eq. (4.2). The supersaturation is given by the concentration of the solution in the vicinity of the growing hydrated crystal which is determined by the dissolution rate of the anhydrous (or lower hydrated) crystal, the growth rate of the hydrate, and the diffusion rate of the ions to the surface of the hydrated crystal (Steiger et al. 2008a).

4.2.4 Combination of Factors

The previous sections discussed the different processes involved in the deterioration of stone through mechanical stresses. However, in nature, these seldom act alone, and the observed damage is the result of their interaction. One of the difficulties

Table 4.3 Comparison of thermal and hydric expansion of different rock types

	Rock type	Thermal expansion coefficient ($\mu m \times m^{-1}K^{-1}$)	Thermal expansion $\Delta T = 40$ K ($\mu m \times m^{-1}$)	Hydric expansion ($\mu m \times m^{-1}$)
Magmatic		8	320	49
Metamorphic	Marble	105	420	70
	Siliceous	8.5	340	500
Sedimentary	Limestone	4	160	70
	Travertine	5	200	20
	Sandstones	11	440	1000

Based on data from Weiss et al. (2004a)
Thermal expansion is calculated for a 40 °C temperature change, assuming linear behavior of the thermal expansion coefficient. Hydric expansion values correspond to maximum water absorption by capillarity (ranging between 1 min and 16 h depending on the stone type) and measurements were made perpendicular to foliation (based on data from Weiss et al. 2004a)

faced when trying to find a remedy to a problem is the identification of the key deteriorating factor, or, if there are several, as is more likely, then it is important to know if these act simultaneously or sequentially (Koestler et al. 1994).

To follow the order used previously, the first combination considered will be that of thermal cycling in conjunction with water. For this purpose, it is important to bear in mind the ranges of expansions that can be expected under normal conditions as summarized in Table 4.3.

For the specific case of marbles, wherein thermal expansion is more relevant than the hydric one, the residual strain left in marbles after thermal cycling decreases after the first cycle; however, if moisture is present, there is a progressive increase in the residual strain. Furthermore, there is no correlation between the amount of residual strain remaining after dry and wet cycling (Koch and Siegesmund 2004). However, a correlation could be detected between the bowing tendencies of different marble types with the residual strain measured from the wet thermal cycling experiments mentioned. The amount of deterioration, and of bowing, can be correlated with the marble fabric. Therefore, the type of marble, the presence of moisture, and thermal cycling all interact in the deterioration and, in the case of marble slabs, their deformation tendencies (see Sect. 3.4.2).

The effect of long-term freeze–thaw cycling for marbles has been studied by Ondrasina et al. (2002). The resulting deterioration ranges from a superficial sugaring to a complete loss of cohesion along grain boundaries. The study was carried out on three marbles, Palissandro (a dolomitic marble containing phlogopite and quartz with pronounced foliation), Sterzing (a calcite with some dolomite and muscovite, slightly foliated marble) and Carrara (a fine-grained calcite marble with thin grayish veins). The samples were left for 6 h at −20 °C. After this, they were stored in a water bath at 20 °C for 2 h. In total, 204 cycles were carried out. The change in their porosity was interesting. While the Sterzing and the Carrara marbles showed a continuous increase in porosity as a function of the number of cycles, the Palissandro marble showed its first increase after 24 cycles

and subsequently did not change significantly. The Carrara marble also showed a significant decrease in the elasticity modulus between the 5th and the 7th cycles, followed by another around the 115th cycle, while the other two marbles did not show such changes, a fact that can be attributed to their dolomite content. The decrease in the elasticity modulus of the Carrara marble correlated to its increase in porosity. This is also a result of the straight grain boundaries of this marble, which results in crack formation along them. The other two marbles, with curved and interlocked grain boundaries, are more resistant to freeze–thaw cycling.

Dolomitic marbles that contain localized inclusions of mica and amphibole minerals, especially prismatic tremolite, are prone to what is called "pock marking", a larger form of pitting. This minor deterioration pattern has been observed in many historical buildings in the northeast US where it freezes, but not in corresponding buildings in the southeast. The damage could, therefore, be attributed to the preferential moisture retention by the platy mica and the fibrous tremolite, which, upon freezing, leads to their detachment, leaving a rounded pock mark behind (Lewin and Charola 1981).

An important point that has to be taken into account when dealing with stones in historical structures is their microenvironment. This point was studied in detail by Turkington et al. (2002). Experiments were carried out on two blocks of Hollington sandstone, an iron-rich quartz sandstone. These were located in a cabinet, and their moisture and temperature were measured as they were subjected to changes in RH and temperature, attained by heating with an infrared lamp that was turned on and off at 15 min intervals. The experiments were run with the blocks dry and with the blocks saturated in water. Furthermore, the blocks were first set flush so that they both received full light, and then the bottom one was receded progressively until it was totally in the shade while the top one remained in the light. The depth and steepness of the thermal gradient established in the near-surface of the stone depends on the thermal properties of the stone and the thermal regime applied. If the stone is in the shade, the amplitude between maximum and minimum temperatures decreases. Nonetheless, steep gradients are still created when environmental temperatures fluctuate and may cause significant stress to the stone. When moisture is present, the thermal gradients are enhanced, since the subsurface layers are slower to respond to indirect heating, i.e. when the blocks are in the shade. Thermal stress is not reduced in these cases, but it is limited to the surface layer. This is relevant in the case of the presence of salts, as these will concentrate at the subsurface layer.

For rocks containing phyllosilicates, such as slates and sandstones, the hydric expansion can be twice as high as the thermal expansion. To illustrate this point, the interesting experimental study combined with numerical modeling carried out by Ožbolt et al. (2008) will be summarized. The aim of the study was to determine the location of crack formation in Heilbronner Schilf sandstone quarry samples. The stone is a fine-grained arenite to feldspar arenite with chlorite cement and secondary feldspar to feldspar cement and has a medium–high compressive strength and elasticity modulus. The study considered hygric, hydric, and thermal cycling, including freezing. One of the samples was constantly monitored via

Acoustic Emission Analysis (AEA) during the cycling to determine when cracks were forming. This proved to occur primarily upon heating after a freezing cycle or during freezing of the water-saturated sample. The most critical stresses were induced during fast changes in temperature when the sample was saturated with water. The fast and high water uptake and the consequent swelling of the sample in combination with rapid heating or drying triggered the crack formation in the sample. Cracks developed preferentially in sharp spikes (notches) and corners (acute angles) of the profiled part of the specimen, and stiff but brittle layers, such as diagenetic iron cementations, also served as points for crack initiation. Crack propagation follows the bedding layering of stone; therefore, stone anisotropy is an important factor to be taken into account. The numerical modeling suggests that the thermal cycling alone does not cause any damage, but, coupled with increased water content, it does more damage than hygric-hydric cycling alone. An important factor is the moisture gradient from the surface to the interior, which causes significant damage.

The aforementioned study did not address the formation of ice, and, to understand the deterioration that freezing water can induce in porous buildings, the crystallization of ice is discussed first.

4.2.4.1 Crystallization of Ice

In contrast to widespread belief, crystallization pressure, not the hydraulic pressure that is caused by the volume expansion during freezing of water, is the primary cause of frost damage (Taber 1929; Everett 1961; Walder and Hallet 1986). The mechanisms of frost damage have been recently reviewed by Scherer and Valenza (2004). A strong argument that crystallization pressure is the primary source of stress during freezing comes from experiments with organic liquids that contract upon freezing (Taber 1930; Beaudoin and MacInnis 1974; Litvan 1978). In these experiments, dilation and damage of various porous materials were observed with liquids that were less dense than their respective solid phase. In this case, the damage can only be explained in terms of crystallization pressure.

Just as in the case of salt crystallization, the crystallization pressure that can be exerted by a confined ice crystal requires that the crystal be in contact with a supersaturated solution. However, in the case of a freezing liquid, the supersaturation is usually expressed in terms of the supercooling of the liquid phase, i.e. the temperature difference between the liquid film at the ice crystal-pore wall interface and the equilibrium freezing temperature. The crystallization pressure generated by an ice crystal in contact with supercooled liquid water is given by

$$\Delta p = \frac{S_{\mathrm{l}} - S_{\mathrm{ice}}}{V_{\mathrm{m,ice}}} (T_{\mathrm{f}} - T) \tag{4.9}$$

where S_{l} and S_{ice} are the entropies of liquid water and ice (respectively), $V_{\mathrm{m,ice}}$ is the molar volume of ice, T_{f} is the freezing temperature, and T is the temperature of

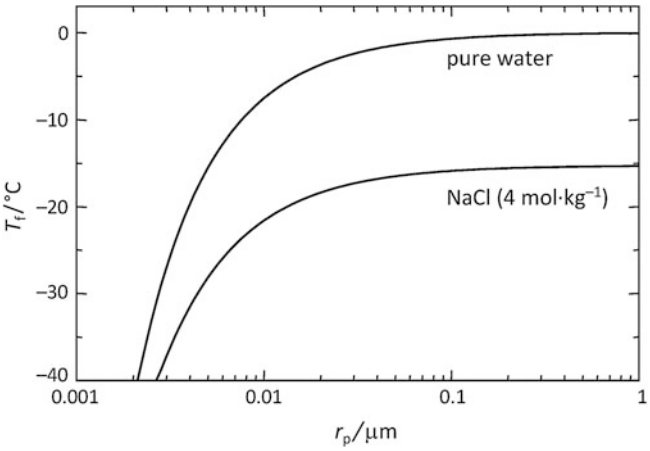

Fig. 4.11 Freezing temperatures (T_f) of water and aqueous NaCl as a function of pore size in a saturated porous material. Adapted from Steiger (2006b)

a supercooled liquid film between the growing ice crystal and the pore wall. It should be noted that the freezing temperature of water is strongly affected by the concentration of dissolved salts, as discussed in more detail below. The supercooling of water in an aqueous solution can also be expressed in terms of supersaturation, i.e. the activity of the water in the supercooled solution. This yields the following equation for the crystallization pressure of a growing ice crystal (Steiger 2004):

$$\Delta p = \frac{RT}{V_{\mathrm{m,ice}}} \ln\left(a_{\mathrm{w}} / a_{\mathrm{w},0}\right) \tag{4.10}$$

where a_{w} is the water activity in the liquid film, and $a_{\mathrm{w},0}$ is the water activity of the saturated solution at the same temperature, i.e. the water activity of the solution in equilibrium with ice at its freezing temperature. While for pure water $a_{\mathrm{w}} = 1$, in salt solutions the water activity is determined by the dissolved salts. In effect, there is a substantial depression of the freezing temperature with an increasing concentration of dissolved salts (see the following section).

In a porous material, there is no uniform temperature at which the pore water freezes. Apart from the concentration of dissolved salts, the freezing temperature is also affected by pore size. A small ice crystal, i.e. a crystal growing in a small pore, has a higher chemical potential and, therefore, a lower freezing temperature than a large crystal. Figure 4.11 depicts freezing temperatures of pure water and of a NaCl pore solution. It is obvious that there is a strong depression of the freezing temperature with decreasing pore size. Therefore, in a porous stone, pure water starts to freeze in large pores and at temperatures only slightly below 0 °C. In small pores (<0.1 µm), water only freezes at significantly lower temperatures, as shown by the upper curve in Fig. 4.11. The same effect is also responsible for

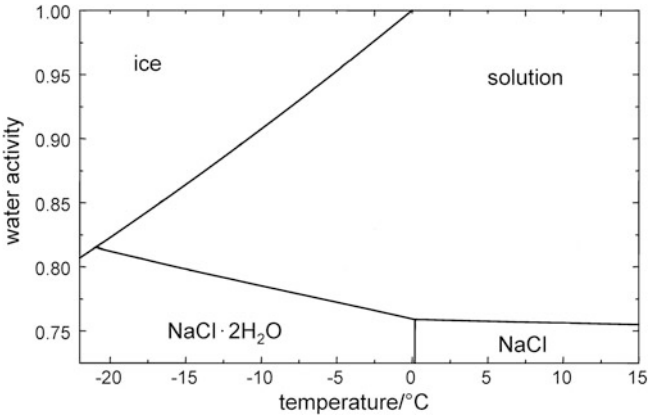

Fig. 4.12 Phase diagram of a sodium chloride solution. Concentration of sodium chloride increases with decreasing water activity. Adapted from Steiger (2004)

the low freezing temperature of salt solutions in small pores. In contrast, there is a significant depression of the freezing temperature in large pores due to the dissolved NaCl.

Similar to the case of growing salt crystals, the pore size dependence of the freezing temperature can be used to derive an expression for the crystallization pressure in small pores from Eq. (4.10). For example Eq. (4.5) applies to the case of a large spherical pore with small entrances. In fact Eq. (4.5) was first derived by Everett (1961) for the special case of frost damage, i.e. the crystallization of ice in porous materials. Different equations may be derived for other pore geometries, e.g. cylindrical pores (Scherer 1999, 2004; Steiger 2006b).

4.2.4.2 Ice Crystallization in Combination with Clays or Salts

It is well known that a salt solution will freeze at a lower temperature than pure water and that the decrease in temperature is proportional to increasing salt concentration—hence, the use of NaCl or $CaCl_2$ as deicing salts to keep pavements free of ice. About 50 % of the world's production of NaCl (estimated at 210 million metric tons) is used for this purpose with the unfortunate result that the salt solutions migrate into neighboring buildings with the consequent introduction of these salts into the masonry and its subsequent deterioration.

Figure 4.12 shows the equilibrium diagram for a sodium chloride solution at different relative humidities, reflected by the water activity of the solution and temperature. Sodium chloride crystallizes as such above 0 °C but, as a dihydrate, below that temperature. The $a_w = 1$ top line corresponds to pure water that freezes at 0 °C. With an increasing sodium chloride concentration, the water activity decreases, and the freezing temperature for ice is shifted below 0 °C.

The graph is valid for a salt-water system. In a porous body, this may vary as a function of the pore diameter. The freezing temperature depression of a salt solution has been calculated to be constant for pore sizes down to 0.1 μm in diameter, i.e. pores that are just at the edge of the capillary pore size (see Fig. 4.11 and Steiger 2006b) so that, for larger pores, the diagram above may be considered valid.

There has been some controversy regarding whether the presence of salts accelerates the damage induced by pure freeze–thaw cycles (Goudie and Viles 1997) since some early laboratory experiments showed that salts could actually reduce the amount of damage (McGreevy 1982). However, subsequent studies have shown that samples from various beds from the same quarry of fine-grained, quartzose sandstone were more damaged when subjected to freeze–thaw cycling where salts, either sodium chloride or sodium sulfate, were present than when only water was present. In general, more deterioration was observed when the samples were vacuum-impregnated with water or the salt solution (Williams and Robinson 1981). Further studies with other salts have confirmed that NaCl is one of the most deteriorating salts under freeze–thaw conditions, and this was attributed to the crystallization of the dihydrate salt (Williams and Robinson 2001). Studies carried out on chalk samples, wherein different salts, such as NaCl, $MgSO_4$, Na_2SO_4, and mixtures of them were subjected to various freeze–thaw cycles with varying conditions and temperatures (minimums were −10 and −30 °C), showed that intense freezing conditions caused more damage than milder conditions and that, in general, the presence of salts increased the observed damage, though the amount of damage depended on the type of salt (Jerwood et al. 1990a). These results were confirmed in subsequent studies carried out under non-saturation conditions that proved less damaging (Jerwood et al. 1990b).

Laboratory freeze–thaw tests carried out with various types of sandstones showed that conventional tests provide limited information regarding the deterioration mechanism occurring within the porous matrix. Mostly, the results reflect the presence of weak areas in the stones, such as discontinuities and preexisting microcracks. The study carried out by Ruedrich and Siegesmund (2007) measured the length change of the samples, both dry and saturated in water prior to freeze–thaw cycling. During dry freeze–thaw cycling, the samples show a linear contraction with decreasing temperatures, from 20 to −20 °C. This behavior changes for water-saturated samples that, upon cooling, first show an expansion at about −2 °C that could be attributed to ice crystallization. This was followed by a subsequent contraction at around −7 to −12 °C, depending on the type of sandstone, which was ascribed to the pressure solution and recrystallization of the ice crystals. Upon heating, an expansion occurs at around 3 °C, followed by a contraction that reaches its maximum at 7 °C. This behavior was followed by most of the sandstones containing some clays and with smaller capillary as well as micro-pores. For sandstones with higher clay content, a significant contraction was observed for the subsequent cooling to −20 °C and was attributed to the clay-bound water that does not freeze.

Samples with different water content were also tested. For some stones, a 70 % water content leads to behavior similar to that at full saturation, and strong residual strains were measured in the first cycle that resulted in macrocrack formation.

Furthermore, the water content determined the length change measured on the samples upon freezing. Also investigated was the influence of the cooling rate. One of the effects was the moving of the expansion maxima from −4 to −7 °C when the cooling rate was increased from 0.05–0.5 K min^{-1}. However, the more slowly cooled samples showed the highest absolute length change.

Field experiments were carried out in Antarctica using welded tuff cubic samples that were either pretreated with water or saturated with solutions of halite, thenardite, or gypsum, respectively, for a week (Matzuoka et al. 1996). Then they were exposed on the ledges of rock walls, where there is a limited supply of moisture. Thus, the samples equilibrated within a few days to the ambient conditions. As a reference, the moisture content in the rocks on site was around 35 %. After 4–5 years, little damage had been suffered by the water-pretreated or gypsum solution saturated samples, while those treated with the thenardite solution had cracked and their edges rounded, and the halite-treated ones had disintegrated completely. The limited damage suffered by the two former samples was attributed to the low moisture available on site, since the tuff had suffered severely during laboratory freeze–thaw cycling (Matzuoka et al. 1996). This data is corroborated with laboratory studies of other tuffs where the amount of water in the sample prior to freeze-thawing is critical (Van Hees et al. 2004).

As usual, the situation for stones in outdoor masonry is different. First of all, the distribution of salt is not homogeneous in the stones, with the subsurface, in general, holding a higher concentration of salt. Since the salt in question is most likely sodium chloride from the application of deicing salts, its concentration will be higher at ground level. Secondly, while freezing or below-freezing temperatures will be found at the surface, the interior of the stone may not be at subzero values. However, if the subzero temperature is relatively constant for some days, then this temperature may already be found some distance into the stone. During the day, if the sun is shining, the surface of the stone may thaw, with a resulting expansion, while the subsurface will continue to be frozen and contracted. This will induce stresses at the freezing front that will result in the typical spalling observed. Furthermore, as the solutions in the stone are not likely to be saturated, as ice forms, the solution will concentrate, lowering the freezing temperature of the remaining solution. Therefore, it is difficult to determine which factor is the most relevant for the particular deterioration observed.

4.2.4.3 Salts and Moisture Changes

Hygric expansion is mostly relevant for phyllosilicates, particularly clays, as discussed in Sect. 4.2.2. However, their swelling behavior in the presence of salts changes significantly as already pointed out by McGreevy and Smith (1984). To illustrate this point, the following experiment, similar to that discussed by Snethlage and Wendler (1997), is described using the clay containing Sander Schilf sandstone that was discussed in Sect. 4.2.2. One sample of the stone was first impregnated with NaCl, and a second sample served as a control. Both

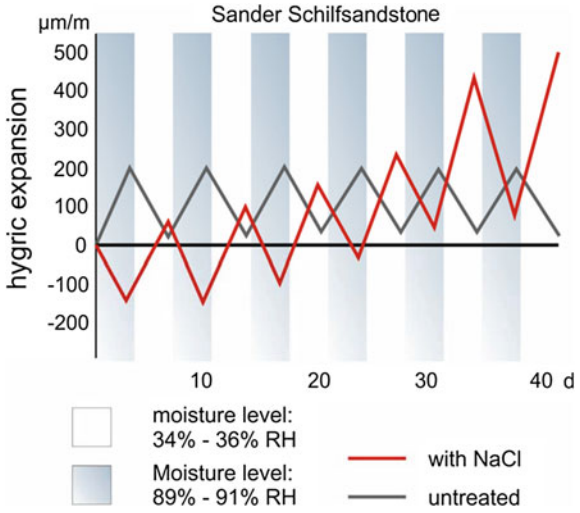

Fig. 4.13 Hygric expansion for a Sander Schilf sandstone sample and for one pre-treated with a NaCl solution. Adapted from Snethlage and Wendler (1997)

samples were dried to ambient conditions (30 % RH and 20 °C) prior to subjecting them to RH cycling between 35 and 90 % RH. The behavior of these samples is shown in Fig. 4.13.

The graph shows that, while the control sample expands upon moisture absorption and contracts upon its loss, the one containing salt has exactly the opposite behavior. Furthermore, for the control sample, the expansion—contraction is constant and reversible over at least ten cycles, while, for the salt-impregnated sample, it increases with cycling becoming irreversible. Similar results were also obtained by pre-treating the stone with $MgSO_4$ and $Ca(NO_3)_2$ solutions (Wendler and Rückert-Thümling 1993). The contraction of the salt-containing sample upon exposure to high RH (above the equilibrium relative humidity of the salt in question) can be the result of the formation of dense hydration layers because of the higher electrolyte content in the stone. Since the expansion of these stones is associated with their clay content, this could be related to the two swelling mechanisms associated with them. The first one corresponds to the crystalline swelling where the incorporation of cations from the salt in the intermediate layers of the clay minerals can result in a reduction of hydration possibilities. The second is associated with the intercrystalline, i.e. osmotic, swelling of these minerals. The thickness of the diffuse electrical double layer at the surface of the clay minerals decreases significantly in the presence of a salt solution as repulsive forces between the clay layers decrease (Scheffer and Schachtschabel 1984).

However, these theories do not take into account the presence of the salts and the role that their crystallization-dissolution plays during the hygric cycling. As has been long known and is discussed in detail in Sect. 4.2.3, when salts crystallize from a saturated solution, there is an expansion in the system, whereas, when they dissolve, there is a contraction. At the beginning of the experiment, both samples

are dry, but the salt-containing sample with the crystallized salt in it will already have been expanded. Subjecting it to high relative humidity, above the DRH of the salt, the salt will deliquesce and go into solution with a net contraction of the system, as shown in the graph.

There is certainly an interaction between the clays and the salts, but it appears that the overall behavior of this system reflects that of the salts rather than that of the clays. However, comparing the salt-induced deterioration of a clay containing stone with that of a similar stone without clays, it is clear that the clays contribute significantly to the overall deterioration.

4.2.4.4 Further Examples

To illustrate the complexity of the problem, a case study is presented that compares two clay-bearing limestones used in the construction of many buildings of historical value in Sicily, Italy (Cultrone et al. 2008). The limestones are the Syracuse limestone (Pietra di Siracusa) and the Melilli limestone (Pietra Bianca di Melilli), both of the Monti Climiti Formation. The Syracuse limestone has been used since Greek and Roman times, while the Melilli one was used for reconstruction of the destroyed eastern part of Sicily after the 1693 earthquake. Quarry samples were characterized through analysis, including mercury porosimetry and ultrasound measurements, the usual tests of water uptake and release, and salt resistance tests. The deterioration patterns were observed in selected monuments and in areas with a comparable environment, such as orientation, height, and rainfall. The Syracuse limestone (SL) showed typical selective weathering where algal nodules were preferentially eroded out—reflecting its nature as a bioclastic packstone—as well as some exfoliation. The Mellili limestone (ML) suffered mostly from differential erosion due to its more homogeneous texture of a bioclastic wackestone.

Both limestones contain over 99.5 % calcite. The main difference is in the acid insoluble residue, which is slightly higher for the ML (0.41 %) than for the SL (0.30 %). Analysis of these fractions showed further differences, the ML having more sand and slightly less clays than the SL. Expansive clays of the smectite group are found in both limestones, but the ML also has kaolinite and illite (hydromica group). Visually, the SL is more compact than the ML.

Their hydric behavior is quite different; ML has a higher capillary water absorption coefficient and absorbs more water than the SL. Furthermore, ML also dries faster than the SL, suggesting a high pore interconnectivity. Their porosity values from forced water absorption are similar (around 27 %), but, for free water absorption, the open porosity of the SL is only 21.6 %, suggesting the presence of bottle necks in the pore system. Similarly, their behavior after 15 cycles of the standard UNI-EN12370 (2001) sodium sulfate salt test was different. The weight loss was nearly 9 % for the SL—mostly by flaking—but only 1 % for the ML. After the tests, the open porosity increased more for the SL than for the ML, reflecting changes in their pore structure. Interestingly, the ultrasound wave

velocities of both stones followed a parallel behavior, decreasing in velocity with an increasing number of salt cycles, but, after 10 cycles, the ultrasound velocity decreased significantly for the SL, indicating higher deterioration, i.e. crack development. This was also confirmed by the pore-size distribution, which had significantly changed.

The laboratory tests could reproduce the observed damage of these stones in the monuments. The apparently more compact SL deteriorates faster than the ML. There is a complex interaction of the mineralogy and texture of the stone that affects the hydric behavior of these stones and, consequently, that of salt crystallization, which, in the present example, was the main deteriorating factor.

Similar deterioration patterns were found for other limestones, such as the French Sébastopol limestone (FSL) and the white tuffeau (WT) (Van et al. 2007). The former contains mainly calcite with some quartz, 80 and 20 %, respectively. The latter has a more complex composition (50 % calcite, 10 % quartz, 30 % opal, 10 % clay and mica). Both stones have a high open porosity, FSL 42 % and WT 48 %. The deterioration patterns observed in monuments constructed with these stones show that, while the FSL tends towards a granular deterioration, the clay containing WT shows delamination.

4.3 Deterioration by Chemical Processes

Chemical damage processes refer to the dissolution or alteration of the mineral constituents of a stone material via chemical reactions. This section provides a brief summary of such reactions and will also discuss the resulting damage patterns in building stones and the changes in the appearance of building façades. Mineral dissolution in building stones is closely related to atmospheric pollution and acid deposition. The origin and changes of this pollution are more thoroughly dealt with in Chap. 5. Here, the focus will be on the chemical reactions in the stone and on the behavior of the reaction products.

4.3.1 Mineral Dissolution Reactions

Many minerals present in rocks and building stones are thermodynamically unstable in the Earth's surface conditions. Therefore, these minerals are undersaturated if they are in contact with natural waters, e.g. rainwater. Mineral dissolution reactions in building stones involve the attack of water and its associated acidity. The H^+-ion attack on the mineral components causes their dissolution and the formation of deterioration products. Some examples of mineral dissolution reactions relevant to stone deterioration are:

$$CaCO_3 + 2H^+ \rightleftharpoons Ca^{2+} + CO_2 + H_2O \tag{4.11}$$

Table 4.4 Ions released from weathering of some common minerals in building materials (Steiger 2003)

Mineral name	Idealized formula	Ions released
Carbonate minerals:		
–Calcite	$CaCO_3$	Ca^{2+}
–Dolomite	$CaMg(CO_3)_2$	Ca^{2+}, Mg^{2+}
Feldspars:		
–Plagioclase feldspar	$Na_xCa_{1-x}\ Al_{2-x}Si_{2+x}O_8$	Na^+, Ca^{2+}
–Microcline (K-feldspar)	$KAlSi_3O_8$	K^+
Clay minerals:		
–Biotite	$K(Mg,Fe)_3AlSi_3O_{10}(OH)_2$	K^+, Mg^{2+}
–Chlorite	$Mg_5Al_2Si_3O_{10}(OH)_8$	Mg^{2+}

$$2KAlSi_3O_8 + 2H^+ + 9H_2O \rightleftharpoons 2K^+ + Al_2Si_2O_5(OH)_4 + 4Si(OH)_4 \quad (4.12)$$

$$Mg_5Al_2Si_3O_{10}(OH)_8 + 10H^+ \rightleftharpoons 5Mg^{2+} + Al_2Si_2O_5(OH)_4 + 4Si(OH)_4 + 5H_2O \quad (4.13)$$

$$Fe_2SiO_4 + \frac{1}{2}O_2 + 3H_2O \rightleftharpoons 2FeOOH + Si(OH)_4 \quad (4.14)$$

Acid attack generally causes the mobilization of metal cations and dissolved silica, $Si(OH)_4$, from the parent minerals. The weathering of silicates also leads to the formation of new mineral compounds, e.g. iron or aluminum oxyhydroxides and clays such as kaolinite, $Al_2Si_2O_5(OH)_4$. Compared to the parent materials, the mineral reaction products are depleted in metal cations relative to Al and Si. Additionally, the product minerals are usually more hydrated. If the parent mineral contains Fe(II), the dissolution reaction usually also involves an oxidation step, as in, for example, Eq. (4.14). Table 4.4 lists the cations released from the weathering of some common mineral constituents of building materials. It can be seen that mineral dissolution reactions lead mainly to the formation of sodium, potassium, magnesium, and calcium salts, i.e. the major cations in natural waters.

The rates of mineral dissolution reactions depend on: (1) the amount and contact time of liquid water available at mineral surfaces; (2) the solubility of the mineral in question; (3) the availability of acidity, i.e. the pH of the aqueous solution in contact with the mineral surface. The major source of liquid water in building stones is precipitation, and damage caused by mineral dissolution reactions often shows a distinct pattern following the exposure to direct rainfall, driving rain, and surface runoff waters, as discussed in more detail below. Most rock-forming minerals exhibit a very low but finite solubility in water. In historical buildings, the amount of rainwater infiltration and the contact times over centuries are sufficiently long enough that mineral dissolution reactions can cause significant damage. The carbonate minerals, i.e. calcite and dolomite, exhibit the highest solubilities, followed by feldspars, clay minerals, and quartz. As a rule of thumb, the solubility increases with decreasing silica content and with an increasing content of calcium and magnesium. According to reactions such as (4.12), (4.13),

and (4.14), the solubility of the rock-forming minerals also increases with decreasing pH, i.e. in acidic solutions. It should be noted that some minerals, such as silicates, also exhibit an increased solubility in alkaline solutions, i.e. at pH above 10. However, in the present context of building stone deterioration, the focus will be limited to the dissolution reactions in acidic solutions, since these are the most common ones.

Carbon dioxide, CO_2, is a major source of acidity in natural waters, and it is the acid responsible for most natural rock weathering on a geological time scale.

The solubility of carbonate materials in water is enhanced in the presence of CO_2 according to the reaction:

$$CaCO_3 + CO_2 + H_2O \rightleftharpoons Ca^{2+} + 2HCO_3^- \tag{4.15}$$

The pH value of unpolluted rainwater in equilibrium with atmospheric CO_2 is about 5.6, i.e. slightly acidic. The equilibrium solubility of calcite in rainwater in equilibrium with atmospheric CO_2 (5.5×10^{-4} mol L^{-1}) is about four times higher than in pure water. Thus, even in the absence of other sources of acidity, there is a natural dissolution reaction of carbonate minerals which is commonly referred to as the karst effect. The pH values of natural river, lake, and ground waters are also affected by rainwater infiltration, but the pH varies depending on the composition of surrounding rocks and sediments. Natural waters in contact with carbonate-rich rocks usually have pH values greater than 7, whilst the groundwater will tend to remain acidic if carbonate rocks are absent, i.e. in the presence of sandstones and other silicate rocks. Although the dissolution rates of silicate minerals are far slower than those of carbonate minerals, the former are also subject to natural chemical weathering (Stumm and Wollast 1990; Drever 1994a, b; Lasaga et al. 1994). The same reactions are responsible for the dissolution of quartz and silicate minerals in building stones; however, in this case, the presence of mortars, generally alkaline, will increase their dissolution.

Acid deposition is the major source of H^+ in building materials and significantly increases the natural rates of mineral dissolution reactions. Here, acid deposition refers to both wet deposition, i.e. acid precipitation, and the dry deposition of gaseous and particulate pollutants into water films on mineral surfaces. In acid rain, the pH values are significantly lower and can reach values of about 4 during the initial rainfall. In acid fog, even lower pH values of about 2–4 can occur, because, there being less water available, the solution is more concentrated. However, in recent years, a continuous increase in the pH of rainwater has been observed at least in North America and Europe.

Atmospheric acidity is closely related to the atmospheric chemistry of sulfur dioxide (SO_2) and the nitrogen oxides (NO, NO_2) which become oxidized to sulfate and nitrate through gas and aqueous phase processes. Most of the nitrates and sulfates of the major cations that are mobilized in mineral dissolution reactions, i.e. the reaction products of acid deposition, are substantially more soluble than the respective parent minerals. Therefore, mineral dissolution reactions cause a substantial loss of cohesion if acid attack and dissolution occur at grain contacts.

Apart from insoluble new minerals such as kaolinite or iron oxyhydroxides, soluble nitrates and sulfates are the major reaction products of acid deposition onto building stones. It is generally not possible to clearly distinguish damage due to the chemical reactions with the rock-forming minerals and subsequent salt stress, as discussed in Sect. 4.4.

A number of studies were carried out to determine the effect of acid deposition on building stones. A useful experimental technique is the collection and analysis of stone runoff solutions (Rönicke and Rönicke 1972; Reddy et al. 1985; Livingston 1986; Cooper 1986; Cooper et al. 1992). Any differences in the concentrations between runoff and incident rainfall must be due to interactions with the stone. For carbonate stones, the excess calcium concentration in runoff solutions provides a direct measure of calcite dissolution. Here, excess calcium concentration refers to a corrected concentration, taking into account contributions from the dry deposition of particles and the calcium concentrations in the incident rainfall itself (Reddy 1988). Data obtained from runoff water experiments were used to determine the relative contributions of the karst effect, the neutralization of acid rain, and the dry deposition of sulfur dioxide (Livingston 1992; Baedeker et al. 1992). It was found that, in urban areas with significant SO_2 pollution, the dry deposition of local sulfur dioxide was dominant (Roekens and van Grieken 1989; Livingston 1992; Steiger et al. 1993; Cardell-Fernández et al. 2002). The mobilization of metal cations as an indicator for the dissolution of silicate minerals, mainly clay minerals and feldspars, was also observed in the runoff from sandstone surfaces (Steiger and Dannecker 1994; Halsey et al. 1995).

Mineral dissolution reactions in sandstone can also be detected by careful analysis of weathered stone samples. Using petrographic analysis of depth profiles in sandstone samples from several buildings in Germany, Mausfeld and Grassegger (1992) obtained distinct profiles of fresh and leached feldspars and a significant increase in the total feldspar content with increasing distance from the exposed stone surface. In a similar study, these authors also found profiles of clay mineral composition in building stones with rather constant compositions in the unweathered interior and distinct profiles close to the surface (Mausfeld and Grassegger 1994). Schäfer and Steiger (2002) measured profiles of cation exchange capacities (CEC) in clay minerals containing sandstones. In all cases, they found distinct profiles with significantly lower CEC close to the exposed stone surfaces, indicating a significant loss of the mineral surface area available to ion exchange processes due to partial dissolution of clay minerals.

While most reaction products of mineral dissolution reactions are very soluble, calcium sulfate is an important exception. Calcium sulfate in the form of gypsum, $CaSO_4 \cdot 2H_2O$, is the major reaction product of the dissolution of carbonate stone, i.e. limestone and marble, and is a ubiquitous compound found in building materials. The properties of gypsum and its role in the deterioration of building stones have been recently reviewed by Charola et al. (2007). Gypsum crusts are preferentially formed on rain-sheltered surfaces of carbonate building materials. According to Camuffo et al. (1982), gypsum crusts occurring on surfaces not directly exposed to rainfall correspond to the black areas that can be clearly

distinguished from the rain-exposed white areas of limestone and marble buildings. In fact, gypsum crusts on buildings in urban environments nearly always appear black. Their black color is caused by the embedding of air pollutant particles originating from a number of different sources, including fly ash, soot, mineral dust, iron oxides or oxyhydroxides, and organic pollutants mostly from combustion reactions, such as combustion engines (e.g. Del Monte et al. 1981; Del Monte and Sabbioni 1984; Nord and Tronner 1991; Whalley et al. 1992; Saiz Jimenez 1993).

There is no doubt that the formation of gypsum crusts on calcareous stones is the result of the preferential dry deposition of sulfur dioxide onto the moist surface of a stone followed by the dissolution of calcite and subsequent precipitation of gypsum. Hence, the major damage mechanism is one of mineral dissolution. The replacement of calcite by gypsum and the growth mechanism of crusts have been studied in detail, both for limestone (Schiavon 1992) and marble (Vergès-Belmin 1994).

Other crusts related to mineral dissolution reactions in calcareous stones are the calcium oxalate films or patinas. Whewellite ($CaC_2O_4 \cdot H_2O$) and weddellite ($CaC_2O_4 \cdot 2H_2O$) are commonly found on Italian marble and limestone monuments and natural carbonatic outcrops (Del Monte et al. 1987; Watchman 1991). In this case, the product of the replacement reaction, i.e. calcium oxalate, is even less soluble than the parent mineral calcite such that a crust is also formed on exposed surfaces. There have been controversial discussions about the origin of these films, many of them orange colored, particularly with respect to the patina called "scialbatura" commonly found on Roman imperial marble monuments (Del Monte and Sabbioni 1987; Lazzarini and Salvadori 1989). Their origin has been attributed to various mechanisms, from geological weathering at outcrops to chemical weathering of intentional treatments or to biological weathering of them, or plain biological activity as summarized elsewhere (Del Monte et al. 1987; Charola et al. 2002). However, biological activity may probably be the major source of oxalate crusts as discussed in Sect. 4.5.

The formation of gypsum crusts on sandstone is less obvious. However, gypsum crusts are commonly found on calcite cemented sandstones (e.g. Zehnder 1982) and nearly calcium-free materials such as quartz sandstone and granite (Whalley et al. 1992; Neumann et al. 1993; Smith et al. 1994). In contrast to calcareous stone, the mechanism of crust formation on sandstone is different, because both sulfate and calcium must originate from external sources. Therefore, the formation of gypsum crusts on non-calcareous stones cannot be considered the result of chemical deterioration of the substrate. Nonetheless, the low solubility of gypsum favors its accumulation in the pore space of these materials. Very often, the pore space close to the surface is completely filled with gypsum deposits (Charola et al. 2007). A characteristic feature at a later stage of the damage process is the complete destruction of the original internal fabric, which is replaced by a secondary gypsum supported fabric (Neumann et al. 1993, 1997; Steiger 2003). Figure 4.14 shows an example of these gypsum crusts on quartzitic sandstone.

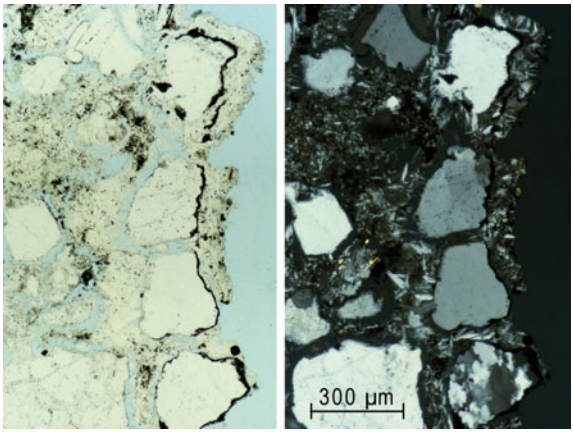

Fig. 4.14 Thin section of gypsum crust on a quartz bound sandstone at Leineschloss (Hanover) with//Nicols (*left*) and X Nicols (*right*). Note the loss of cohesion of the surface quartz grains due to secondary gypsum growth. The gypsum crystals growing on the original thin black surface layer resulted from the subsequent development of a leak above this area. Reproduced with permission from Neumann et al. (1993)

In contrast to marble and limestone, black discolorations often appear more evenly distributed on sandstone and granite surfaces. Their occurrence is not restricted to sheltered areas; rather, intensely black thin films are preferentially found on surfaces that are frequently wetted by rainfall or runoff. These discolorations often appear as homogeneous black layers firmly attached to and tracing the stone surface. Following Nord and Ericsson (1993), we prefer the term "thin black layer" for this kind of surface deposits that have to be clearly distinguished from gypsum crusts. A more detailed discussion of their composition and morphology is provided by Steiger (2003).

4.3.2 Surface Recession Rates on Calcareous Stone

In contrast to sheltered areas, surfaces on limestone and marble façades that are freely exposed to wind and rain usually appear as white areas. In these areas, rainwater runoff dominates. Hence, there is a significant contribution of the karst and the acid dissolution effects, and the reaction product gypsum is dissolved and removed by the runoff water. The surface recession in such exposed areas is a direct measure of the integral material loss due to acid deposition and dissolution of calcite and the karst weathering effect. Several attempts have been made to determine the resulting surface recession. The lowering of the surface can be measured with a high resolution micrometer, using reference points such as lead plugs (Sharp et al. 1982) or unweathered mineral constituents (Winkler 1987). Using lead plugs as references Sharp et al. (1982) found average recession rates of 0.078 mm a^{-1} for the period 1718–1980 measured on a Portland limestone balustrade at St. Paul's Cathedral. This value was later confirmed by re-measurements of Trudgill et al. (1989). However, both studies revealed substantial spatial variation, making comparisons of different data sets, e.g. for different exposures, difficult. Winkler (1987), using unweathered hornblende as a reference, determined average surface recession rates

of 0.026 mm a^{-1} on ribs of Georgia marble columns at the Chicago Field Museum of Natural History. Attewell and Taylor (1990) determined the recession on Carrara marble tombstone surfaces by measuring the lowering with reference to lead-filled letters of the inscriptions. They obtained average recession rates of (0.002–0.014) mm a^{-1} for exposure periods of about 10–100 years at different sites near Durham, UK. The lowest rates were observed at rural sites, and the highest recession rates were obtained in industrial areas.

Several authors determined the surface recession rates on tombstones by comparing upper and lower slab thicknesses. Using this method Baer and Berman (1983) found marble recession rates of 0.014 mm a^{-1} and 0.018 mm a^{-1}, respectively, for urban sites in Philadelphia and New York and 0.008 mm a^{-1} for a suburban site in Long Island. With the same method Feddema and Meierding (1987) obtained average annual recession rates of 0.035 mm a^{-1} for marble tombstones in highly polluted downtown Philadelphia for a period of some 150–200 years exposure. In contrast, they obtained annual rates of <0.005 mm a^{-1} at rural sites and (0.014–0.018) mm a^{-1} for moderately polluted sites over approximately the same period of time.

Recession rates can also be calculated from weight loss data determined in exposure experiments. Weber (1985) obtained recession rates up to 0.062 mm a^{-1} for porous Austrian limestones exposed for one year in Vienna. Jaynes and Cooke (1987) carried out an extensive two-year exposure study at 25 sites in Southeast England. They obtained recession rates for Portland limestone ranging from 0.010 mm a^{-1} at rural sites to 0.016 mm a^{-1} at central London sites. They also calculated recession rates from the weight loss data of a 10 year (1955–1965) exposure study with Portland limestone carried out by Honeyborne and Price (1977). Their weight data yielded recession rates of 0.029 mm a^{-1} in central London and 0.010 mm a^{-1} in Garston. Though careful interpretation is required, it appears that the reduced recession rates in central London reflect the decrease in air pollution levels. Baedeker et al. (1992) used weight loss data for samples of Indiana limestone and Vermont marble that were exposed in the United States National Acid Precipitation Assessment Program (NAPAP) to determine recession rates. The recession rates range from 0.015 to 0.024 mm a^{-1} for marble and from 0.020 to 0.058 mm a^{-1} for limestone. Similar values were obtained using an interferometric technique to determine the erosion rate. The trend observed by Jaynes and Cooke (1987) is confirmed by more recent data from the UN ECE Program on Effects on Materials (Kucera et al. 2007). In this program, Portland limestone was exposed over a 4-year period at 49 sites, most of them spread all over Europe with additional sites in Russia, Israel, the US, and Canada. The recession rates determined from weight loss data hardly exceeded values of 0.010 mm a^{-1} even at the most polluted urban and industrial sites; for rural sites, recession rates were typically <0.004 mm a^{-1}.

Another approach to determining surface recession rates is the collection and analysis of runoff water, as mentioned before (Reddy et al. 1985; Cooper 1986). Extensive runoff water measurements were also carried out at the NAPAP exposure sites (Reddy 1988). Surface recessions were calculated from the excess

calcium concentrations in the runoff water, yielding rates in the range from 0.007 to 0.008 mm a^{-1} for marble and from 0.007 to 0.010 mm a^{-1} for limestone (Baedeker et al. 1992). These values are less than half of the rates that were determined from weight loss and interferometric data. The reason for the deviation is simply that runoff experiments only measure stone dissolution rates. The calculation of recession rates is based on the assumption that a calcite grain is only lost if it is completely dissolved. However, a much smaller degree of calcite dissolution may be sufficient to weaken the grain contacts, resulting in a loss of cohesion. In this case, the material loss occurs mainly as sanding. In runoff experiments with Portland limestone in Dublin, Cooper et al. (1992) calculated total surface recession rates from both excess calcium concentrations, i.e. reflecting the influence of dissolution, and total particulate matter suspended in the runoff water, i.e. reflecting the recession via particulate loss. The total recession rates they obtained range from 0.013 to 0.039 mm a^{-1}.

The range of recession rates in the studies mentioned so far shows significant scatter, reflecting the variety of materials, pollutant concentrations, exposure conditions, and times of these studies and, of course, the different experimental approaches used. In several of the studies, substantial scatter also occurred on a point to point basis, again reflecting the complexity of the erosion process due to mineral dissolution involving large variation in local microclimatic conditions, orientation of surfaces, and material inhomogeneities. Considering all these points, the results of the studies appear to be in reasonable accordance and allow an assessment of average recession rates for calcareous materials. One of the major influences appears to be the orientation of the exposed surface, as the incident rainfall intensity is much higher on horizontal than on vertical surfaces.

4.4 Action of Salts

There is no question that salts are probably the single most damaging factor for stone deterioration. Several reviews have been written summarizing this topic (Charola 2000; Doehne 2002), and several conferences on this single topic have taken place over the past 10 years (Leitner et al. 2003; Simon and Drdácky 2006; Ottosen et al. 2008, to name a few).

The deteriorating effect of salts is mostly reflected in the patterns that have been grouped under the detachment category of the ICOMOS-ISCS Glossary (Vergès-Belmin 2008). Within this category, blistering, delamination, scaling, and disintegration are considered, as the glossary focuses on the form of the deterioration, not its origin (Chap. 6, Table 6.1). From practical experience gained over the years, it has been concluded that deterioration induced by salts forms a continuum between the granular disintegration and scaling, delamination, and blistering patterns, as shown in Fig. 4.15 (Snethlage and Wendler 1997). Whether one pattern or the other develops will depend on the type of material, e.g. sandstone or marble, and, more importantly, the conditions under which the salt crystallizes.

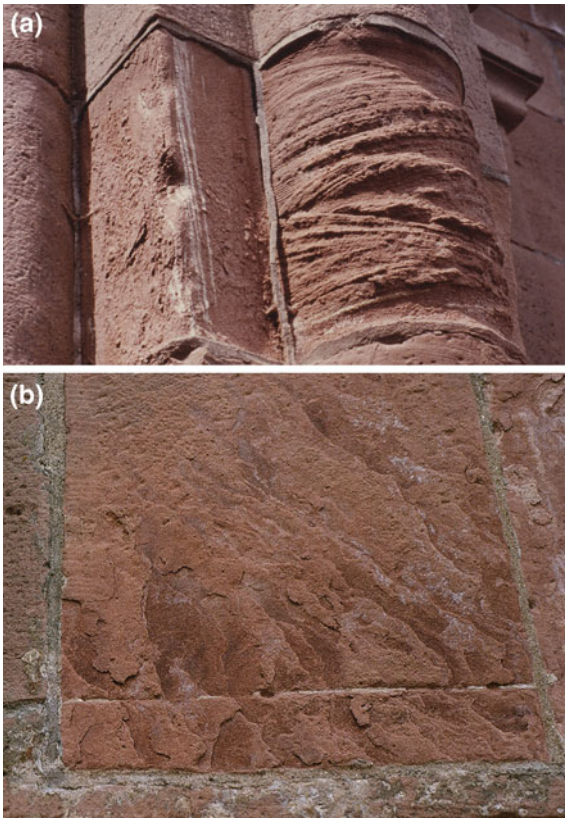

Fig. 4.15 Salt-induced deterioration (by magnesium sulfate) of Bunter sandstone at Kaiserpfalz (Gelnhausen, Germany): **a** Incipient flaking (*left block*) and sanding following the bedding plane (*right block*); **b** Scaling parallel to bedding

The amount of water available during crystallization, which depends on the porosity of the stone and the environmental conditions, will affect the habit in which the salts crystallize. This topic has been studied extensively by Arnold and Zehnder over many years (Arnold and Küng 1985; Arnold and Zehnder 1985; Zehnder and Arnold 1989; Arnold and Zehnder 1991).

It should be remembered that, when dealing with clay-bearing stones such as some sandstones or marly limestones, the moisture retention of the clays tend to accumulate salts in these layers so that the scaling pattern of a thin surface flake may result in the formation of thicker layers spalling off, i.e., the properly called delamination.

Another pattern is alveolization, or honeycomb formation, which has been found on many different rock types, such as limestones, sandstones, and volcanic stones, among others (see Fig. 4.16). This cavernous-like pattern is most commonly found in coastal areas, but also in other regions, and ranges from smaller cavities to larger ones, referred to as "tafoni" and eventually leading to overhangs. The reason for this characteristic weathering can be attributed to the presence of salts on the stone and wind in the environmental conditions. What role the nature

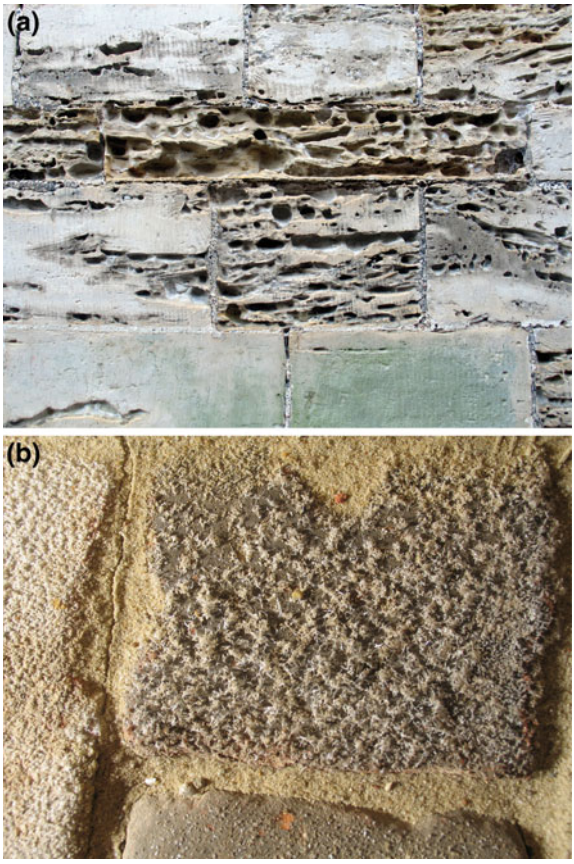

Fig. 4.16 Salt-induced deterioration: **a** Alveolization (Kromborg Castle, Copenhagen, Denmark); **b** Salt efflorescences on sandstone flagstones (Marienkirche Salzwedel, Germany); Photos: Hans-Jürgen Schwarz, Ri-Con, Hanover, Germany

and heterogeneity of the stone play is still under study. Pauly (1976) carried out one of the pioneering studies by reproducing this weathering pattern in the laboratory. Many studies have been carried out since then, as summarized by Goudie and Viles (1997).

The formation of efflorescences is yet another important deterioration pattern, though, if their growth occurs only on the surface, it does not cause major damage. The problem is that, since stone is porous, where efflorescences are found, subflorescences will also be present, and these cause damage.

While many studies have been devoted to elucidating why and how salt crystallization causes damage to stone, fewer, or less successful, studies have been carried out in the field, because the number of variables present makes it difficult to determine the leading factors in the observed deterioration. However, an enlightening study was carried out in the Romanesque crypt of the Cathedral of Basel, Switzerland for several months (Zehnder and Schoch 2009). The study was based on an in situ automated monitoring system of the indoor conditions coupled with image-capturing devices. Thus, correlations could be obtained for the

crystallization and deliquescence periods of the salts present in the masonry with changes in temperature and RH in the air as well as on the surface, as will be discussed in detail in the following sections. The actual development of mirabilite, epsomite, and gypsum efflorescence was documented in a degree of detail not previously achieved.

The study confirmed that small changes in RH within the moderate relative humidity range in the crypt triggered the crystallization and dissolution cycles. Consequently, although reducing changes in RH will diminish the intensity of the damage, it does not eliminate it, because keeping RH constant in a large environment where people carry out activities is practically impossible.

4.4.1 Sources of Salts in Building Materials

Deposition of acidity from the atmosphere is an important source of salt enrichment in building materials. The major anions associated with atmospheric acid-forming species are sulfate and nitrate. Therefore, the processes described in Sect. 4.4 lead to the enrichment of sulfates and nitrates of calcium for the case of mortars and calcitic stones, as well as those of sodium, potassium, and magnesium in the case of other stone materials. In addition to these salts formed through chemical reaction, there is also a direct input of salts from the atmosphere. For example, in a marine environment, sea salt has an important presence in the local atmosphere. On a global scale, emissions of sea salt droplets ejected from the oceans are considered one of the most important primary sources of the atmospheric aerosol (Blanchard and Woodcock 1980). Sea salt particles will undergo both wet and dry deposition, the major processes leading to their enrichment in building materials.

In contrast to anthropogenic air pollutants whose concentrations have changed dramatically during the last centuries (Brimblecombe and Rohde 1988), the enrichment of sea salt in historical buildings has been progressing continuously for far longer periods of time. Salt accumulations found today represent an integral effect of sea salt deposition, beginning as of the building's construction time. Experience from many monuments located at coastal sites suggests that the deposition and enrichment of sea salt can be a major cause of decay (e.g. Theoulakis and Moropoulou 1988; Zezza and Macrì 1995). An example is shown in Fig. 4.17.

Sea salt particles in the atmosphere have a chemical composition very similar to that of bulk seawater. The contribution of the six ions sodium, magnesium, potassium, calcium, chloride, and sulfate amounts to >99 % by mass of the total solids dissolved. The major ions, sodium and chloride, account for 85.6 % of the bulk sea salt. Oceans have a remarkably uniform composition, and it can be assumed that the relative abundances of the major ions have not significantly changed over time. Therefore, the relative abundances of the major constituents can be used as tracers for sea salt deposition (Zappia et al. 1989). It has been

Fig. 4.17 Sea-salt-induced deterioration at Santa Marija Ta' Cwerra church (Malta); Photo: B. Fitzner, Geological Institute, RWTH Aachen University

shown that the enrichment of sea salt in buildings in coastal environments is considerably variable depending on a number of different influences, including environmental parameters and the geometry and constructional details of a building (Steiger et al. 1997).

Deicing salts, as they lower the freezing temperature of water, have been used for decades to improve traffic safety on roads and sidewalks and millions of tons of salt have already been applied. The most commonly used deicing salt is NaCl, which is inexpensive and readily available. Sometimes $CaCl_2$, $MgCl_2$, and carnallite ($KMgCl_3 \cdot 6H_2O$) are also used. These salts depress the freezing point to lower temperatures and have an additional thermal effect caused by the exothermic dissolution reaction. Transport of deicing salt into the surroundings causes an impact on roadside vegetation, soil, groundwater, and masonry. In fact, the use of deicing salt is a major source of chloride accumulation in masonry near ground level. Figure 4.18 shows efflorescences of deicing salt on a stairway in downtown Basel with an obvious impact on the adjacent masonry (Siedel 2009). Due to the harmful environmental effects of NaCl, alternative deicers such as CMA (calcium magnesium acetate), potassium acetate, and mixtures of potassium and sodium formate are now frequently used. Hence, in the future, there might also be a significant input of these organic anions into building stone.

Another very important source of salts in buildings is ground moisture carried into masonry by rising damp in the absence of damp-proof coursing. Considering a structure in hydraulic contact with the saturated ground, water is absorbed and slowly moves upwards in the wall (Fig. 4.19). Above ground level, the wall is

Fig. 4.18 Efflorescences of deicing salt on a stairway in downtown Basel. Reproduced with permission from Siedel (2009)

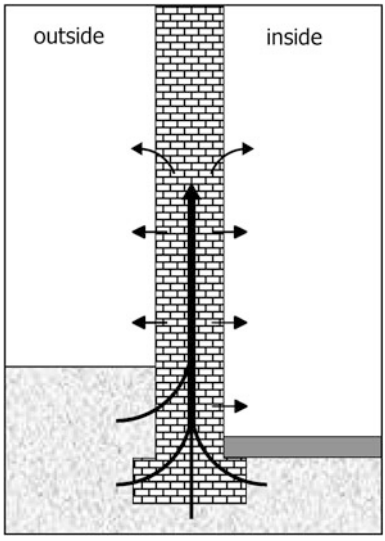

Fig. 4.19 Moisture transport in masonry affected by rising damp

subject to evaporation, and rising damp is a result of the competition between the rate of capillary absorption and the evaporation rate (Hall and Hoff 2002, 2007).

The composition of groundwater is largely determined by the time of contact and the nature of the geological materials it is moving through. The major constituents of natural ground and surface waters that can penetrate building materials are sodium, potassium, magnesium, calcium, chloride, sulfate, and bicarbonate. Additional constituents may be leached from surface soils. For example, nitrate is an important contaminant in surface soils, originating from the use of fertilizers, animal waste, and the oxidation of organic nitrogen. Therefore, ground moisture penetrating the base of a building that is used as a stable can carry substantial

amounts of nitrates into the masonry. Similarly, a significant input of nitrate into the walls of churches may arise from the use of the surrounding soils as cemeteries.

Initially, ground moisture is a dilute solution of groundwater vertically transported due to capillary rise. However, above ground level, moisture evaporates from the wall, and the solution becomes more and more concentrated while still being subject to capillary rise. As the solution becomes saturated during transport, any further evaporation will cause crystallization and immobilization of the salt. In effect, a zone of salt enrichment evolves some distance above ground level. The height of the accumulation zone is dependent on the rate of evaporation and the solubility of the salt. The maximum height is given as the upper limit of the capillary rise of moisture, i.e. the height at which the evaporation rate equals the supply of moisture from below. It has to be noted, however, that evaporation rates are significantly lower in the presence salts. This is the result of a strong depression of the vapor pressure above concentrated salt solutions (see Sect. 4.4.3). Therefore, with increasing salt enrichment, the maximum height of capillary rise increases.

In particular, old buildings are very often insufficiently insulated against rising ground moisture. Arnold and Zehnder (1989, 1991) provide a detailed discussion of salt transport and accumulation in walls affected by rising damp based on extensive observations of a number of old buildings that were subjected to ground moisture over long periods of time. During capillary rise and evaporation, the less soluble salts will reach saturation earlier than salts of greater solubility, resulting in a fractionation of the salts according to their solubilities. The composition of the pore solution continuously changes during transport, and only the very soluble salts are transported as concentrated brine solutions to the upper evaporation zone. Arnold and Zehnder (1989, 1991) provide vertical profiles of ion concentrations in the zone affected by rising damp from a number of buildings. Maxima of salt enrichment were observed at heights from 0.5 m to about 3 m above ground level, and the profiles provide evidence of salt fractionation.

The use of alkaline materials, e.g. Portland cement, cleaning products, and consolidation materials, such as water glass, can be an important source of salts in buildings (Arnold and Zehnder 1991). Generally, these materials release sodium and potassium hydroxide and carbonate, which can react with salt mixtures already present in a masonry, forming new, often more damaging salt mixtures.

Sometimes, the present day salt contamination of a building may be directly related to a particular use of the building in a former time. Use as a stable leading to nitrate contamination arising from animal waste has already been mentioned. Other examples include the use of a building or part of it for storage, e.g. for rock salt or gun powder (black powder) etc., thus, leading to direct salt input into masonry. Another example is Angkor Wat in Cambodia (see Fig. 4.20), which was overgrown by the jungle over a period of about 400 years. The bats inhabiting it roosted in the interior of the temple towers, producing tons of guano. Bat guano is strongly enriched with a number of salts, but mainly contains phosphates and nitrates that were transported into the walls of the temple via uncontrolled water flow through leakages (Hosono et al. 2006; Siedel et al. 2008).

Fig. 4.20 Salts partially originating from bat guano at Angkor Wat (Cambodia)

4.4.2 Common Salts in Building Stones

Depending on the nature of the sources, the salt mixtures that are found in building materials are formed by several different ions. Typically, chlorides, nitrates, sulfates, carbonates, and bicarbonates of sodium, potassium, magnesium, and calcium are the most common. These salts are commonly referred to as "soluble salts". However, their solubilities differ by orders of magnitude and, consequently, the components of such complex salt mixtures may be either present in dissolved form, i.e. in pore solutions, or as crystallized salts within the pore system. Salts dissolved in a pore solution are subject to capillary transport, for instance, with rising ground moisture or rainwater penetrating the stone. In contrast, crystallized salts are less mobile and may accumulate. Crystalline solids formed during drying may either form efflorescences on the stone surface or they can crystallize as subflorescences within the pore space of the stone. Crystal growth on the stone surface is usually not harmful as long as the growing crystals are not confined. However, during the formation of crystalline deposits in pores, so-called subflorescences, growing crystals may become confined and can then generate substantial stress, as discussed before.

Upon evaporation of water, a pore solution becomes more concentrated and finally reaches saturation with one or more solid phases. From a pore solution containing the above-mentioned ions, a large number of different crystalline salts can be precipitated. In addition to all possible and electrically neutral binary cation–anion combinations, there is also a large number of double salts containing

more than two different ions that can be precipitated from a mixed solution. In addition, several salts can exist in anhydrous and different hydrated forms, e.g. sodium sulfate can exist as the anhydrous $NaSO_4$ (thenardite) and as the decahydrate $Na_2SO_4 \cdot 10H_2O$ (mirabilite). Only considering solutions of the most common ions in building materials, i.e. Na^+, K^+, Mg^{2+}, Ca^{2+}, Cl^-, NO_3^-, SO_4^{2-}, CO_3^{2-}, and HCO_3^-, about 70 different evaporite minerals can be precipitated in the temperature range of −40 to +40 °C (see Table 4.5). About half of these minerals have, in fact, been detected in building stones (see compilations by Arnold and Zehnder 1991, Nord and Tronner 1991, Allmann and Kraus 2003).

As discussed in more detail in Sect. 4.4.3, it is difficult to predict the precipitation sequences in mixed salt solutions. However, due to solubility limitations, there are certain restrictions for the composition of brine solutions evolving during transport and evaporation. As Hardie and Eugster (1970) have pointed out, the solubilities of the calcium and magnesium carbonates and of gypsum ($CaSO_4 \cdot 2H_2O$) are so low compared to all other salt minerals of interest that they provide a chemical divide. The major pathways of fractionation and brine evolution from solutions initially containing Na^+, K^+, Mg^{2+}, Ca^{2+}, Cl^-, NO_3^-, SO_4^{2-}, CO_3^{2-}, and HCO_3^- are summarized in Fig. 4.21. The solubilities of the alkaline earth carbonates is about 2 orders of magnitude lower than that of gypsum and about 4–5 orders of magnitude lower than that of the remaining salts. The evaporation of water from such solutions always leads to the crystallization of the alkaline earth carbonates, i.e. calcite, dolomite, or nesquehonite ($MgCO_3 \cdot 3H_2O$). Thus, concentrated pore solutions cannot contain calcium or magnesium and carbonate ions at the same time (Steiger 2003).

A carbonate-rich salt mixture is typically observed in building stones as the result of the application of alkaline materials such as Portland cement or water glass. These materials release alkalinity, initially in the form of calcium hydroxide that is neutralized by atmospheric acidic gases—mainly carbon dioxide and sulfur dioxide. If there is sufficient excess alkalinity compared to the dissolved alkaline earth elements, the resulting salt system is characterized as a mixture of mainly alkali carbonates, bicarbonates, and sulfates together with chlorides and nitrates originating from other sources (Fig. 4.21). Such a carbonate-rich salt mixture is called a type III mixture (Steiger 2003) and the efflorescences and subflorescences that result from it may contain typical crystalline phases such as trona, $Na_3H(CO_3)_2 \cdot 2H_2O$, thermonatrite, $Na_2CO_3 \cdot H_2O$, thenardite, Na_2SO_4, darapskite, $Na_3(SO_4)(NO_3) \cdot H_2O$, and burkeite, $Na_6CO_3(SO_4)_2$ (e.g. Charola and Lewin 1979; Arnold 1985; Arnold and Zehnder 1991; von Konow 2002; Bionda 2006).

If the sum of the calcium and magnesium concentrations exceeds the total carbonate concentration, a carbonate-poor solution will evolve due to the precipitation of the alkaline earth carbonates. Then, due to its low solubility compared to all other salts, gypsum is precipitated next and acts as a second divide. If the initial calcium concentration exceeds that of sulfate, a sulfate-poor, type I solution evolves. Here, the term "sulfate-poor" only refers to the composition of the pore solution. There might also be a high sulfate concentration in the stone; however, as long as there is more calcium, all sulfate is essentially immobilized as gypsum.

Table 4.5 Solid phases in the Na^+–K^+–Mg^{2+}–Ca^{2+}–Cl^-–NO_3^-–SO_4^{2-}–CO_3^{2-}–HCO_3^-–H_2O system from –45 °C to about 50 °C

Formula (name)	Formula (name)
Chlorides	$CaCl_2 \cdot 6H_2O$ (antarcticite)
NaCl (halite)	$MgCl_2 \cdot 6H_2O$ (bischofite)
$NaCl \cdot 2H_2O$ (hydrohalite)	$MgCl_2 \cdot 8H_2O$ (magnesium chloride octahydrate)
KCl (sylvite)	$MgCl_2 \cdot 12H_2O$ (magnesium chloride dodecahydrate)
$CaCl_2 \cdot 2H_2O$ (sinjarite)	
$CaCl_2 \cdot 4H_2O$ (calcium chloride tetrahydrate)	
Nitrates	
$NaNO_3$ (nitratine)	$Ca(NO_3)_2 \cdot 4H_2O$ (nitrocalcite)
KNO_3 (niter)	$Mg(NO_3)_2 \cdot 2H_2O$ (magnesium nitrate dihydrate)
$Ca(NO_3)_2$ (calcium nitrate)	$Mg(NO_3)_2 \cdot 6H_2O$ (nitromagnesite)
$Ca(NO_3)_2 \cdot 2H_2O$ (calcium nitrate dihydrate)	$Mg(NO_3)_2 \cdot 9H_2O$ (magnesium nitrate nonahydrate)
$Ca(NO_3)_2 \cdot 3H_2O$ (calcium nitrate trihydrate)	
Sulfates	
Na_2SO_4(V) (thenardite)	$MgSO_4 \cdot 1.25H_2O$ (magnesium sulfate 1.25 hydrate)
Na_2SO_4(III) (sodium sulfate, phase III)	$MgSO_4 \cdot 2H_2O$ (sanderite)
$Na_2SO_4 \cdot 7H_2O$ (sodium sulfate heptahydrate)	$MgSO_4 \cdot 2.5H_2O$ (magnesium sulfate 2.5 hydrate)
$Na_2SO_4 \cdot 10H_2O$ (mirabilite)	$MgSO_4 \cdot 4H_2O$ (starkeyite)
K_2SO_4 (arcanite)	$MgSO_4 \cdot 5H_2O$ (pentahydrite)
$CaSO_4$ (anhydrite)	$MgSO_4 \cdot 6H_2O$ (hexahydrite)
$CaSO_4 \cdot 1/2H_2O$ (bassanite)	$MgSO_4 \cdot 7H_2O$ (epsomite)
$CaSO_4 \cdot 2H_2O$ (gypsum)	$MgSO_4 \cdot 11H_2O$ (meridianiite)
$MgSO_4 \cdot H_2O$ (kieserite)	
Carbonates	
$NaHCO_3$ (nahcolite)	$KHCO_3$ (kalicinite)
$Na_2CO_3 \cdot H_2O$ (thermonatrite)	$K_2CO_3 \cdot 3/2H_2O$ (potassium carbonate hydrate)
$Na_2CO_3 \cdot 7H_2O$ (sodium carbonate heptahydrate)	$MgCO_3 \cdot 3H_2O$ (nesquehonite)
$Na_2CO_3 \cdot 10H_2O$ (natron)	$MgCO_3 \cdot 5H_2O$ (lansfordite)
Double salts	
$Na_3NO_3SO_4 \cdot H_2O$ (darapskite)	$Na_6Mg(SO_4)_4$ (vanthoffite)
$K_3Na(SO_4)_2$ (glaserite, aphthitalite)	$Na_7K_3Mg_2(SO_4)_6(NO_3)_2 \cdot 6H_2O$ (humberstonite)
$Na_2Mg(SO_4)_2 \cdot 4H_2O$ (astrakanite, bloedite)	$KCaCl_3$ (chlorocalcite)
$Na_2Mg(SO_4)_2 \cdot 5H_2O$ (konyaite)	$KCa(NO_3)_3 \cdot 3H_2O$ (potassium calcium nitrate trihydrate)
$Na_2Ca(SO_4)_2$ (glauberite)	$K_2Ca(SO_4)_2 \cdot H_2O$ (syngenite)
$Na_4Ca(SO_4)_3 \cdot 2H_2O$ (eugsterite)	$K_2Ca_5(SO_4)_6 \cdot H_2O$ (gorgeyite)
$KMgCl_3 \cdot 6H_2O$ (carnallite)	$CaMg_2Cl_6 \cdot 12H_2O$ (tachyhydrite)
$KMgSO_4Cl \cdot 3H_2O$ (kainite)	$Na_3H(CO_3)_2 \cdot 2H_2O$ (trona)
$K_2Mg(SO4)_2 \cdot 4H_2O$ (leonite)	$Na_6(SO_4)_2CO_3$ (burkeite)
$K_2Mg(SO_4)_2 \cdot 6H_2O$ (schoenite, picromerite)	$Mg_5(CO_3)_4(OH)_2 \cdot 4H_2O$ (hydromagnesite)

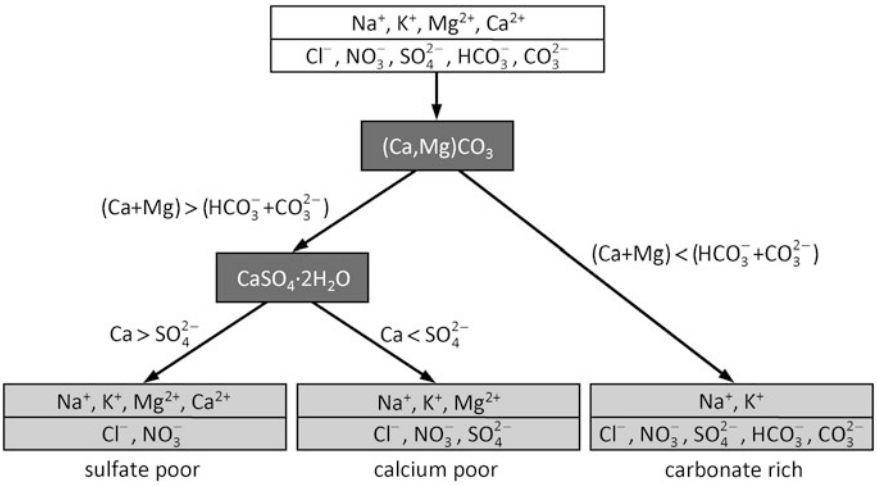

Fig. 4.21 Evolution of concentrated solutions of major types of hygroscopic salt mixtures. Adapted from Steiger (2003)

Because of its low solubility, calcium sulfate is far less mobile in building stone than any of the remaining salts (Charola et al. 2007).

The mobility of a salt may be conveniently defined as the total amount of salt present in the pore space that could be dissolved in the amount of water filling the pore completely. For example, in a natural stone with a water-accessible porosity of 10 %, the mobility of gypsum is only about 0.1 g kg^{-1}, while, in the same material, the mobility of NaCl is 14 g kg^{-1} (Steiger 2003). Typically, the concentration of calcium sulfate in historical masonry exceeds its mobility by several orders of magnitude. Hence, only a very small fraction of calcium sulfate present in the pores can be dissolved, even if the pore space is saturated with water. In other words, gypsum, once deposited in the pore space of a building material, tends to continue accumulating over time. Nonetheless, it will also undergo dissolution and crystallization phenomena.

Typically, the solubilities in sulfate-poor (type I) mixtures are very high, particularly if there are significant relative abundances of calcium or magnesium. Type I solutions are very often found in masonry affected by rising damp. Numerous examples can be found in the literature (e.g. Arnold and Zehnder 1991; Zezza et al. 1995; Klenz Larsen 1999, 2004; Schlütter et al. 2003; Sawdy and Price 2005; Weber and Burszán 2008; Brajer and Klenz Larsen 2008; Cooper 2008). The typical fractionation of such mixtures during capillary rise and evaporation of ground moisture has been discussed in detail by Arnold and Zehnder (1991). The least soluble components of type I pore solutions are halite, NaCl, niter, KNO_3, and nitratine, $NaNO_3$, which are, therefore, often found in efflorescences of the salt accumulation and damage zones in walls affected by rising damp. In contrast, the very soluble alkaline earth chlorides and nitrates are hardly ever expected to crystallize under normal climatic conditions in buildings. Due to their solubility,

the latter salts often show the strongest enrichment and form a distinct zone above the damage zone in masonry that often appears moist due to their extreme hygroscopicity, as discussed in the following section.

If a pore solution contains more sulfate than calcium, a type II solution evolves upon evaporation. Such a sulfate-rich (or calcium-poor) type of solution composition typically evolves as a result of air pollution attacks to (calcitic) sandstones. In this case, the major reaction products next to gypsum are other sulfates and nitrates listed in Table 4.5. Apart from gypsum, the typical crystalline solids are alkali nitrates, thenardite, magnesium sulfate hydrates, darapskite, and other sulfate-containing double salts such as glaserite (aphthitalite), $K_3Na(SO_4)_2$, schoenite, $K_2Mg(SO_4)_2{\cdot}6H_2O$, astrakanite, $Na_2Mg(SO_4)_2{\cdot}4H_2O$, and syngenite, $K_2Ca(SO_4)_2{\cdot}H_2O$. Additionally, the evaporation of seawater leads to calcium-poor type salts with halite and carnallite, $KMgCl_3{\cdot}6H_2O$, as the major crystalline phases (Braitsch 1971).

In general, it should be noted that salts are not necessarily found where they are formed. For example, salts formed as reaction products of acid deposition are not always found at the stone surface, except for the case of gypsum, which, because of its relatively low solubility, tends to accumulate in the "black crusts" that develop on rain-protected areas. The remaining salts are far more soluble. Their mobilities are one or two orders of magnitude higher than that of gypsum. In effect, unless these salts are present in extremely high concentrations exceeding their mobility, they are usually completely dissolved if the pore space of the stone is filled with water, for example, via the infiltration of rainwater. Therefore, these salts are subject to capillary transport during both the infiltration and the subsequent drying. A similar fractionation mechanism by combined transport and sequential crystallization, which was discussed before for capillary rise and evaporation, is also valid for horizontal transport. This may result from water infiltration as a consequence of roof leaks and broken gutters and downpipes, leading to distinct salt concentration depth profiles in the masonry. For example, Fig. 4.22 depicts a salt profile measured in a sandstone monument. The building is located in a rural environment in Southern Germany where the local air pollution level is low and it is expected that there is a significant contribution of acid rain to the total deposition of acidity.

Magnesium, sulfate, and nitrate are the major constituents of the salt system, whilst the calcium concentration is only of minor importance. The maximum salt concentration (1.1 % w/w total salts) is found at depths of about 6–9 mm. Considering the porosity of the stone and the solubilities in the salt mixture, it can be concluded that, apart from gypsum, all other salts will be completely dissolved if rainwater penetrates the stone. As water evaporates from the stone, salts will crystallize out, resulting in fractionation, as discussed before. For the given salt mixture, it can be simply deduced from available solubility data (see discussion below) that, apart from gypsum, epsomite ($MgSO_4{\cdot}7H_2O$) will be precipitated first. This is in accordance with the profile in Fig. 4.22 showing a strong enrichment of magnesium and sulfate at a distance of 6–9 mm from the surface, whilst the remaining ions are more evenly distributed and are, therefore, probably present in dissolved form. Clearly, the profile shown only reflects an intermediate state.

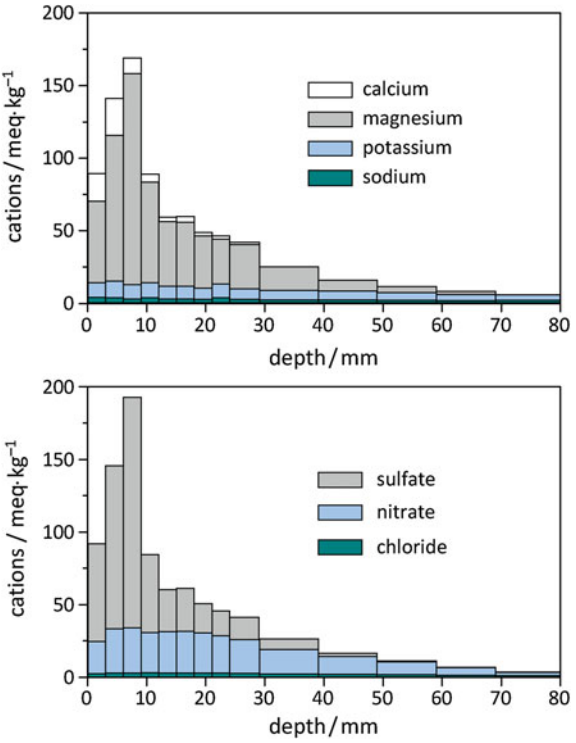

Fig. 4.22 Salt profile in sandstone from Schloss Weissenstein, Pommersfelden. Adapted from Steiger (2003)

The distribution of the various ions within masonry is only a snapshot in time, as it is the result of a dynamic process affected by continuous transport and phase transformations of the salts. Even if no liquid water reaches the masonry, moisture condensation from changes in temperature and relative humidity as well as the hygroscopicity of materials, including the crystallized salt and its solution, make this system a dynamic one.

4.4.3 Interaction of Salts with the Environment

Salt damage in building stones is the result of confined crystal growth within the pore space. There are various phase changes involving crystal growth, including the crystallization from supersaturated solutions, the change of the state of hydration, and chemical reactions resulting in the growth of new minerals at the expense of previously deposited phases. The dynamics of this process are controlled by the interaction of the salts present in the pore space with the surrounding climatic conditions. Unfavorable climatic conditions result in repeated cycles of crystallization-dissolution or hydration–dehydration. Under such conditions, stone and other building materials are subject to rapid decay.

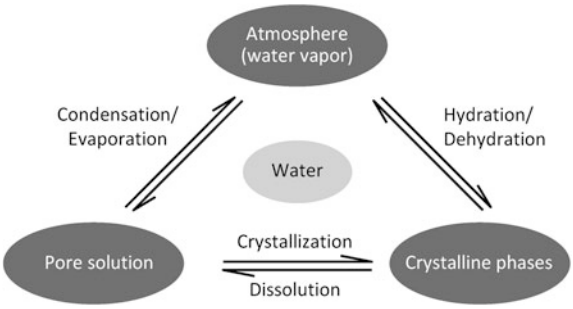

Fig. 4.23 Phase transitions of salts in building materials. Adapted from Steiger (2005c)

One obvious climatic influence that can cause cyclic crystallization events is exposure to rainfall. Salts accumulated in the pores are dissolved in rainwater penetrating the stone, and, during the subsequent drying process, the salts crystallize out again and can generate stress. Depending on the amount of salt in the stone, the frequency of rainfall, the exposure of the stone surface to driving rain, and the drying characteristics (largely determined by the properties of the stone and the local microclimatic conditions), such cyclic crystallization processes can cause severe damage to salt-contaminated building stone. However, rainwater is not the only source of liquid water in building materials. In sheltered areas or inside a building, the dynamics of salt damage in porous materials is largely determined by the interaction of the salts present in the pore space and the surrounding atmosphere, i.e. temperature and relative humidity (Arnold and Zehnder 1991). The basic thermodynamics of the underlying phase equilibria have been reviewed by Steiger (2005c). This section provides a brief overview of the crystallization behavior of single salts and salt mixtures.

4.4.3.1 Single Salts

The different interactions between water vapor and crystalline phases are depicted in Fig. 4.23. If a salt is subjected to a slowly increasing relative humidity, the deliquescence or saturation relative humidity (DRH) point will be reached, wherein the solid begins to absorb water vapor, forming a saturated solution. At the deliquescence relative humidity, DRH, three phases can be found in equilibrium: the saturated solution, the solid salt mineral, and water vapor in the ambient air. As the relative humidity is further increased, the solid phase dissolves completely and the solution becomes more dilute. If the dilute salt solution is then subjected to a decreasing relative humidity, water starts to evaporate from the solution until saturation is reached at the saturation or deliquescence humidity DRH. Below this humidity, a solution is not stable, and only a solid phase can coexist with the vapor phase. Therefore, any further decrease in RH will cause the crystallization of the salt and complete evaporation to dryness. It is obvious that fluctuations in the ambient RH across the deliquescence humidity of a salt in a porous stone will cause crystallization-dissolution cycles and rapid decay. The deliquescence humidities of

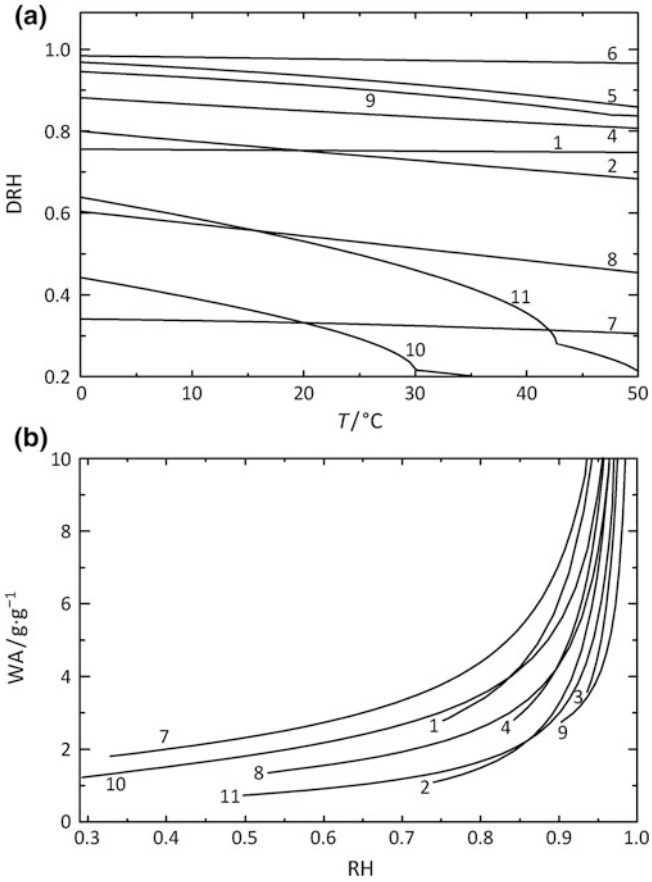

Fig. 4.24 Deliquescence humidities (**a**) and hygroscopic moisture uptake (**b**) of several salts commonly found in building materials: *1* NaCl, *2* $NaNO_3$, *3* Na_2SO_4, *4* KCl, *5* KNO_3, *6* K_2SO_4, *7* $MgCl_2{\cdot}6H_2O$, *8* $Mg(NO_3)_2{\cdot}6H_2O$, *9* $MgSO_4{\cdot}7H_2O$, *10* $CaCl_2{\cdot}6H_2O$, *11* $Ca(NO_3)_2{\cdot}4H_2O$

common salts in building materials cover the whole range of typical ambient relative humidities (see Fig. 4.24). For convenience, values of DRH for several important salts are listed at round temperatures in Table 4.6.

Above the deliquescence relative humidity, a salt is dissolved completely and the amount of water uptake is determined by the equilibrium between salt solution and water vapor in the ambient air. At equilibrium, the activity of water, a_w, in a salt solution equals the relative humidity of the surrounding atmosphere.

$$a_w = \frac{p_w}{p_{w,0}} = \mathrm{RH} \tag{4.16}$$

Here, p_w and $p_{w,0}$ are the actual vapor pressure and the saturation vapor pressure of water vapor, respectively. It follows that $a_w = 1$ for pure water. Any

Table 4.6 Deliquescence humidities and hydration–dehydration equilibrium humidities of several salts at round temperatures from 0 to 50 °C

	0 °C	10 °C	20 °C	30 °C	40 °C	50 °C
Deliquescence humidities						
NaCl	75.9	75.6	75.4	75.2	75.0	74.8
$NaNO_3$	80.1	77.7	75.3	72.8	70.4	68.0
Na_2SO_4[a]	98.8[b]	97.8[b]	95.6[b]	90.1[b]	87.9	88.4
KCl	88.3	86.7	85.0	83.5	82.1	80.7
KNO_3	97.0	95.5	93.7	91.5	88.9	85.9
$MgCl_2{\cdot}6H_2O$	34.1	33.7	33.1	32.4	31.5	30.5
$Mg(NO_3)_2{\cdot}6H_2O$	61.3	58.6	55.7	52.5	49.2	45.7
$MgSO_4{\cdot}7H_2O$	94.5	93.1	91.3	89.1	86.3	83.2[c]
$CaCl_2{\cdot}6H_2O$	44.3	39.4	33.3	21.6[d]	18.4[d]	16.3[e]
$Ca(NO_3)_2{\cdot}4H_2O$	63.8	58.8	53.1	46.0	35.5	21.3[f]
Equilibrium humidities						
Na_2SO_4(V)–$Na_2SO_4{\cdot}10H_2O$	60.6	68.2	76.4	85.3	–	–
$MgSO_4{\cdot}6H_2O$–$MgSO_4{\cdot}7H_2O$	30.2[g]	37.5[g]	46.7	57.7	70.6	–
$MgSO_4{\cdot}H_2O$–$MgSO_4{\cdot}7H_2O$	36.1	41.1	46.7	53.0	60.0	67.7 [g]
$MgSO_4{\cdot}4H_2O$–$MgSO_4{\cdot}6H_2O$	32.0[g]	35.4[g]	39.1[g]	43.3[g]	48.4[g]	54.4[g]

[a] Na_2SO_4(V) (thenardite)
[b] $Na_2SO_4 \cdot 10H_2O$
[c] $MgSO_4 \cdot 6H_2O$
[d] $CaC_{l2} \cdot 4H_2O$
[e] $CaC_{l2} \cdot 2H_2O$
[f] $Ca(NO_3)_2 \cdot 3H_2O$
[g] metastable

deviation from the equilibrium causes either evaporation of water from the solution (if $a_w > p_w/p_{w,0}$) or condensation of water vapor (if $a_w < p_w/p_{w,0}$). The water activity depends on the composition and concentration of a salt solution and can be experimentally determined by measuring the equilibrium humidity above a salt solution of a given composition. The rate of evaporation is controlled by the difference between the ambient RH and the water activity. Therefore, concentrated salt solutions with low water activity present in the ground moisture zone slow down the evaporation rate significantly and, thus increasing the capillary rise height, as discussed before (see Sect. 4.4.1).

Once a large amount of salt is accumulated in a porous material, the hygroscopic moisture uptake may be the major source of liquid water in the material. This is illustrated in Fig. 4.24 by the hygroscopic water uptake curves for a number of common salts above their respective deliquescence humidities. Above approximately 80 % RH, most salts absorb such a large quantity of water that the water-accessible pore space of the material can be entirely filled with a salt solution if there is sufficient salt enrichment. Considering, for example, a stone material with a total porosity of 15 % that contains 1 % by weight NaCl, the water-accessible pore space is completely filled with a NaCl solution at 91 % RH. Such a solution formed by the hygroscopicity of the salt is subject to capillary

transport, which might be the reason that salts in masonry can be transported to much greater heights than would be expected by simply assuming transport via capillary rise of ground moisture (Klenz Larsen 1999).

The hygroscopicity of a salt is characterized by both the water uptake curves shown in Fig. 4.24 and the deliquescence humidity. In both respects, magnesium and calcium chloride are the most hygroscopic salts. If these salts are enriched in masonry, they will always be responsible for high moisture content in the masonry given their low DRH of about 30 % RH at ambient temperatures. This is also the reason why these salts rarely crystallize out and, therefore, do not induce any crystallization damage. In contrast, other salts have very high deliquescence humidities and will hardly ever go into solution. For example, the deliquescence humidity of K_2SO_4, arcanite, remains above 97 % at near-ambient temperatures. It is unlikely that this salt dissolves in the absence of another source of liquid water such as rainfall. Finally, gypsum is not hygroscopic at all (DRH > 99.9 %). It is important to remember that water–vapor adsorption is a surface phenomenon. Therefore, the size of the crystals present and their distribution in the masonry will affect the amount of water sorbed.

A number of salts exist in anhydrous and various hydrated forms in which water molecules are part of the crystal lattice of the salt mineral. The most prominent example of that type of equilibrium is the hydration–dehydration equilibrium of anhydrous sodium sulfate (thenardite) and the decahydrate (mirabilite). Many salts found in building materials form different hydrates (see Table 4.5). As already discussed in Sect. 4.2.3, the crystal growth of a hydrated phase can be an important cause of damage. From a thermodynamic point of view, the equilibrium is determined by the relative humidity. If the RH increases above a critical value, the anhydrous or lower hydrated form of a salt picks up moisture from the air, forming a higher hydrated state. For example, in the case of calcium nitrate, several such transitions exist. At 20 °C, the critical RH values for the formation of the di-, tri-, and tetrahydrates are 8.3, 12.4 and 20.5 % RH, respectively. The corresponding phase equilibria are the following:

$$Ca(NO_3)_2(s) + 2H_2O \rightleftharpoons Ca(NO_3)_2 \cdot 2H_2O(s) \tag{4.17a}$$

$$Ca(NO_3)_2 \cdot 2H_2O(s) + H_2O \rightleftharpoons Ca(NO_3)_2 \cdot 3H_2O(s) \tag{4.17b}$$

$$Ca(NO_3)_2 \cdot 3H_2O(s) + H_2O \rightleftharpoons Ca(NO_3)_2 \cdot 4H_2O(s) \tag{4.17c}$$

The tetrahydrate, nitrocalcite, is the highest hydrated form of calcium nitrate. The deliquescence humidity of $Ca(NO_3)_2 \cdot 4H_2O$ equals 53.1 %. A water uptake curve and the complete phase diagram of the system $Ca(NO_3)_2$–H_2O is depicted in Fig. 4.25. Thick solid lines represent deliquescence humidities, i.e. the equilibrium conditions for the coexistence of the various solid phases and a saturated solution. Above these curves, a solution is the stable phase. Thin solid lines are the coexistence curves of two solid phases, i.e. they represent the hydration-dehydration equilibria. At very low temperatures, a solution is not stable, and, hence, the stable phases below −28.5 °C are ice and $Ca(NO_3)_2 \cdot 4H_2O$. At temperatures

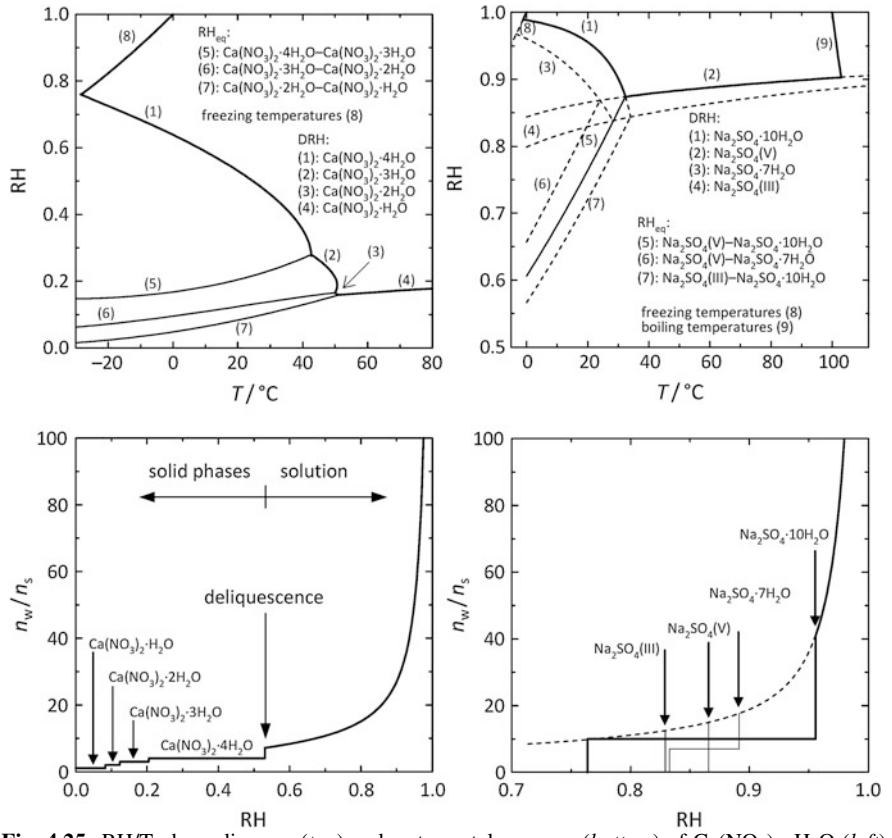

Fig. 4.25 RH/T phase diagram (*top*) and water uptake curves (*bottom*) of $Ca(NO_3)_2$–H_2O (*left*) and Na_2SO_4–H_2O (*right*); dashed curves represent metastable equilibria

between −28.5 and 0 °C, two equilibria have to be considered. A solution can either be in equilibrium with ice (line 8) or with $Ca(NO_3)_2{\cdot}4H_2O$ (line 1). The latter curve represents the deliquescence humidity of the tetrahydrate which is stable from −28.5 to 42.7 °C. At a higher temperature, the lower hydrates also have ranges of stable existence.

Calcium nitrate is a very hygroscopic salt with low deliquescence humidity. In effect, the various hydration–dehydration equilibria occur at even lower humidity, and it is unlikely that dehydration of nitrocalcite can occur under typical climatic conditions in buildings. In fact, this is the reason why the lower hydrates have never been identified in building stones. Similarly, the lower hydrated forms of the very hygroscopic salts, bischofite, $MgCl_2{\cdot}6H_2O$, antarcticite, $CaCl_2{\cdot}6H_2O$, and nitromagnesite, $Mg(NO_3)_2{\cdot}6H_2O$, will hardly crystallize under normal conditions. Due to their hygroscopicity and high solubility, these salts are also most efficient at depressing the freezing temperature of water.

In contrast to the alkaline earth chlorides and nitrates, sodium sulfate is much less hygroscopic, and the formation of Na_2SO_4 solutions requires very humid conditions, particularly at temperatures below 25 °C. Therefore, in the absence of other sources of liquid water, typical fluctuations in ambient temperature and relative humidity are such that hydration–dehydration reactions are more likely to occur than deliquescence–crystallization cycles. However, the situation with this salt becomes a lot more complicated due to the formation of metastable phases. Apart from thenardite, Na_2SO_4(V) and mirabilite, there are two additional phases, namely, the heptahydrate $Na_2(SO_4)\cdot 7H_2O$ (Rijniers et al. 2005; Hamilton et al. 2008) and the anhydrous polymorph Na_2SO_4(III) (Grossi et al. 1997; Rodriguez-Navarro et al. 2000; Linnow et al. 2006).

The phase diagram of the system Na_2SO_4–H_2O and the water uptake curve were recently updated and are also shown in Fig. 4.25 (Steiger and Asmussen 2008). Due to the presence of the metastable phases, the phase diagram is considerably more complicated than previously assumed. However, both metastable phases were identified in experimental studies where, for kinetic reasons, they were formed instead of the stable phases. A more detailed discussion of the phase diagram and the importance of the metastable salts for understanding the damage mechanism of sodium sulfate crystallization in stone can be found in the literature (e.g. Espinosa-Marzal and Scherer 2008; Hamilton et al. 2008; Steiger and Asmussen 2008).

There are also other salts commonly found in building materials whose crystallization behavior is characterized by the formation of metastable phases. In the case of calcium sulfate, gypsum, $CaSO_4\cdot 2H_2O$, is the major phase found even at very low relative humidity, although anhydrous $CaSO_4$ (anhydrite) is the thermodynamically stable phase under such conditions (Charola et al. 2007). The dehydration of gypsum is hindered for kinetic reasons. Considering the ubiquitous presence of very high gypsum concentrations in building materials, it is beneficial that it is obviously not subject to extensive dehydration–rehydration cycles.

Even more complex is the behavior of the magnesium sulfate hydrates. In the $MgSO_4\cdot nH_2O$ series, all compounds with n = 11, 7, 6, 5, 4, 3, 2.5, 2, 1.25, and 1 exist. However, the only thermodynamically stable phases are meridianiite (n = 11), epsomite (n = 7), hexahydrite (n = 6), and kieserite (n = 1). An updated phase diagram of the system, considering both stable and metastable phases, was presented recently by Steiger et al. (2011). Meridianiite is only stable at subzero temperatures. In addition, the magnesium sulfate hydrates are only deliquescent at high relative humidities. As changes in the state of hydration require lower relative humidities, they are more likely to occur under typical ambient conditions. Laboratory experiments have shown that, due to sluggish kieserite formation, metastable phases are the major dehydration products of epsomite and hexahydrite (Chipera and Vaniman 2007; Wang et al. 2009; Steiger et al. 2011). In these experiments, the tetrahydrate starkeyite, $MgSO_4\cdot 4H_2O$, was found as the most abundant compound under near-ambient conditions (see Table 4.6).

Several common salts do not form hydrated phases, e.g. $NaNO_3$, KNO_3, KCl, and K_2SO_4. Their phase diagrams are particularly simple and are characterized by

their deliquescence humidities (see Fig. 4.24). The hydrated form of sodium chloride is hydrohalite, $NaCl{\cdot}2H_2O$, which, however, is only formed at subzero temperatures. Similarly, there exist higher hydrated phases of magnesium chloride and nitrate (see Table 4.5) that are only stable at low temperatures.

4.4.3.2 Salt Mixtures

From the phase diagrams discussed so far, the properties of a single salt in porous stone can be easily predicted. Crystallization damage may be avoided by maintaining the relative humidity of the air either permanently below or above the deliquescence humidity. If the RH is kept below the deliquescence humidity, the salt remains in solid form, and, at humidities above the saturation value, the salt remains in solution the whole time. Similar arguments apply to the equilibrium humidity of a hydration reaction. However, contamination with a single salt is extremely uncommon, and, unfortunately, the situation becomes a lot more complicated for mixed systems compared to pure salts as the concept of the saturation humidities of the individual salts no longer applies to mixtures (Price and Brimblecombe 1994; Steiger and Dannecker 1995; Steiger and Zeunert 1996). In fact, salt efflorescences on walls containing complex salt mixtures have been observed at considerably lower relative humidities than would have been expected from the saturation humidities of the respective pure salts (Arnold and Zehnder 1991).

The more complex behavior in salt mixtures can be easily understood considering the influences on solubility equilibria in mixed solutions. The equilibrium constant (the thermodynamic solubility product) of the dissolution reaction [Eq. (4.3), Sect. 4.2.3] is given by

$$\ln K_{MX} = \nu_M \ln m_M + \nu_M \ln \gamma_M + \nu_X \ln m_X + \nu_X \ln \gamma_X + n \ln a_w \qquad (4.18)$$

where γ_M and γ_X are the activity coefficients, and m_M and m_X are the molalities of the cation M and the anion X in the saturated solution. It is obvious that the solubility of a salt is strongly affected by the presence of a second salt which might have one ion in common, i.e. increasing either m_M or m_X. The second salt will also affect the solubility if it does not have a common ion, as it influences the activity coefficients of the ions M and X. As an example, Fig. 4.26a depicts the solubilities of NaCl and $NaNO_3$ in their respective mixed solutions. Due to the common ion effect, the solubilites of both salts decrease with increasing concentration of the respective second salt. The crystallization pathways of mixed solutions upon the evaporation of water can be readily deduced from the solubility diagram. For example, if water evaporates from a solution of initial composition A, the solution becomes more concentrated and the solution composition moves along line AB. Reaching point B, the solution is saturated with respect to $NaNO_3$, and, upon continued evaporation, this salt will start to crystallize out. As $NaNO_3$ is removed, the composition of the solution changes; the nitrate concentration decreases while the NaCl concentration still increases due to ongoing evaporation. Therefore, the crystallization of $NaNO_3$ continues and the composition of the solution moves

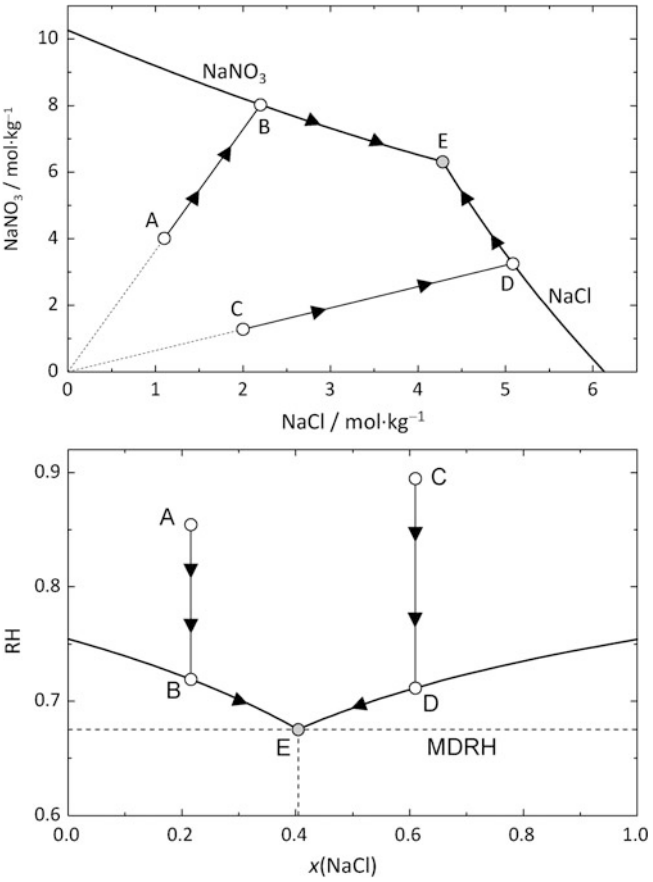

Fig. 4.26 Solubilities (**a**) and saturation humidities (**b**) in the NaCl–$NaNO_3$–H_2O system at 19 °C

along the solubility curve of $NaNO_3$ until the solution reaches saturation, also with respect to NaCl at point E, which is the drying point of this system. Any further evaporation causes the crystallization of both solids to complete dryness. A solution of initial composition C follows a similar crystallization pathway. In this case, however, the first solid that crystallizes is NaCl, and $NaNO_3$ is only precipitated at the crystallization end point.

The relative humidities in equilibrium with the respective saturated solutions are depicted in Fig. 4.26b. The mixture composition is expressed in terms of the mole fraction of chloride. It can be seen that the relative humidity in equilibrium with solution A is RH_{eq} = 86 %. In order to reach saturation with $NaNO_3$, the RH has to be decreased to 72.5 %, which is the equilibrium or saturation humidity of solution B. $NaNO_3$ starts to crystallize below this humidity. The crystallization end point is reached at 67.5 % RH. In comparison with the two single salts, the crystallization of $NaNO_3$ starts at a slightly lower RH than for a pure $NaNO_3$

solution (72 % instead of 75 %), while the crystallization of NaCl starts at a significantly lower RH (67.5 % instead of 75 %). For the solution with initial composition C (RH_{eq} = 89 %), NaCl starts to crystallize at 71.5 %. Upon further evaporation, more NaCl is precipitated and $NaNO_3$ crystallizes at 67.5 %, i.e. far below its single salt DRH. This simple example explains why the formation of efflorescences on walls containing complex salt mixtures occurs at significantly lower RH than implied by the deliquescence humidities of the pure salts.

The behavior of a single salt at a given temperature can be sufficiently characterized by a single value of DRH. If the humidity remains above this RH, the salt remains dissolved; however, if it drops below the DRH, the salt will crystallize. In contrast, a range of relative humidity is required to characterize the crystallization properties of salt mixtures. The upper RH limit depends on mixture composition and is given by the saturation RH curves of the two salts, as shown in Fig. 4.26b for NaCl and $NaNO_3$. Above these saturation humidities, the salt mixture remains in solution the whole time. Thus, these curves define the RH below which the crystallization of a solid phase starts. The lower RH limit is given by the relative humidity in equilibrium with the solution that is saturated in both solids. This relative humidity is called the mutual DRH (MDRH). The MDRH is the lowest RH at which a mixed solution of two or more salts can still exist. The MDRH is also the RH at which the dry salt mixture, provided that the two solids are intimately mixed, first acquires water vapor and forms a saturated solution. The MDRH is always lower than the DRH of any single salt in the mixture. In the range between the MDRH and the crystallization humidities, a salt solution and crystalline deposits coexist. In effect, the crystallization of one salt from a mixed solution does not occur at a specific value but rather across a range of relative humidities (Price and Brimblecombe 1994; Steiger and Dannecker 1995; Steiger and Zeunert 1996).

The simple example of a NaCl–$NaNO_3$ mixture also provides insight into the process of salt fractionation during transport, as mentioned before. Depending on the initial mixture composition, one of the two solids is first precipitated. If salt crystallization occurs during the transport of the solution, the first salt is immobilized while the solution enriched with the second salt is still subject to transport. Considering evaporation of a mixed solution from a porous stone, one component of the mixture, for example, $NaNO_3$ in the case of solution composition A in Fig. 4.26, crystallizes first and might form an efflorescence on the stone surface during the initial drying phase. With ongoing evaporation, the drying front eventually moves into the interior of the stone where the remaining salt mixture continues to crystallize as a subflorescence. It is important to note that the composition of an efflorescence generally is not representative of the salts that are present in the interior.

Fractionation also has important consequences for the deliquescence behavior of salt mixtures. If the dry salts do not form an intimate mixture, the MDRH is not the relative humidity at which the salts pick up moisture again and form a solution. As a result of the fractionation, there are salt deposits consisting of more or less only a single salt. Consequently, deliquescence occurs at the DRH of this single salt. In effect, there is an offset between the drying point of the mixed solution, i.e.

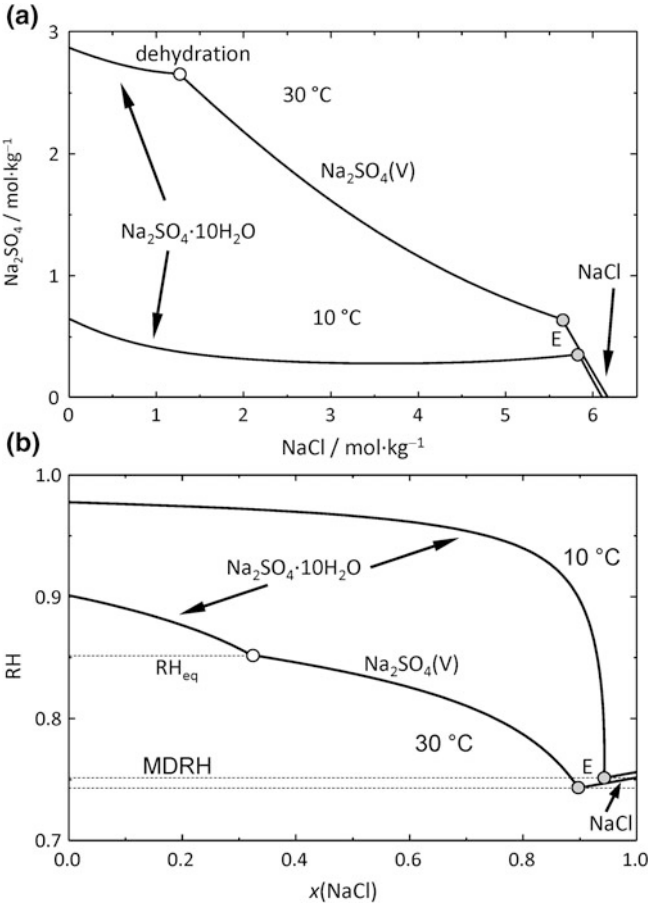

Fig. 4.27 Solubilities (**a**) and saturation humidities (**b**) in the NaCl–Na_2SO_4–H_2O system at 10 and 30 °C

the MDRH of this mixture, and the actual deliquescence humidity, which is the DRH of one of the mixture components.

The discussion so far has only considered a very simple situation, i.e. a mixture with only three different ions and with two crystalline salts that neither form different hydrated states nor double compounds. Moving to different mixture compositions, particularly including sulfate as one of the components, the solubility diagrams become more complicated. Examples including the thenardite-mirabilite equilibrium in the presence of NaCl are shown in Fig. 4.27. According to Eq. (4.18), the solubility of a hydrate salt also depends on the water activity a_w. In addition to the common ion effect and the influence on the ion activity coefficients, there is also an influence of the components of a mixture on the water activity. With increasing concentration of a salt solution, the water activity decreases, resulting in a solubility increase at high concentrations of the second

salt. This is the reason for the course of the mirabilite solubility curve at 10 °C (Fig. 4.27a). However, according to Eq. (4.7), the dehydration equilibrium is also determined by the water activity. While mirabilite dehydration does not occur at 10 °C (even in saturated NaCl solutions), much lower NaCl concentrations, i.e. far higher water activities are sufficient at 30 °C. The reason for this behavior is the strong temperature dependence of the thenardite-mirabilite equilibrium (see Fig. 4.25). At low temperatures, the dehydration equilibrium humidity is lower than the deliquescence humidity of the salt mixture. At temperatures above 18 °C, the dehydration humidity exceeds the deliquescence humidity and the dehydration or rehydration occurs in the presence of a solution. In the presence of hygroscopic salts such as magnesium chloride, this effect is even more pronounced. This might have important implications, as hydration and dehydration reactions are known to be sluggish in the absence of liquid water (Charola and Weber 1992; Doehne 1994; Steiger et al. 2008a). Therefore, hydration reactions that can cause damage in porous stone can be significantly accelerated in salt mixtures. It is important to note, however, that the presence of other salts does not influence the values of the equilibrium humidity of a hydration–dehydration equilibrium. Hence, the equilibrium curve for the thenardite-mirabilite equilibrium that is shown in Fig. 4.25 also applies to salt mixtures.

Another significant complication in the behavior of salt mixtures arises from the fact that the salts commonly found in building materials form a large number of double salts, i.e. salts that are comprised of three or more different ions. Figure 4.28 shows solubility diagrams including the common double salts astrakanite (bloedite), $Na_2Mg(SO_4)_2{\cdot}4H_2O$, glaserite (aphthitalite), $K_3Na(SO_4)_2$, and darapskite, $Na_3NO_3SO_4{\cdot}H_2O$. Further double salts are listed in Table 4.5. Astrakanite is one of the rare examples of a congruently soluble double salt that is found in building materials. If a compound dissolves congruently, the solution and the solid have the same stoichiometric composition. For example, the dashed line in Fig. 4.28a represents the composition of an equimolar mixture of Na_2SO_4 and $MgSO_4$, i.e. a mixture of the same mixing ratio as in the double salt astrakanite. Evaporation of water from a solution of that composition yields first saturation with respect to the double salt which would crystallize out. Since precipitation of astrakanite does not change the solution composition, the equimolar solution behaves just like a single salt. The salt crystallizes out if the ambient RH drops below its saturation humidity, and the dry double salt picks up moisture and forms a solution as the RH is increased to its deliquescence humidity again.

Unfortunately, most of the double salts that are found in building materials are incongruently soluble. For example, the dashed line in Fig. 4.28b represents the stoichiometric composition of aphthitalite, i.e. a 3:1 molar mixture of K_2SO_4 and Na_2SO_4, respectively. It is obvious that evaporation of such a solution at 15 °C yields saturation with respect to arcanite (K_2SO_4) and not aphthitalite. As a consequence, a saturated solution of aphthitalite is supersaturated with respect to arcanite.

Therefore, if the double salt dissolves in a limited amount of water, arcanite would crystallize out instead. It is obvious that the crystallization behavior of

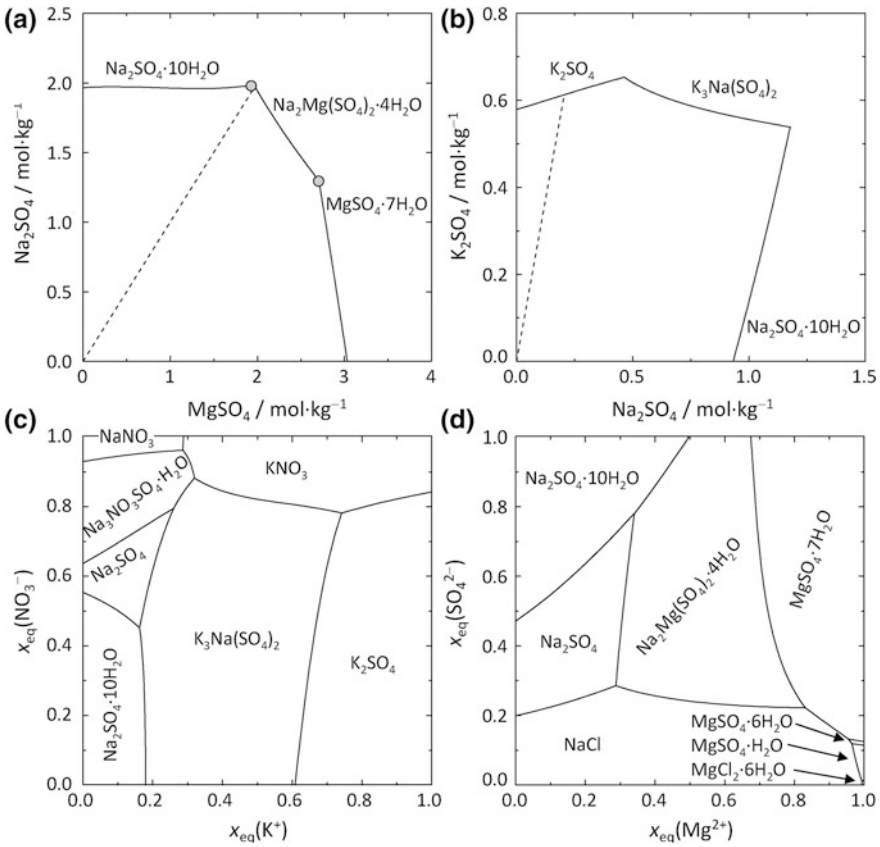

Fig. 4.28 Solubilities in **a** The Na_2SO_4–$MgSO_4$–H_2O system at 25 °C, **b** The Na_2SO_4–K_2SO_4–H_2O at 15 °C, **c** The Na^+–K^+–NO_3^-–SO_4^{2-}–H_2O system at 25 °C, and **d** The Na^+–Mg^{2+}–Cl^-–SO_4^{2-}–H_2O system at 25 °C

incongruently soluble double salts is considerably more complicated than that of single salts. Although the formation of double salts has been frequently observed in buildings, only a few laboratory investigations of salt damage in porous stone have been carried with salt mixtures including double salt formation. A recent study of De Clercq (2008) confirms the complex behavior of such mixtures.

The phase diagrams of slightly more complex mixtures that comprise four different ions, two cations and two anions, are also shown in Fig. 4.28. For the sake of simplicity, the solubilities are given as so-called Jänecke projections, i.e. the water content of the saturated solutions is not shown. All possible mixtures of the four ions are represented in terms of charge-equivalent mole fractions of the cations and the anions, respectively, i.e. the fractional contribution of each cation to the total number of positive charges and the contribution of each anion to the total number of negative charges. The corners of the square diagram, therefore,

represent the four pure salts. For example, Fig. 4.28c depicts the solubility diagram of a mixed system containing sodium, potassium, sulfate, and nitrate. Therefore, in this diagram, the corners represent the four salts sodium sulfate, sodium nitrate, potassium sulfate, and potassium nitrate. The lines in the interior of the square are the saturation curves for solutions coexisting with two solid phases. These curves define the crystallization fields of the different mineral phases that would first crystallize out for a given mixture composition. According to the phase rule, a maximum of three different solids can coexist with a mixed solution containing four different ions. The corresponding isothermal invariant points are given as the intersections of the two salt coexistence curves.

In the $Na^+-K^+-NO_3^-{}-SO_4^{2-}-H_2O$ system, there are seven different crystalline phases that have a range of stable existence at 25 °C. These are anhydrous potassium nitrate (niter), sodium nitrate (nitratine) and potassium sulfate (arcanite), thenardite and mirabilite, and the double salts darapskite and glaserite. A lot of information about the crystallization properties of the four-component system can be readily derived from the diagram. First, it is obvious that the double salts, particularly aphthitalite, have large stability fields and will, therefore, easily form in this four-component system. Second, it can be seen that only certain mineral combinations represent a stable assemblage. For example, niter can coexist with both double salts, with nitratine and arcanite, but with neither thenardite nor mirabilite. Similarly, in the $Na^+-Mg^{2+}-Cl^-{}-SO_4^{2-}-H_2O$ phase diagram (Fig. 4.28d), NaCl (halite) can coexist with the various $MgSO_4$ hydrates, but there is no stable assemblage of bischofite, $MgCl_2{\cdot}6H_2O$, with either thenardite or mirabilite. Also in this system, there is a large stability field of a double salt (astrakanite), while the very soluble and hygroscopic bischofite only has an extremely small range of stable existence.

4.4.3.3 Modeling of Crystallization Pathways in Salt Mixtures

Phase diagrams as those shown in Fig. 4.28 allow the prediction of complete crystallization pathways as discussed before for the NaCl–$NaNO_3$ mixture. For practical applications, it is impossible to conduct all the necessary measurements for a huge number of mixture compositions. In order that phase equilibria can be predicted, a model approach is more appropriate (Price 2000; Steiger 2005c). It follows from Eq. (4.7) that calculating solubility equilibria in mixed salt systems requires (a) values of the equilibrium constants, K_{MX}, in the temperature range of interest and (b) activity coefficients of the aqueous species as a function of solution composition and temperature. The ion interaction model from Pitzer (1991) has been successfully applied for the prediction of ion activities in complex, mixed electrolyte solutions. The model parameters, including the thermodynamic solubility product, are determined from available experimental data for single salts and simple mixtures (Steiger et al. 2008b). Once the model is parameterized, it can be used to predict crystallization pathways and the critical climatic conditions for complex salt mixtures that are present in building materials.

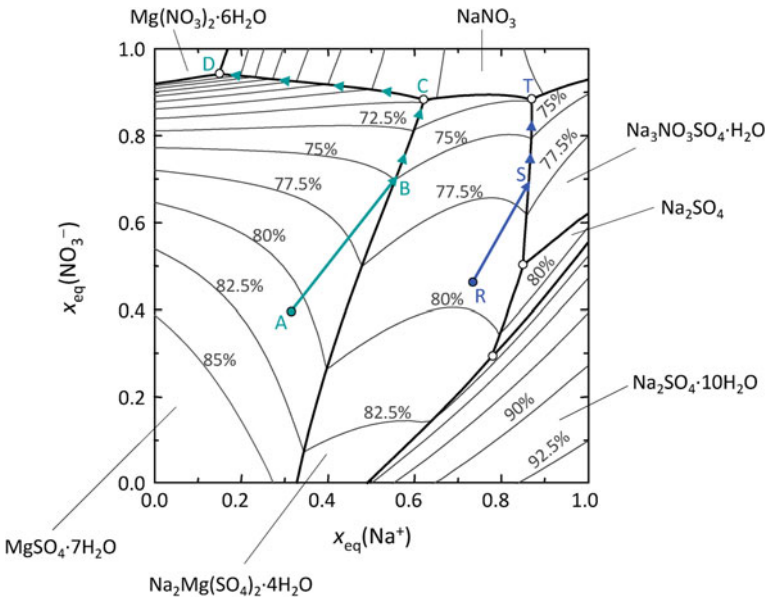

Fig. 4.29 Solubilities and saturation humidities in the system Na^+–Mg^{2+}–NO_3^-–SO_4^{2-}–H_2O at 25 °C. Adapted from Steiger et al. (1998)

The use of such a model approach is illustrated in Fig. 4.29, which represents a calculated phase diagram of the four-component system $Na^+-Mg^{2+}-NO_3^--SO_4^{2-}-H_2O$. For any solution composition, the crystallization pathway can be readily predicted from the phase diagram. For example, epsomite would crystallize out first from a solution of composition A. Due to the crystallization of epsomite, the solution becomes depleted in magnesium and sulfate. Hence, the solution composition moves along line AB, which is the extension of the straight line connecting point A, the solution composition, with the composition of the solid phase, i.e. the corner representing pure $MgSO_4$. As more water evaporates, epsomite continues to crystallize until the solution is also saturated with respect to astrakanite at point B.

Further removal of water then causes the simultaneous crystallization of epsomite and astrakanite until, at point C, the solution is also saturated with respect to nitratine. The solution is now saturated with respect to three solids. However, point C is not the crystallization end-point for a solution of initial composition A, but C is rather a transformation point. Assuming full equilibrium between the solution and the solids already precipitated, further removal of water would lead to the complete dissolution of astrakanite and the precipitation of nitratine instead. Then, the solution composition moves along the line CD. Finally, point D is the drying point of the solution of initial composition A.

The equilibrium model can also be used to calculate the relative humidity in equilibrium with a solution of any composition. Equilibrium humidities of saturated

solutions are particularly important, as they indicate the critical relative humidities below which a solution of a given composition starts to crystallize. In Fig. 4.29, these critical values are plotted as lines of equal saturation humidity. As in the examples discussed before, it is obvious that there is a considerable decrease in the saturation humidities of the different solids in the presence of other ions.

Such diagrams can be used to obtain critical ranges of relative humidity, within which fluctuations cause crystallization or other phase changes. For example, in a solution of composition A, epsomite starts to crystallize at about 81 % RH, which has to be compared to the saturation humidity of 90.3 % of a pure $MgSO_4$ solution at the same temperature. Further decreasing the relative humidity, the solution also becomes saturated with astrakanite at 75 % RH. At about 70 % RH, the double salt redissolves and nitratine starts to precipitate instead. Finally, the crystallization end-point of solution A is reached at a relative humidity of 50 % RH, yielding a mixture of epsomite, niter, and nitromagnesite, $Mg(NO_3)_2{\cdot}6H_2O$.

It is important to note, however, that completely different crystallization pathways result for other solution compositions. For example, the composition of solution R in Fig. 4.29 is in the astrakanite stability and, therefore, follows a different crystallization pathway. Astrakanite starts to crystallize from this solution slightly below 80 % RH, and the remaining solution becomes depleted in sodium, magnesium, and sulfate according to the stoichiometric composition of astrakanite, i.e. $x_{eq}(Na) = 0.5$, $x_{eq}(NO_3^-) = 0$. Hence, the solution composition moves along line RS, reaching saturation with the second double salt darapskite at about 77 % RH (point S). Below this RH, both double salts crystallize simultaneously until the solution composition reaches point T at 75 % RH. Point T is the drying point of solution R, and hence, the dry salt mixture consists of astrakanite, darapskite, and niter. Different pathways are obtained for other solution compositions.

The salt mixtures found in building materials are typically more complex, and it is usually not possible to represent the complete phase diagram of such a mixed system in a simple two-dimensional diagram. However, using a model, it is still possible to calculate the crystallization pathways for any mixture composition. It is possible to predict the critical conditions of climatic conditions that would cause crystallization or hydration processes that could possibly cause material damage. There are several possible applications of thermodynamic models in the conservation of building materials (Steiger 2005c), and a number of very useful applications, using experimentally-determined salt mixture compositions in samples from various building materials as model input data, can be found in the literature (Steiger 1996; Sawdy 2001; Bionda and Storemyr 2002; Schlütter et al. 2003; Sawdy and Price 2005; Bionda 2006; Price 2007; Klenz Larsen 2007; Prokos 2008; Zehnder and Schoch 2009).

In many of these studies, the programs RUNSALT and ECOS (Environmental Control of Salts) were used to calculate the crystallization pathways of salt mixtures from a number of different objects. ECOS was developed in a collaborative project funded by the European Commission (Price 2000). The use of ECOS requires an ionic analysis of a sample taken from the building or the salt-contaminated material in question. The program is then able to predict the crystallization

pathways for specified conditions of RH and temperature. RUNSALT is an improved interface to the fundamental thermodynamic model that was subsequently developed by Bionda (2006).

4.5 Biodeterioration of Stone

From the biological point of view, stone is an extreme environment. It is poor in nutrients and suffers large changes in moisture content, with wind and rain wearing away its surface while the sun provides perniciously high UV radiation. Nevertheless, stone is inhabited by microorganisms in all climate regions of the Earth, ranging from the cold Antarctic to temperate and tropical areas to the hot deserts and rocky shores in all places (Warscheid and Braams 2000; Selbmann et al. 2005; Sterflinger 2005). The microorganisms can be epilithic, i.e. living on the rock surface, or endolithic when living within pores and fissures of the stone, and they can grow in both terrestrial as well as aquatic habitats.

Microorganisms, plants, and animals play a considerable role in the formation of rocks. The so-called "banded iron formations" are a result of iron oxidation due to oxygen release by cyanobacteria; carbonate sediments are formed by precipitation resulting from the algal and bacterial CO_2 uptake from seawater at continental edges; massive carbonate rocks were created by the shells of bryozoans, corals, and mollusks; microbes catalyze the diagenesis of crystalline or amorphous components in rock. Finally, they play a major role in the weathering of rock. Geomicrobiologists even postulate that the weathering of rock in the presence of microbes is some ten thousand times faster than without them, the latter being a mere theoretical hypothesis because there are no sterile rock surfaces on Earth. Whereas the alteration of rocks in the natural environment is referred to as bioweathering, the damage of stone in man-made objects is called biodeterioration (Allsopp et al. 2003; Scheerer et al. 2009).

A biopatina refers to the aesthetic chromatic modification of the material caused by the growth of some organisms but with no visible surface deterioration. On the other hand, the staining that may remain on the stone after the biological organisms have disappeared is called a biogenic discoloration.

The most decisive factor of microbial growth is the availability of water. Therefore, porous stones that are able to retain large amounts of water are easily colonized by a wide variety of bacteria and fungi. Stones with lower porosity or those that easily dry after rain events will not be colonized as easily. Primary colonization requires longer times, and the species diversity of this colonization is generally more restricted.

Bacteria generally need high water activity ($a_w > 0.98$). Fungi and lichen are able to grow at much lower water activity ($a_w > 0.65$) and tolerate periods of complete dryness in a dormant state. However, bacteria are able to tolerate high salt concentrations on and inside of stone (Rivadeneyra et al. 2004). For this reason, very humid and salty environments, such as foundations and plinth walls

on exterior facades, are often inhabited by salt-tolerating bacteria but are nearly free of fungal growth. The exception is the growth of some fungal species like *Hortaea werneckii* and *Wallemia ichthyophaga* growing on salty walls in exterior and interior environments (Gunde-Cimerman et al. 2009). Exposed stone surfaces receiving high UV radiation, and with drastic changes in humidity resulting from rain events followed by dry spells, are usually inhabited by black fungi and by cyanobacteria forming dark green and brown crusts on and within natural stone. Algal films are common in extremely damp semi-basements, on pavement, and on terraces.

4.5.1 Organisms Involved in Biodeterioration

4.5.1.1 Bacteria

Bacteria are small and mostly single-cell organisms, their size ranging between 1 and 5 μm but up to 100 μm in some special genera. Bacteria are common inhabitants of soil, and their presence is essential for the function of all ecosystems on Earth. In one gram of agricultural soil, there are up to 10^9 bacterial cells, while, in a porous stone, there might be up to 10^6 cells inhabiting its surface, pores, cracks, and fissures. Because of their remarkable capability of processing materials, ranging from degradation of organic compounds, i.e. hydrocarbons and plastics, to their capability of using carbon monoxide, hydrogen, and minerals as energy sources, bacteria are able to cope with nearly all environmental conditions. However, in arid and semi-arid areas, they are rare, while fungi and lichen, being more tolerant to drier conditions, are predominant. Nonetheless, in extremely dry environments, bacteria can grow as endobionts in the thalli of lichens. Although single bacteria cannot be seen with the naked eye, they can produce visible deterioration phenomena such as discoloration, sanding, and etching of stone.

Chemoheterotrophic Bacteria

By definition, chemoheterotrophic bacteria are those that need organic carbon sources for growth. On and in stone, nutrients for heterotrophic bacteria are available from the metabolites of autotrophic bacteria, from airborne organic contamination and dripping water, from animal feces, and from organic compounds that may sometimes be present in the substrate itself.

Chemoheterotrophs can degrade a wide variety of substances, including natural materials from plants and animals, as well as man-made substances such as polycyclic aromatic hydrocarbons (PAHs) derived from traffic; resins or waxes used for the consolidation of stone; and methylcellulose or other organic additives commonly used in slurries and coatings. From this capability, it can be easily deduced that the growth of bacteria on rock can be significantly enhanced by the addition of organic carbon. Chemoheterothrophs produce organic pigments and a

wide range of organics acids. For this reason, they are important deteriorating agents of stone, causing color change and biogenic corrosion. Filamentous bacteria—actinomycetes—inhabit stone more effectively than most of the single-cell bacteria. This can be attributed to their filamentous growth as well as to their effective utilization of various nitrogen and carbon sources (Saarela et al. 2004).

Chemolithotrophic Bacteria

The chemolithotrophic bacteria—in contrast to the heterotrophs—do not depend on organic carbon sources. Their growth is based on the oxidation of minerals containing iron, sulfur, manganese, or ammonia. Ammonia oxidizers preferentially occur in very damp environments where ammonia is available, e.g. plinths and foundations in the vicinity of animal stables or damaged canalizations. During the process of ammonia oxidation, both nitrite and nitrate ions are released and can lead to the formation of nitrous and nitric acids and the corrosion of natural stone, mortar, and even concrete. On undisturbed stone surfaces, iron and manganese oxidation by bacteria leads to the formation of desert varnish, a dense blackish-brown layer covering the rock surface. Rock varnish occurs on a variety of substrates, including stone and ceramics in diverse environments (O'Grady 2005). Iron and sulfur oxidizing bacteria produce sulfurous and sulfuric acid and are biotechnologically used for the leaching of copper, iron, uranium, and gold from ore-containing rocks.

Phototrophic Bacteria and Micro-Algae

Phototrophic bacteria occur on all stones if sufficient light and water are available. "Phototrophic" means that these bacteria are able, from the absorption of sunlight, to generate the energy they need for the maintenance of their metabolism, growth, and propagation. This process is called photosynthesis and is also used by higher plants and algae. Phototrophic bacteria build up cell material by incorporating CO_2 and transforming it into carbohydrates such as sugar, using the same biochemical mechanism of higher plants. This is called the Calvin-cycle.

In nature, there are some phototrophic bacteria that need sulphur in addition to water, sunlight, and CO_2. These do not produce oxygen. They perform an "anoxic" photosynthesis. These bacteria are either pigmented purple "phototrophic purple bacteria" or green "green anoxygen phototrophs". Both, however, require high a_w values, and their growth is restricted to aqueous environments. Therefore, the organisms can develop on stones found in small lakes and tarns, where the water might seasonally become anoxic. Only in very rare cases might they affect stone monuments in the vicinity of such aqueous environments. For example, parts of the remnants of the Temple of Artemis in Ephesus (Turkey)—one of the Seven Wonders of the World—are located within and underneath a brackish-water tarn that turns completely red with the bloom of purple bacteria in summer, and that results in the purple coloration of the white calcareous limestone (Fig. 4.30).

The most important and predominant group of phototrophic organisms on rocks and stones are cyanobacteria (Crispim and Gaylarde 2004). Cyanobacteria,

Fig. 4.30 Ephesus, Turkey: the rosy stain on white calcareous limestone is caused by bacteria-forming blooms in the brackish water of the pond overlaying the subterranean parts of the Artemision

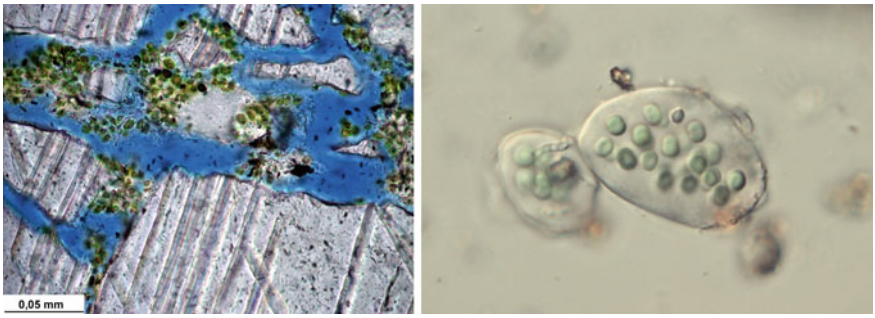

Fig. 4.31 Gloeocapsalean cyanobacteria with thick, gel-like capsules that protect them against desiccation and chemical attack

formerly called blue-green algae, colonize stone in all climate regions of the Earth. The basic pigment produced by cyanobacteria is the chlorophyll necessary for their photosynthesis. Due to the chlorophyll, cyanobacteria appear as green layers on stone or as parallel subsurface bands inside it. In highly sun-exposed environments, they also produce other pigments for sun protection. Due to the presence of carotenoids and scytonemin pigments in their cells, cyanobacterial layers might also appear orange or dark brown. While dry cyanobacterial layers may appear dark black, this does not mean that they are dead. In fact, they regain full metabolic activity and fresh green color upon wetting.

There are different morphological types of cyanobacteria on stone: The most frequent are the single-cell cyanobacteria with cells encapsulated in a thick layer of slime that helps the bacteria to keep water and that protects them from chemical attack or drying (Fig. 4.31). The genera *Gloeocapsa* and *Chroococcus* are typical representatives. Another morphological type is represented by filamentous cyanobacteria that might even produce a dense sheath around their filaments for protection. Due to their sheath and slime capsules, cyanobacteria are able to live with low amounts of water and to survive long periods of desiccation in a resting state.

Fig. 4.32 St. Virgil's chapel (Vienna, Austria): halophilic bacteria and archaea cause a rosy stain on the salt-attacked stone surface of the Medieval monument

On stone, cyanobacteria often occur in close association with algae and lichen, the relative abundance of the groups being determined by the climate and exposure to light and other factors in the immediate vicinity. In general, cyanobacteria are regarded as highly resistant to UV-radiation and desiccation. Due to their phototrophic lifestyle, they do not depend on any organic nutrients, although some of them are able to use organic compounds as a dietary supplement. Their ability to adapt to different light qualities, a process called chromatic adaptation, allows cyanobacteria to develop on stone in archeological hypogea with low light intensities, as in the cases of crypts, caves, and catacombs. There, they might be one of the most important deterioration agents for wall paintings and inscriptions. In such subsurface environments, *Eucapsis*, *Leptolyngbya*, *Scytonema*, and *Fischerella* have been the most frequently encountered cyanobacterial taxa (Albertano 2003).

Green layers of micro-algae cannot be distinguished from cyanobacterial layers with the naked eye, and, in fact, most biofilms in humid or wet environments are a complex mixture of both groups. Although the physiology of green micro-algae is similar to that of cyanobacteria—both depend on light and water and are photosynthetic—micro-algae are less stress resistant and need more water. An algal biofilm is a good indicator of a constant water supply. In architectural objects, the presence of green micro-algal films should be regarded as a sign of constructional defects that allow water infiltration.

Halophilic Bacteria and Archaea

Archaea are bacteria-like organisms that are supposed to have been among the first organisms to colonize the Earth more than 3 billon years ago. Archaea—formerly called archaebacteria—tolerate very high temperatures and extreme salt stress. For the latter reason, they are frequently found on stone and mortar with a high load of chlorides, such as NaCl from deicing salt and sulfates or nitrates from agricultural fertilization, and when sufficient humidity is available. The soluble salts migrate

Fig. 4.33 Side, Turkey: black micro-colonial fungi on a marble surface

into the pore space of the stones, and, as soon as the water evaporates from the stone surface, the salts start crystallizing out forming dense salt crusts. Salt crusts as well as salt efflorescences provide a suitable environment for moderately halotolerant and extremely halophilic (salt-loving) bacteria and archaea. *Salinisphaera*, *Halobacillus*, *Rubrobacter*, and *Bacteroidetes* are common, moderately halophilic bacteria. The most important genera of archaea are *Halococcus* and *Halobacterium*. Many species of the halophilic archaea produce pink or purple pigments, leading to a typical pink stain on stone or mortar surfaces (Fig. 4.32).

4.5.1.2 Fungi

Fungi, in contrast to most bacteria, are multi-cellular organisms forming dense three-dimensional networks of hyphae (cell filaments) on and in stones. Hyphal growth enables fungi to spread over surfaces and to penetrate porous stone. Fungi may be the most important endoliths on building stone because their activity is high and they are extremely corrosive (Sterflinger 2000; Scheerer et al. 2009). Depending on the physical properties of the material, fungi may be found over 1 cm deep in the stone.

There are two major morphological and ecological groups of stone-inhabiting and -dwelling fungi. These are adapted to different environmental conditions. In moderate or humid climates, the fungal communities on rock are dominated by hyphomycetes (mold) that form mycelia (hyphal networks) in the porous space of the stones. Since the settlement of spores from the air is the first step for fungal colonization, the species' diversity of stone fungi is rather similar to the diversity of common airborne spores. *Alternaria*, *Cladosporium*, *Epicoccum*, *Aureobasidium*, and *Phoma* are the most important species. In arid and semi-arid environments, such as those found in the Mediterranean area, the climate conditions are too extreme for most of the hyphomyces, and, therefore, the communities shift towards the so-called black yeasts and microcolonial fungi. Black fungi belonging to the genera *Hortaea*, *Sarcinomyces*, *Knufia*, *Capnobotryella*, *Exophiala*, and *Trimmatostroma* form small black colonies on and inside the stone and often occur in close association with lichen (Fig. 4.33) (Sterflinger 2005).

Some other genera of black fungi are lichenicolous, i.e. they inhabit not the bare stone but the lichen thallus itself. Black fungi on stone have a remarkable resistance against desiccation and tolerate periods of complete dryness for several months. Their growth is extremely slow because most of their energy is spent in the production of thick cell walls and melanin to shelter them against desiccation, erosion, UV-radiation, and chemical attack. Moreover, they produce large amounts of sugars—trehalose, a disaccharide—and polyols that serve as intracellular protection. Those substances are necessary in order to shelter their cell functions and enzymes against heat, desiccation, and salt stress.

Fungi are especially resistant against heat, and a stone surface exposed to the sunlight might heat up to 80 °C without affecting the fungi. Due to the thick walls they develop, fungi also resist chemical attack and, therefore, resist biocides and other anti-microbial treatments. Black fungi dwell deep inside granite, calcareous limestone, and marble. In addition, they deteriorate those stones both via chemical and mechanical attack. The phenomenon of biopitting—the formation of pits with sizes ranging up to 2 cm in diameter and depth in stone—is caused by black fungi. Biopitting occurs predominantly on marble and limestone. Due to the strong melanization of the cell walls, stones colonized by these fungi show black spots or can be completely covered by a black layer. In addition to outdoor environments, black fungi are also found on the rock surfaces of caves and catacombs (Saarela et al. 2004), especially where the naturally high humidity has been actively decreased in order to suppress algal growth on precious wall paintings.

4.5.1.3 Lichens

Lichens are composed of a pair of symbiotic organisms: an algae or cyanobacteria in close spatial and physiological association with a fungus. Both partners form a physiological and morphological entity called a thallus. There are different kinds of lichen: foliose lichens form a coral-like, scrubby thallus; fruticose lichens form a leaf-like thallus on the bark of trees or on rocks; squamulose lichen form a flat thalli with small lobes on the top. On rocks and stone, crustose lichens are the predominant form (Fig. 4.34).

Crustose lichens are strongly adhered to the surface of the rock. When most of the thallus is formed on the rock and only single hyphae (filaments) penetrate the substrate, the lichens are called epilithic. When most of the thallus is inside the cracks and fissures of the substrate and only the fruiting bodies are visible on the surface, they are called endolithic lichens. The symbiosis between fungi and algae/cyanobacteria enables the lichen to live on nutrient-poor and arid stone surfaces. The algal partner, also called the photobiont, produces sugar through photosysthesis and CO_2 fixation that feeds the fungal partner. This helps the fungus to survive in nutrient-poor conditions. On the other hand, the algae profits from the sheltering action of the fungus that protects it from UV-radiation and desiccation. The fungus forms a dense crust around an inner layer, the latter being composed of loose hyphae associated with the algal cells. For nearly all the lichenized fungi,

Fig. 4.34 Lichen crusts growing on calcareous sandstone and forming a landscape-like pattern

the symbiotic lifestyle is necessary, while most of the algae and cyanobateria could live autonomously under suitable environmental conditions. In other words, most lichenized fungi can only live in association with the respective cyanobacterium or algae.

All over the world, lichens are the most common colonizers of calcareous stone. They appear on every stone surface that is not cleaned regularly (Gaylarde and Gaylarde 2005). Lichens are very sensitive to heavy metals and high concentrations of SO_2. Therefore, stone monuments in cities in industrialized countries, such as Paris or Munich, had lost most of their lichens by the 1960s and 1970s. In contrast, monuments in rural areas, such as Angkor Wat in Cambodia or the Maya temples in Mexico, are extensively covered by lichen thalli. Today, lichens are re-conquering the urban areas in industrialized western countries because of the decreased SO_2 concentration and better air quality.

Lichens are colorful, and a surface covered with crustose lichens will appear as a landscape with green, white, gray, black, yellow, and orange areas. Lichens penetrate the rock with their hyphae and with fruiting bodies. This creates a pattern of pitting in calcareous rock. Lichens play an important role in the deterioration of stone, and the pros and cons of removing lichen from a stone surface is discussed in the following section.

4.5.2 Processes of Biodeterioration and Biodegradation

4.5.2.1 Surface Alteration Phenomena and Biogenic Layers

Bacteria, archaea, fungi, algae, and lichens produce a wide variety of organic pigments that have different functions for the organisms: Chlorophyll is the photosynthetic pigment enabling cyanobacteria and algae to absorb sunlight for energy production. Chlorophyll appears in different shades of green, varying from

light blue-green to deep moss-green and nearly black when the photosynthetic microbial mat becomes dry. In the dry state, the cells of the cyanobacterial biofilm are in a passive state with minimal metabolism. Once water is available again, they regain full metabolic activity within a few minutes and return to their green color.

Carotenoids, orange, yellow, red, brown, and purple pigments, are produced by photosynthetic organisms as supporting pigments for photosynthesis and by many others as a UV absorber and protective agent. Melanin has a dark brown or black color that serves to protect the cells against UV-radiation and some radioactive radiation (Dadachova et al. 2007), as well as desiccation, mechanical destruction, and chemical attack. Moreover, it plays a predominant role in the ability of fungi to attack and penetrate hard substances. Melanin is produced by many fungi and especially by the black microcolonial fungi, such as the *Phaeococcomyces*, *Sarcinomyces*, *Knufia*, and *Capnobotryella* that specialize in colonizing stones. The dark brown scytonemin pigment is incrusted in the cell walls and the sheath of some filamentous cyanobacteria that inhabit bare rock surfaces in very sun-exposed areas (Ortega-Morales et al. 2005), such as the plateaus in the Andes (South America) and Table Mountain of Cape Town (South Africa). The dark biogenic coloration of the stone surfaces increases sunlight absorption, thus amplifying physical stress via temperature cycling.

Organic pigments are located both in the cell walls and in the cell of the organism itself. Some are also excreted by the organisms actively, while others are excreted and liberated into the environment after the death and decomposition of the cells. Especially in calcareous rocks, such as limestone and marble, organic pigments are incorporated into the stone, where they remain stable. For this reason, a biogenic stain may be found many decades after the organisms that produced the pigment have died. This alteration is called a biogenic discoloration.

Organisms may cause an aesthetic, chromatic modification of the material, generally not involving visible destruction or material loss, and the alteration phenomenon is then called a biopatina.

A biofilm is defined as a layer formed by microorganims that are normally embedded in slime or in a gelatinous capsule composed of extracellular polymers (EPS) (Kemmling et al. 2004). EPS contain mainly anionic sugars accompanied by proteins, lipids, pigments, and nucleic acids. The thickness of a biofilm ranges from several microns up to 5 mm or more. Above this thickness, it is referred to as a biogenic layer. Biogenic layers are formed by crustose epilithic lichens, cyanobacteria, and algae. On exposed stone surfaces, bacterial biofilms are rare because of the low water activity in the environment. However, the inner surfaces of a stone, i.e. pore walls, fissures, and cracks, may well be inhabited by bacterial biofilms. Such inner biofilms are composed of bacterial cells, and their EPS layers can influence the physical properties of the substrate considerably. Biofilms are effective in clogging pores while increasing water uptake and retention within the stone, and they can hamper water diffusion and evaporation (May 2003). As a consequence, chemical weathering processes, such as dissolution, are enhanced. Bacterial slimes are sticky. Therefore, dirt particles, dust, pollen, and fly ash are trapped by the biofilm. This deposition may serve to feed the bacteria and, thus,

increase the biofilm formation, resulting in an increasingly dirty appearance of the surface with the consequent aesthetic damage.

Fungi, due to their special mycelial morphology, do not form biofilms; they either form single clump-like colonies that can merge into a dense fungal crust or they form mycelial networks on the top and inside of the stone. Fungi may also spread over the stone surface with thin "running hyphae" and drill their way into the stone with very thin penetration hyphae. Foot-like penetration pegs and appressoria, hyphal "pressing" organs, help them to induce mechanical stress with the pressure they exert on individual crystals or stone grains.

4.5.2.2 Bio-Chemical and Bio-Mechanical Alterations

Stone micro-organisms not only inhabit the stone surface (called epilithic) but also penetrate the stone to depths of several millimeters and even centimeters. When they inhabit fissures and crevices in the stone, they are called chasmo-endolithic, while, when they invade the pore system, they are called crypto-endolithic. Due to chemical and mechanical actions and processes, the endolithic growth can considerably influence the physical and chemical properties of the stone and lead to accelerated deterioration and weathering.

The deteriorating effect of epi- and endolithic lichens is based upon the induced chemical and mechanical processes and are, therefore, relevant to the conservation of building stone (Lisci et al. 2003). The contraction and expansion of the lichen thallus following wet-dry cycles causes mechanical stress via the disruption of the grain or crystal structure of the stone. Loosened stone particles accumulate within the lower thallus layer but get lost completely upon removal of the lichen from the surface (Gadd 2007).

Lichens, through their release of organic acids or complexing agents, can leach out Mg, Na, K, Ca, Fe, and even Si and other elements from the stone matrix. After a lichen thallus has disappeared or fallen from the substrate, the surface is rougher and, therefore, more vulnerable to chemical and physical processes of weathering. However, an intact lichen crust might well serve to protect the stone surface sheltering it against wind and rain erosion as well as sunlight-induced stresses (Warscheid and Braams 2000). The damage that the lichen crust may induce is smaller than the subsequent deterioration upon its removal. Therefore, it is important to assess whether it is really necessary to remove a lichen crust from stone monuments.

Among the most important alteration phenomena caused by lichens and fungi is the formation of point-like millimetric or submillimetric shallow cavities called biopits. These pits generally have a cylindrical or conical shape and are not interconnected, although transition patterns to interconnected pits can also be observed. The merging of micropits during a proliferating process might even result in macropitting, with sizes ranging up to 2 cm both in depth and diameter. Micropitting is predominantly caused by lichen, whose fruiting bodies and hyphen penetrate the rock through chemical dissolution. Oxalic acid is the most

predominant acid produced by lichens, and its excretion leads to the formation of calcium oxalate crystals through the chemical reaction of the acid with calcareous stones (Monte 2003). Crusts of calcium oxalate, including two main crystal types—whewellite (the monohydrate form) and wheddelite (the dihydrate form)—may be a result of biogenic oxalic acid production. Micropitting is observed in all climatic regions of the Earth where lichens colonize stone surfaces. The phenomenon occurs predominantly on calcareous stones but also on gneiss and granite.

Macropitting is a phenomenon that mainly occurs in arid and semi-arid areas where black microcolonial fungi are common inhabitants of stone. Although black microcolonial fungi also inhabit limestone and granite, the phenomenon of biopitting seems to be restricted to crystalline calcareous rocks, i.e. marbles. Black fungi have been found to penetrate the stone by both mechanical and chemical processes that are not yet fully understood. In fact, the fungi form colonies inside the stone and mechanically loosen and disrupt stone layers and individual crystals. The process is progressive, resulting in large lesions on the stone surface within a time frame of several decades. In addition, cyanobacteria are frequently observed in depressions, lesions, and interiors of stone. The mechanism of their boring activity is not yet understood.

Fungi, heterotrophic bacteria, and cyanobacteria produce various organic acids as products of a very central metabolic pathway, the so-called citric-acid cycle. The production of acids is significantly influenced by the nutrients present and the availability of trace-elements necessary for their metabolism, e.g. Mg, Fe, or Mn. Increasing environmental pollution—by providing nutrients for the micro-organisms—can increase acid production and, thus, enhance stone decay (Wright 2002). Organic acids, such as oxalic, gluconic, succinic, malic, fumaric, citric, and acetic are produced by stone-inhabiting organisms and are excreted into the environment. Their chemical action causes carbonate dissolution as well as the etching of quartz crystals and corrosion of other minerals present. Depending on the structure and chemical composition of the stone, acid attack may result in the sugaring of marble, the sanding of limestone and sandstone, and the corrosion of other minerals, i.e. feldspars and micas. The corrosion of mica and feldspar minerals results in their size change and leads to decohesion of the stone matrix. Therefore, granites and volcanic tuffs, the latter through the glassy matrix, can be attacked by fungal and bacterial organic acids (Sterflinger 2000). Especially citric and oxalic acid chelate the ions produced by stone dissolution, enhancing this process by removing one of the reaction products.

Inorganic acids are produced by chemolitotrophic bacteria that derive their energy from the oxidation of ammonium or reduced sulfur compounds, resulting in the formation of nitrous (HNO_2), nitric (HNO_3), sulfurous (H_2SO_3), and sulfuric (H_2SO_4) acids. These are highly corrosive to natural stones as well as concrete and cement.

The respiration activity of bacteria and fungi inhabiting the pores and fissures of stone raises the concentration of CO_2 in the porous spaces. When the pores contain water, the CO_2 can form carbonic acid that solubilizes calcite in limestone and other stones. Carbonic acid is a weak acid and, therefore, not as aggressive as the

other acids mentioned. Nonetheless, it is corrosive and the resulting deterioration patterns, e.g. sugaring, etching, etc., are similar.

Biomineralization and especially the biogenic precipitation of calcium carbonate are widespread processes catalyzed by bacteria. Microorganisms from stone surfaces, including most of the common bacteria associated with building stone, have been found to be able to precipitate $CaCO_3$ in the form of calcite. Ehrlich (2009) defined microbial mineral formation as either "active", involving enzymes or metabolic products, or "passive", where the microorganism serves as a crystallization nucleus for calcium carbonate precipitation. Since organisms are in contact with the available precursors required for crystal formation, new mineral material is produced on the stone.

In summary, biogenic weathering and biodeterioration are the results of various interacting features and abilities of the micro-organisms. The biogenic factors leading to deterioration of stone cannot be clearly distinguished from merely physical and chemical weathering. They are part of it. Therefore, weathering processes must always be regarded as a result of combined factors acting together. Biodeterioration contributes significantly to the overall deterioration of stone and other building materials such as concrete, mortar, slurries and paint coatings, glass, and metals used in architecture (Piñar and Sterflinger 2009).

4.6 Final Remarks

The last section of this chapter discusses biodeterioration. However, it limits itself mostly to microorganisms and some of what may be called visually perceptible biocolonization by fungi, algae, and lichens. The deterioration induced by the growth of higher vegetation, especially large trees that can induce severe structural damage with their roots, has already been mentioned in the mechanical processes section. Nonetheless, animals can also contribute to the deterioration of structures and/or their materials. For example, ants *(Camponotus punctulatus)* in the area of northeast Argentina, eastern Paraguay, and southeast Brazil, dig out a lot of earth to build their nearly conical nests above ground, from half a meter to one meter in height and one meter in diameter. The tunnels they dig to obtain the earth, if below a structure, may induce ground subsidence with consequent mechanical damage to the structure above it. Such damage has been identified in some of the structures of the Santísima Trinidad Jesuit Mission in Paraguay (Cedrola and Charola 2009). Birds have been known to selectively pick out grains from limestone and sand grains from mortars, while pigeons present a soiling problem when they roost on buildings. Similarly, bats' guano is a soluble salt source, particularly for phosphates and nitrates, which may be leached into a structure. Four-legged animals can also can contribute to the deterioration of stone: dogs, by their habit of marking objects; cattle and horses, by using monuments as scratching posts.

However, the worst biodeterioration agent is man himself. Not considering catastrophic events such as wars, there are plenty of other examples that condemn

him. To begin with, poor design in buildings, especially detailing, leads to water flowing over walls with the consequent biocolonization of the surface as mentioned in the last section. Then, there is the ubiquitous problem of poor maintenance. Faulty gutters and downspouts allow water penetration into walls, with the resulting problem of hygric expansion of the materials, leading to, if salts are present, their solubilization, mobilization, and eventual recrystallization, or to freeze–thaw damage.

These problems are subsequently followed by the eventual restoration of the building. It is not the aim to criticize those restorations carried out in the past that used some conservation materials that would not be used now, but rather the ones where past experience was not properly applied. This is best illustrated with the by-now classic example of the restoration of the Parthenon by N. Balanos, carried out in the period between the two world wars. Although, in principle, the original method of joining blocks was to be followed, i.e. metal pins or clamps embedded in lead, this was not correctly implemented; poor quality iron was used, and sometimes cement or similar materials were used for filling the holes. Since the condition of the joints between the blocks was not perfect, water penetrated and corroded the iron elements, leading to their expansion with the consequent mechanical damage to the marble blocks, as became evident some 20 years after the intervention.

Another case is given by the structural retrofitting interventions carried out after an earthquake without taking into account the real behavior of the structures, both in the original and the modified condition, which left them more susceptible to subsequent quakes (Binda et al. 1999; Penazzi et al. 2000). Another instance reflects the poor choice in restoration materials that may turn out to be incompatible, depending on their location in the structures, as illustrated by the deterioration the pinnacles of St. Peter's and Paul's Cathedral in Brno (Bayer 2006). In the 19th century, the church suffered a Neogothic reconstruction, wherein two types of stone were used, sandstone and limestone, though the latter was originally also identified as a sandstone with a calcium-dolomite binder. This was used for the more delicately carved elements. Consequently, the limestone finials were set on top of the sandstone blocks of the pinnacles. With increasing air pollution, the limestone was attacked with the resulting formation of gypsum. This salt, being more soluble than the calcite, migrated into the sandstone block, deteriorating it heavily through recrystallization cycles. While the limestone finial was slowly eroded, the sandstone block immediately below it deteriorated heavily. Knowledgeable stone craftspeople would not have made this error.

One last example serves to illustrate the totally irreversible damage that can be inflicted upon an object. The object is the 17th century alabaster sarcophagus of the Duke Melchior von Hatzfeld in Laudenbach, which deteriorated over time and suffered several restorations. Between 1982 and 1984, the sarcophagus underwent a total acrylic impregnation (AVT), a method described in detail in a subsequent chapter (Sect. 7.10) after preliminary tests on sample slabs proved successful. The process involved several steps: drying at 100 °C for several days, vacuum treatment and subsequent flooding with methyl methacrylate monomer, and heating to

80 °C for in situ polymerization. Initially, the sarcophagus showed good superficial strengthening, but warping and cracking became evident some months later and continued to increase with time. The origin of this damage can be attributed to impregnation process, which involved subjecting the object to temperatures of 100 °C and to vacuum, causing the partial dehydration of the gypsum ($CaSO_4 \cdot 2H_2O$). The consequent heterogeneous material was, therefore, not uniformly impregnated. Upon exposure to the humid environment in the church where it is located, rehydration of the gypsum with its accompanying expansion took place, and a new restoration had to be implemented (Grassegger 2002).

As described in this chapter, deterioration of stone is a complex process. Many advances have been made in understanding the mechanisms underlying it, such as salt crystallization—definitely the single-most important deterioration factor—clay swelling, and thermal deformation of marbles. These advances include mathematical modeling that contribute both in identifying the critical factors that act under given conditions and in determining the amount of damage to be expected for a specified material subjected to certain stresses, as exemplified by the study of Derluyn et al. (2008). However, little has been done with regards to applying this knowledge in practice. Otherwise, how can we explain why a predeteriorated stone, such as flame-finished granite, is used in new construction instead of a plain sawed one that would last far longer? Why does the repair of faulty gutters take place only after severe damage to the masonry has occurred? This happens not only in the case of private houses but also for buildings of historical and artistic value.

While our understanding of materials and their deterioration increases, the gap between the theoretical understanding of the problem and the application of a solution to the practical situation is widening. Perhaps developing an expert system, similar to the Monument Damage Diagnostic System for the identification of structural patterns via an atlas (Binda et al. 2010; de Vent et al. 2010), could help to put into practice the extensive knowledge that has been gained. For this purpose, mathematical modeling is of fundamental importance.

References

Albertano P (2003) Methodological approaches to the study of stone alteration caused by cyanobacterial biofilms in hypogean environments. In: Koestler RJ, Koestler VH, Charola AE, Nieto Fernandez FE (eds) Art, biology and conservation: biodeterioration of works of art. The Metropolitan Museum of Art, New York, pp. 302–315

Alessandrini G, Peruzzi R, Manganelli del Fá C, Vannucci S, Tampone G, Cecchi R (1979) Investigation on the degradation of stones: VIII. The working effects on the Candoglia Marble. In: Proceedings of the 3rd international congress on stone deterioration and conservation. Universitá degli Studi di Padova, Padua, pp. 411–428

Allmann R, Kraus K (2003) Salze in historischem Mauerwerk. Ber Dt Min Ges Beih Eur J Mineral 15:5–6

Allsopp D, Seal K, Gaylarde CC (2003) Introduction to Biodeterioration. Cambridge University Press, Cambridge

Anderson RL, Ratcliffe I, Greenwell HC, Williams PA, Cliffe S, Coveney PV (2010) Clay swelling—a challenge in the oilfield. Earth Sci Rev 90:201–216

Angeli M, Bigas JP, Benavente D, Menéndez B, Hébert R, David C (2007) Salt crystallization in pores: quantification and estimation of damage. Environ Geol 52:205–213

Angeli M, Benavente D, Bigas JP, Menéndez B, Hébert R, David C (2008) Modification of the porous network by salt crystallization in experimentally weathered sedimentary stones. Mater Struct 41:1091–1108

Arnold A (1985) Moderne alkalische Baustoffe und die probleme bei der Konservierung von Denkmälern. Bayerisches Landesamt für Denkmalpflege. Arbeitshefte 31:152–162

Arnold A, Küng A (1985) Crystallization and habit of salt efflorescences on walls I. In: Félix G (ed) Proceedings of the 5th international congress on deterioration and conservation of stone. Presses Romandes, Lausanne, pp 255–267

Arnold A, Zehnder K (1985) Crystallization and habit of salt efflorescences on walls II. In: Félix G (ed) Proceedings of the 5th international congress on deterioration and conservation of stone. Presses Romandes, Lausanne, pp 269–277

Arnold A, Zehnder K (1989) Salt weathering on monuments. In: Zezza F (ed) The conservation of monuments in the mediterranean Basin. Grafo Edizioni, Bari, pp 31–58

Arnold A, Zehnder K (1991) Monitoring wall paintings affected by soluble salts. In: Cather S (ed) The conservation of wall paintings. Getty Conservation Institute, Los Angeles, pp 103–135

Attewell PB, Taylor D (1990) Time-dependent atmospheric degradation of building stone in a polluting environment. Environ Geol Water Sci 16:43–55

Baedeker PA, Reddy MM, Reimann KJ, Sciammarella CA (1992) Effects of acidic deposition on the erosion of carbonate stone—experimental results from the U.S. National Acid Precipitation Assessment Program (NAPAP). Atmos Environ 26B:147–158

Baer NS, Berman S (1983) Marble tombstones in national cemeteries as indicators of stone damage: General methods. In: Preprints 76th annual meeting of the APCA. Air Pollution Control Association, Atlanta, No. 83–5.7

Ballirano P, Melis E (2009) Thermal behaviour and kinetics of dehydration of gypsum in air from in situ real-time laboratory parallel-beam X-ray powder diffraction. Phys Chem Min 36:391–402

Bayer K (2006) Gypsum-an overlooked corrosive factor for some silicate sandstones in Czech Republic. In: Simon S and Drácky A (eds) European research on cultural heritage. State of the art studies, vol 5. Institute of Theoretical and Applied Mechanics, Prague, pp. 97–108

Beaudoin JJ, MacInnis C (1974) The mechanism of frost damage in hardened cement paste. Cem Concr Res 4:139–147

Becker GF, Day AL (1905) The linear force of growing crystals. Proc Wash Acad Sci 7:283–288

Becker GF, Day AL (1916) Note on the linear force of growing crystals. J Geol 24:313–333

Benavente D, Cueto N, Martínez Martínez J, García del Cura MA, Cañaveras JC (2007) The influence of petrophysical properties on the salt weathering of porous building rocks. Environ Geol 52:215–224

Bernabe Y (1991) Pore geometry and pressure dependence of the transport properties in sandstones. Geophysics 56:436–446

Bertagnagi A, Franzini M, Gratziu C, Spampinato M (1983) Il marmocotto in natura e nei monumenti. Rend Soc It Min Petrol 39:39–46

Binda L, Anzani A (1997) Structural behavior and durability of stone masonry. In: Baer NS, Snethlage R (eds) Saving our architectural heritage. Wiley, Chichester, pp 113–150

Binda L, Gambarotta L, Lagomarsino S, Modena C (1999) A multilevel approach to the damage assessment and seismic improvement of masonry buildings in Italy. In: Bernardini A (ed) Seismic damage to masonry buildings. Balkema, Rotterdam, pp 170–195

Binda L, Saisi A, de Vent IAE, van Hees RPJ, Naldini S (2010) Structural damage in masonry. Description and interpretation of crack patterns: basis for finding the damage causes. Rest Build Mon 16:77–98

Bionda D (2006) Modelling indoor climate and salt behaviour in historical buildings: a case study. Dissertation, Swiss Federal Institute of Technology, Zurich

Bionda D, Storemyr P (2002) Modelling the behavior of salt mixtures in walls: a case study from Tenaille von Fersen. In: von Konow T (ed) The study of salt deterioration mechanisms. Decay of brick walls influenced by interior climate changes. Suomenlinnan hoitokunta, Helsinki, pp 95–101

Blanchard DC, Woodcock AH (1980) The production, concentration, and vertical distribution of the sea-salt aerosol. Ann NY Acad Sci 338:330–347

Bourgès A, Fehr KT, Simon S, Snethlage R (2008) Correlation between micro-structure and the macroscopic behaviour of sandstones. Rest Build Monum 14:157–166

Braitsch O (1971) Salt deposits, their origin and composition. Springer, Berlin

Brajer I, Klenz Larsen P (2008) The salt reduction treatment on the wall paintings in Thirsted Church. In: Salt weathering on buildings and stone sculptures. Technical University of Denmark, Lyngby, pp. 219–228

Brimblecombe P, Rodhe H (1988) Air pollution—historical trends. Durability Build Mater 5:291–308

Bühmann C, DeVilliers JM, Fey MV (1988) The mineralogy of four heaving clays. Appl Clay Sci 3:219–236

Camuffo D, Del Monte M, Sabbioni C, Vittori O (1982) Wetting, deterioration and visual features of stone surfaces in an urban area. Atmos Environ 16:2253–2259

Cardell-Fernández C, Vleugels G, Torfs K, Van Grieken R (2002) The process dominating Ca dissolution of limestone when exposed to ambient atmospheric conditions as determined by comparing dissolution models. Environ Geol 43:160–171

Cecchi R, Tampone G, Vannucci S (1978) Effetti delle techniche di rifinitura della Pietra Serena fiorentina VII. Boll Ingegneri 1:3–22

Cedrola ML, Charola AE (2009) Biodeterioro de materiales porosos inorgánicos. In: Charola AE, Magadan ML (eds) Manual Báscio de conservación para las Misiones Jesuíticas Guaraníes. WMF, New York, pp 52–62

Charola AE (2000) Salt in the deterioration of porous materials. J Am Inst Conserv 39:327–343

Charola AE (2004) Stone deterioration in historic buildings and monuments. In: Kwiatkowski D, Löfvendahl (eds) Proceedings of the 10th international congress on deterioration and conservation of stone. ICOMOS Sweden, Stockholm, pp. 3–14

Charola AE, Lewin SZ (1979) Efflorescence on building stones—SEM in the characterization and elucidation of the mechanism of formation. Scan Electron Microsc 79(I):379–387

Charola AE, Weber J (1992) The hydration–dehydration mechanism of sodium sulfate. In: Delgado Rodrigues J, Henriques F, Telmo Jeremias F (eds) Proceedings of the 7th international congress on deterioration and conservation of stone. LNEC, Lisbon, pp. 581–590

Charola AE, Aires Barros L, Centeno SA, Basto MJ, Koestler RJ (2002) Analysis of colour traces found on the cloister of the Jeronimos monastery in Lisbon. Restor Build Monum 8:447–474

Charola AE, Pühringer J, Steiger M (2007) Gypsum: a review of its role in the deterioration of building materials. Environ Geol 52:339–352

Chatterji S, Jensen AD (1989) Efflorescence and breakdown of building materials. Nordic Concr Res 8:56–61

Chipera SJ, Vaniman DT (2007) Experimental stability of magnesium sulfate hydrates that may be present on Mars. Geochim Cosmochim Acta 71:241–250

Chkirda S, Kintrup H, Müller-Rochholz J (1999) Sorptionsmessungen von Baumberger Kalksandstein mit kapazitiven Feuchtefühlern. Berichtsband 69, 10. Feuchtetagung, Berlin, p. 18

Cooper TP (1986) Saving buildings from the weather. Technol Irel 32–35

Cooper BD (2008) Prevention of deterioration from salt contamination in heritage artefacts. In: Salt weathering on buildings and stone sculptures. Technical University of Denmark, Lyngby

Cooper TP, O'Brien PF, Jeffrey DW (1992) Rates of deterioration of Portland limestone in an urban environment. Stud Conserv 37:228–238

Correns CW, Steinborn W (1939) Experimente zur Messung und Erklärung der sogenannten Kristallisationskraft. Z Krist A101:117–135

Coussy O (2004) Poromechanics. Wiley, Chichester

Crispim CA, Gaylarde CC (2004) Cyanobacteria and biodeterioration of cultural heritage: a review. Microb Ecol 49:1–9. doi:10/s0024800310525
Cultrone G, Russo LG, Calabrò C, Uroševic M, Pezzino A (2008) Influence of pore system characteristics on limestone vulnerability: a laboratory study. Environ Geol 54:1271–1281
Dadachova E, Bryan RA, Huang X, Moadel T, Schweizer AD (2007) Ionizing radiation changes the electronic properties of melanin and enhances the growth of melanized fungi. PLoS ONE 2:e457
De Clercq H (2008) The effect of other salts on the crystallization damage to stone caused by sodium sulphate. In: Salt weathering on buildings and stone sculptures. Technical University of Denmark, Lyngby, pp 307–315
de Quervain F, Jenny V (1951) Verhalten der Bausteine gegen Witterungseinflüsse in der Schweiz. In: Schweizerische Geotechnische Kommission (ed) Beiträge zur Geologie der Schweiz, Geotechnische Serie, vol 30. Lieferung, Kümmerly and Frey, Geographischer Verlag, Berlin, pp 1–66
de Vent IAE, Naldini S, van Hees RPJ, Binda L, Saisi A (2010) Definition of structural damage patterns: a structural damage atlas. Rest Build Mon 13:167–186
Del Monte M, Sabbioni C (1984) Gypsum crusts and fly ash particles on carbonatic outcrops. Arch Meteorol Geophys Bioclimatol B 35:105–111
Del Monte M, Sabbioni C (1987) A study of the patina called 'scialbatura' on imperial Roman marbles. Stud Conserv 32:114–121
Del Monte M, Sabbioni C, Vittori O (1981) Airborne carbon particles and marble deterioration. Atmos Environ 15:645–652
Del Monte M, Sabbioni C, Zappia G (1987) The origin of calcium oxalates on historical buildings, monuments and natural outcrops. Sci Total Environ 67:17–39
Delgado Rodrigues J (1996) Conservation of granitic rocks with application to the megalithic monuments. Conclusion report project STEP CT90-110. In: Vicente MA, Delgado Rodrigues J, Acevedo J (eds) Degradation and conservation of granitic rocks in monuments. Protection and conservation of European cultural heritage research report No. 5. European Commission Directorate General XII. Brussels, pp 178–189
Derluyn H, Poupeleer AS, Van Gemert D, Carmeliet J (2008) Salt crystallization in hydrophobic porous materials. In: De Clercq H, Charola AE (eds) Hydrophobe V. Water repellent treatment of building materials. Aedificatio, Freiburg, pp 97–108
Dionisio A, Aires Barros L (2004) Fire effects on stone materials. The case of Lisbon's Cathedral. In: Proceedings of the 6th international symposium. Conservation of monuments in the mediterranean Basin, (CD) Lisbon, pp 143–147
Dionisio A, Rodrigues M, Sequeira Braga MA, Andre H, Waerenburgh JC, Rojas DP, Basto MJ, Matias MJ, Aires Barros L (2005) Study of heat induced colour modifications in limestone used in monuments. Rest Build Mon 11:199–210
Doehne E (1994) In situ dynamics of sodium sulfate hydration and dehydration in stone pores: observations at high magnification using the environmental SEM. In: Zezza F, Ott H, Fassina V (eds) Conservation of monuments in the Mediterranean Basin, Proceedings of the 3rd international symposium, Venice, pp 143–150
Doehne E (2002) Salt weathering: a selective review. In: Siegesmund S, Weiss T, Vollbrecht A (eds) Natural stones, weathering phenomena, conservation strategies, and case studies, Special publication 205. Geological Society, London, pp 51–64
Drever JI (1994a) Durability of stone: mineralogical and textural perspectives. In: Krumbein WE, Brimblecombe P, Cosgrove DE, Staniforth S (eds) Durability and change. Wiley, Chichester, pp 27–39
Drever JI (1994b) The effect of land plants on weathering rates of silicate minerals. Geochim Cosmochim Acta 58:2325–2332
Ehrlich HL (2009) Geomicrobiology, 5th edn. CRC, Boca Raton 606p
Espinosa-Marzal RM, Scherer GW (2008) Crystallization of sodium sulfate salts in limestones. Environ Geol 56:605–621

Espinosa-Marzal RM, Scherer GW (2009) Crystallization pressure exerted by in-pore confined crystals. In: Ling HI, Smyth A, Betti R (eds) Poromechanics IV, Proceedings of the 4th Biot conference on poromechanics. DE-Stech Publications, Lancaster, pp 1013–1018

Espinosa-Marzal RM, Scherer GW (2010) Mechanisms of damage by salt. In: Smith BJ, Gomez-Heras M, Viles HA, Cassar J (eds) Limestone in the built environment: present-day challenges for the preservation of the past. Geological Society, London, Special Publications 331, pp 61–77

Espinosa-Marzal RM, Hamilton A, McNall M, Whitaker K, Scherer GW (2011) The chemomechanics of crystallization during rewetting of limestone impregnated with sodium sulfate. J Mater Res 26:1472–1481

Evans IS (1970) Salt crystallization and rock weathering: a review. Rev Geomorph Dyn 19:153–177

Everett DH (1961) The thermodynamics of frost damage to porous solids. Trans Faraday Soc 57:1541–1551

Feddema JJ, Meierding TC (1987) Marble weathering and air pollution in Philadelphia. Atmos Environ 21:143–157

Flatt RJ (2002) Salt damage in porous materials: how high supersaturations are generated. J Cryst Growth 242:435–454

Flatt RJ, Steiger M, Scherer GW (2007) A commented translation of the paper by C.W. Correns and W. Steinborn on crystallization pressure. Environ Geol 52:187–203

Franzen C, Mirwald PW (2004) Moisture content of natural stone: static and dynamic equilibrium with atmospheric humidity. Environ Geol 46:391–401

Franzini M, Gratziu C, Spampinato M (1983) Degradazione del marmo per effetto di variazione di temperatura. Rend Soc It Min Petrol 39:47–58

Fredrich JT, Wong TE (1986) Micromechanics of thermally induced cracking in three crustal rocks. J Geophys Res 91:12743–12764

Fritz (1922) Steinverbiegungen als Verwitterungserscheinungen. Die Denkmalpflege 24(7):53–55

Gadd GM (2007) Geomycology: biogeochemical transformations of rocks, minerals and radionuclides by fungi, bioweathering and bioremediation. Mycol Res 111:3–49

Gaylarde CC, Gaylarde PM (2005) A comparative study of the major microbial biomass of biofilms on exteriors of buildings in Europe and Latin America. Int Biodeterior Biodegradation 55:131–139

Ginell WS (1994) The nature of changes caused by physical factors. In: Krumbein WE, Brimblecombe P, Cosgrove DE, Staniforth S (eds) Durability and change. Wiley, Chichester, pp 81–94

Gómez-Heras M, Smith BJ, Fort R (2008) Influence of surface heterogeneities of building granite on its thermal response and its potential for the generation of thermoplasty. Environ Geol 56:547–560

Goudie A, Viles H (1997) Salt weathering hazards. Wiley, Chichester

Grassegger G (2002) Restorations of the sarcophagus of Duke Melchior von Hatzfeld-the accompanying scientific and technical investigations. Otto Graf J 13:141–154

Grimmer AE (1984) A glossary of historic masonry deterioration problems and preservation treatments. Department of the interior. National Park Service Preservation Assistance Division, Washington, DC

Grissom CA, Charola AE, Wachowiak MJ (2000) Measuring surface roughness: back to basics. Stud Conserv 45:73–84

Grossi CM, Esbert RM, Suárez del Rio LM, Montato M, Laurenzi-Tabasso M (1997) Acoustic emission monitoring to study sodium sulphate crystallization in monumental porous carbonate stones. Stud Conserv 42:115–125

Gunde-Cimerman N, Ramos J, Plemenitas A (2009) Halotolerant and halophilic fungi. Mycol Res 113:1231–1241

Hajpál M, Török A (2004) Mineralogical and color changes of quartz sandstones by heat. Environ Geol 46:311–322

Hall C, Hoff WD (2002) Water transport in brick, stone and concrete. Taylor and Francis, London

Hall C, Hoff WD (2007) Rising damp: capillary rise dynamics in walls. Proc Roy Soc A 463: 1871–1884

Halsey DP, Dews SJ, Mitchell DJ, Harris FC (1995) Real time measurements of sandstone deterioration: a microcatchment study. Build Environ 30:411–417

Hamilton A, Hall C, Pel L (2008) Sodium sulfate heptahydrate: direct observation of crystallization in a porous material. J Phys D 41:212002

Hardie LA, Eugster HP (1970) The evolution of closed-basin brines. Mineral Soc Am Spec Pap 3:273–290

Hodgman CD, Weast RC, Shankland RS, Selby SM (eds) (1963) Handbook of chemistry and physics. The Chemical Rubber Publishing Co, Cleveland

Honeyborne DB, Price CA (1977) Air pollution and the decay of limestones. Building Research Establishment. Garston, BRE Note 117/77

Hosono T, Uchida E, Suda C, Ueno A, Nakagawa T (2006) Salt weathering of sandstone at the Ankor monuments, Cambodia: identification of the origin of salts using sulfur and strontium isotopes. J Archaeolog Sci 33:1541–1551

Jaynes SM, Cooke RU (1987) Stone weathering in Southeast England. Atmos Environ 21:1601–1622

Jerwood LC, Robinson DA, Williams RBG (1990a) Experimental frost and salt weathering of chalk I. Earth Surf Proc Land 15:611–624

Jerwood LC, Robinson DA, Williams RBG (1990b) Experimental frost and salt weathering of chalk II. Earth Surf Proc Land 15:699–708

Julien A (1883) The decay of building stones in New York City. Am Arch Build News 13:76–77

Kemmling A, Kamper M, Flies C, Schieweck O, Hoppert M (2004) Biofilms and extracellular matrices on geomaterials. Environ Geol 46:429–435

Kessler DW (1919) Physical and chemical tests on the commercial marbles of the US. NBS Technologic Paper 123. Government Printing Office, Washington, DC

Kleber W (1959) Einführung in die Kristallographie. VEB Verlag Technik, Berlin

Klenz Larsen P (1999) Desalination of painted brick vaults. Ph.D. thesis, The National Museum of Denmark, The Technical University of Denmark, Lyngby

Klenz Larsen P (2004) Moisture measurements in Thirsted Church. J Architect Conserv 10:22–35

Klenz Larsen P (2007) The salt decay of medieval bricks at a vault in Brarup Church, Denmark. Environ Geol 52:375–383

Koch A, Siegesmund S (2004) The combined effect of moisture and temperature on the anomalous expansion behaviour of marble. Environ Geol 46:350–363

Koestler RJ, Brimblecombe P, Camuffo D, Ginell WS, Graedel TE, Leavengood P, Petushkova J, Steiger M, Urzì C, Vergès-Belmin V, Warscheid T (1994) How do external environmental factors accelerate change? In: Krumbein WE, Brimblecombe P, Cosgrove DE, Staniforth S (ed) Durability and change. The science, responsibility, and cost of sustaining cultural heritage. Dahlem workshop reports. Wiley, Chichester, pp 149–163

Kucera V, Tidblad J, Kreislova K, Knotkova D, Faller M, Reiss D, Snethlage R, Yates T, Henriksen J, Schreiner M, Melcher M, Ferm M, Lefèvre RA, Kobus J (2007) UN/ECE ICP Materials dose-response functions for the multi-pollutant situation. Water Air Soil Pollut Focus 7:249–258

Lasaga AC, Soler JM, Ganor J, Burch TE, Nagy KL (1994) Chemical weathering rate laws and global geochemical cycles. Geochim Cosmochim Acta 58:2361–2386

Lazzarini L, Salvadori O (1989) A reassessment of the formation of the patina called 'scialbatura'. Stud Conserv 34:20–26

Leitner H, Laue S, Siedel H (eds) (2003) Mauersalze und Architekturoberflächen. Hochschule für Bildende Künste, Dresden

Lewin SZ (1974) Book review. Stud Conserv 19:249–252

Lewin SZ, Charola AE (1981) Stone decay due to foreign inclusions. In: The conservation of stone II. Part A. Centro per la conservazione delle sculture all'aperto, Bologna, pp 205–217

Linnow K, Zeunert A, Steiger M (2006) Investigation of sodium sulfate phase transitions in a porous material using humidity and temperature controlled X-ray diffraction. Anal Chem 78:4683–4689

Lisci L, Monte M, Pacini E (2003) Lichens and higher plants on stone: a review. Int Biodeterior Biodegr 51:1–17

Litvan GG (1978) Adsorption systems at temperatures below the freezing point of the adsorptive. Adv Colloid Interface Sci 9:253–302

Livingston RA (1986) Evaluation of building deterioration by water runoff. In: Davis G (ed) Building performance: function, preservation, and rehabilitation. ASTM, Philadelphia, pp 181–188

Livingston RA (1992) Graphical methods for examining the effects of acid rain and sulfur dioxide on carbonate stones. In: Delgado Rodrigues J, Henriques F, Telmo Jeremias F (ed) Proceedings of the 7th international congress on deterioration and conservation of stone. Laboratorio Nacional de Engenheria Civil, Lisbon, pp 375–386

Madsen FT, Müller-Vonmoos M (1989) The swelling behaviour of clays. Appl Clay Sci 4:143–156

Malaga-Starzec K, Lindquist JE, Björn S (2002) Experimental study on the variation in porosity of marble as function of temperature. In: Siegesmund S, Weiss, T, Vollbrecht A (eds) Natural stone, weathering phenomena, conservation strategies and case studies. Geol Soc Special Publication No. 205. The Geological Society, London, pp 81–88

Matthes S (1987) Mineralogie. Springer, Heidelberg, p 417

Matzuoka N, Moriwaki K, Hirakawa K (1996) Field experiments on physical weathering and wind erosion in an Antarctic cold desert. Earth Surf Proc Land 21:687–699

Mausfeld SA, Grassegger G (1992) Abbauprozesse an Feldspäten und Tonmineralen unter den Bedingungen der Bauwerksverwitterung. Z dt geol Ges 143:23–39

Mausfeld SA, Grassegger G (1994) The changing environment of pore solutions in natural building stones during immission accelerated weathering processes. In: Zezza F, Ott H, Fassina V (eds) Proceedings of the 3rd international symposium conservation of monuments in the Mediterranean Basin, Venice, pp 129–135

Selbmann L, Hoog GS De, Mazzaglia, A, Friedmann EI, Onofri S (2005) Fungi at the edge of life: cryptoendolithic black fungi from the Antarctic desert. In: de Hogg GS (ed) Fungi of the Antarctic: evolution under extreme conditions. Stud Mycol 51:1–32

McGreevy JP (1982) 'Frost and salt' weathering: further experimental results. Earth Surf Proc Land 7:475–488

McGreevy JP, Smith BJ (1984) The possible role of clay minerals in salt weathering. Catena 11:169–175

McKinstry HA (1965) Thermal expansion of clay minerals. Amer Mineral 50:212–222

Monte M (2003) Oxalate film formation on marble specimens caused by fungus. J Cult Herit 4:255–258

Mortensen H (1933) Die "Salzsprengung" und ihre Bedeutung für die regionalklimatische Gliederung der Wüsten. Petermans Mitteilungen aus Justus Perthes geographischer Anstalt 79:130–135

Neumann H–H, Steiger M, Wassmann A, Dannecker W (1993) Aufbau und Ausbildung schwarzer Gipskrusten und damit zusammenhängender Gefügeschäden von Naturwerksteinen am Beispiel des Leineschlosses (Hannover). In: Snethlage R (ed) Jahresberichte steinzerfall–steinkonservierung band 3–1991. Verlag Ernst and Sohn, Berlin, pp 151–167

Neumann H–H, Lork A, Steiger M, Juling H (1997) Decay patterns of weathered quartz sandstones: evidence for gypsum induced structural changes. In: Sveinsdóttir EL (ed) Proceedings of the 6th euro seminars on microscopy applied to building materials. Icelandic Building Research Institute, Reykjavik, pp 238–249

Nielsen AE (1964) Kinetics of precipitation. Pergamon, Oxford

Nord AG, Ericsson T (1993) Chemical analysis of thin black layers on building stone. Stud Conserv 38:25–35

Nord AG, Tronner K (1991) Stone weathering. Conservation Institute of National Antiquities, Stockholm, pp 24–44

O'Grady C (2005) The occurrence of rock varnish on stone and ceramic artifacts. Rev Conserv 5:35–42

Ondrasina J, Kirchner D, Siegesmund S (2002) Freeze-thaw cycles and their influence on marble deterioration: a long term experiment. In: Siegesmund S, Weiss T, Vollbrecht A (eds) Natural stones, weathering phenomena, conservation strategies, and case studies, Special Publication 205. Geological Society, London, pp 9–18

Ortega-Morales BO, Gaylarde CC, Englert GE, Gaylarde PM (2005) Analysis of salt-containing biofilms on limestone buildings of the Mayan culture at Edzna, Mexico. Geomicrobiol J 22:261–268

Ottosen LM, Rörig-Dalgaard I, Klenz Larsen P, Brajer I, Bøllingstoft P, Marciniak M, Svane M (eds) (2008) Salt weathering on buildings and stone sculptures. Technical University of Denmark, Copenhagen

Ožbolt J, Grassegger G, Van der Beken P, Periškić G, Reinhard HW (2008) Experimental and numerical study of hygro-thermo-mechanical properties of "Schilfsandstein" from Baden/Württemburg. Env Geol 56:535–546

Pauly JP (1976) Maladie alvéolaire. Conditions de formation et d'évolution. In: Rossi Manaresi R (ed) The conservation of stone I. centro per la consrvazione delle sculture all'aperto. Bologna, pp 55–80

Penazzi D, Valluzzi MR, Cardani G, Binda L, Baronio G, Modena C (2000) Behaviour of historic masonry buildings in seismic areas: lessons learned from the Umbria-March earthquake. Proceedings of the 12th international conference of IBBMac, vol 1. Universidad Politécnica, Madrid, pp 217–235

Piñar U, Sterflinger K (2009) Microbes and building materials. In: Cornejo DN, Haro JL (eds) Building materials: properties, performance and applications. Nova Publishers, New York, pp 163–188

Pitzer KS (1991) Ion interaction approach: theory and data correlation. In: Pitzer KS (ed) Activity coefficients in electrolyte solutions. CRC Press, Boca Raton, pp 75–153

Price CA (1978) The use of the sodium sulphate crystallisation test for determining the weathering resistance of untreated stone. In: UNESCO/RILEM international symposium, Paris, vol 3.6, pp 1–23

Price CA (ed) (2000) An expert chemical model for determining the environmental conditions needed to prevent salt damage in porous materials. Protection and conservation of the European cultural heritage research report No. 11. Archetype Publications, London

Price CA (2007) Predicting environmental conditions to minimise salt damage at the Tower of London: a comparison. Environ Geol 52:369–374

Price CA, Brimblecombe P (1994) Preventing salt damage in porous materials. In: Preventive conservation: practice, theory and research. International Institute for Conservation, London, pp 90–93

Prokos P (2008) Equilibrium conditions of marine originated salt mixtures: an ECOS application at the archaeological site of Delos, Greece. Salt weathering on buildings and stone sculptures. Technical University of Denmark, Lyngby, pp 139–148

Reddy MM (1988) Acid rain damage to carbonate stone: a quantitative assessment based on the aqueous geochemistry of rainfall runoff from stone. Earth Surf Proc Land 13:335–354

Reddy MM, Sherwood S, Doe B (1985) Limestone and marble dissolution by acid rain. In: Félix G (ed) Proceedings of the 5th international congress on deterioration and conservation of stone. Presses Polytechniques Romandes, Lausanne, pp 517–526

Reeder R, Markgraf SA (1986) High temperature crystal chemistry of dolomite. Am Mineral 71:795–804

Rijniers LA, Huinink HP, Pel L, Kopinga K (2005) Experimental evidence of crystallization pressure inside porous media. Phys Rev Lett 94:075503

RILEM PEM-25 (1980) Recommended tests to measure the deterioration of stone and to assess the effectiveness of treatment methods. Mater Struct 13:175–253

Rivadeneyra MA, Párraga J, Delgado R, Ramos-Cormenzana A, Delgado G (2004) Biomineralization of carbonates by Halobacillus trueperi in solid and liquid media with different salinities. FEMS Microbiol Ecol 48:39–46
Rodriguez-Navarro C, Doehne E (1999) Salt weathering: influence of evaporation rate, supersaturation and crystallization pattern. Earth Surf Proc Land 24:191–209
Rodriguez-Navarro C, Hansen E, Sebastián E, Ginell W (1997) The role of clays in the decay of ancient Egyptian limestone sculptures. J Am Inst Cons 36:151–163
Rodriguez-Navarro C, Doehne E, Sebastian E (2000) How does sodium sulfate crystallize? Implications for the decay and testing of building materials. Cem Concr Res 30:1527–1534
Roekens E, van Grieken R (1989) Rates of air pollution induced surface recession and material loss for a cathedral in Belgium. Atmos Environ 23:271–277
Rönicke G, Rönicke R (1972) Über den Mechanismus der zerstörenden Wirkung der Luftverunreinigung am Freiburger Münster. Dt Kunst- Denkmalpfl 30:57–64
Royer-Carfagni GF (1999) On the thermal degradation of marble. Int J Rock Mech Min Sci 36:119–126
Ruedrich J, Siegesmund S (2007) Salt and ice crystallization in porous sandstones. Environ Geol 52:225–249
Ruedrich J, Weiss T, Siegesmund S (2002) Weathering of treated marbles. Geol Soc Spec Publ 205:254–272
Ruedrich J, Kirchner D, Seidel M, Siegesmund S (2005) Beanspruchungen von Naturwerksteinen durch Salz- und Eiskristallisation im Porenraum sowie hygrische Dehnungsvorgänge. Z Dt Ges Geowiss 156:58–73
Ruedrich J, Bartelsen T, Dohrmann R, Siegesmund S (2011) Moisture expansion as a deterioration factor for sandstone used in buildings. Environ Earth Sci 63:1545–1564
Saarela M, Alakomi HL, Suihko ML, Maunuksela L, Raaska L, Mattila-Sandholm T (2004) Heterotrophic microorganisms in air and biofilm samples from Roman catacombs, with special emphasis on actinobacteria and fungi. Int Biodet Biodegr 54:27–37
Sage JD (1988) Thermal microfracturing of marble. In: Marinos PG, Kouis GC (eds) Engineering geology of ancient works, monuments and historic sites. Balkema, Rotterdam, pp 1013–1018
Saiz Jimenez C (1993) Deposition of airborne organic pollutants on historic buildings. Atmos Environ 27B:77–85
Salles F, Douillard JM, Denoyel R, Bildstein O, Julien M, Beurroies I, Van Damme H (2009) Hydration sequence of swelling clays: evolution of specific surface area and hydration energy. J Colloid Interface Sci 333:510–522
Sánchez Pastor N, Aldushin K, Jordan G, Schmahl WW (2010) K^+ -Na^+ exchange in phlogopite on the scale of a single layer. Geochim Cosmochim Acta 74:1954–1962
Sawdy A (2001) The kinetics of salt weathering of porous materials: stone monuments and wall paintings. Ph.D thesis, Institute of Archaeology, University College, London
Sawdy A, Price CA (2005) Salt damage at Cleeve Abbey, England. Part I: a comparison of theoretical predictions and practical observations. J Cult Heritage 6:125–135
Schäfer M, Steiger M (2002) A rapid method for the determination of cation exchange capacities of sandstone: preliminary data. In: Siegesmund S, Weiss T, Vollbrecht A (eds) Natural stone, weathering phenomena, conservation strategies and case studies. Geological Society London, Special Publications 205:431–439
Scheerer S, Ortega-Morales O, Gaylarde C (2009) Microbial deterioration of stone monuments—an updated overview. Adv Microbiol 66:97–139
Scheffer F, Schachtschabel P (1984) Lehrbuch der bodenkunde, 11th edn. Enke Verlag, Stuttgart
Scherer GW (1999) Crystallization in pores. Cem Concr Res 29:1347–1358
Scherer GW (2004) Stress from crystallization of salt. Cem Concr Res 34:1613–1624
Scherer GW, Valenza JJ (2004) Mechanisms of frost damage. In: Young F, Skalny J (eds) Materials science of concrete VII. The American Ceramic Society, Westerville, pp 209–246
Schiavon N (1992) Decay mechanism of oolitic limestones in an urban environment: King's College Chapel, Cambridge and St Luke's Church, London. In: Webster RGM (ed) Stone

cleaning and the nature, soiling and decay mechanisms of stone. Donhead, London, pp 258–267
Schlütter F, Juling H, Steiger M (2003) Schädigung von chlorid- und nitratbelastetem Ziegelmauerwerk: Kryo-REM-Untersuchungen zur Wirkungsweise eines Salzgemisches. In: Leitner H, Laue S, Siedel H (eds) Mauersalze und architekturoberflächen. Hochschule f, Bildende Künste, pp 72–78
Schmölzer A (1936) Zur entstehung der verwitterungsskulpturen an bausteinen. Chem Erde 10:479–520
Sebastián E, Cultrone G, Benavente D, Linares Fernández L, Elert K, Rodriguez-Navarro C (2008) Swelling damage in clay-rich sandstones used in the church of San Mateo in Tarifa (Spain). J Cult Heritage 9:66–76
Senkayi AL, Dixon JB, Hossner RL (1981) Transformation of chlorite to smectite through regularly in stratified intermediates. Soil Sci Soc Am J 45:650–656
Sharp AD, Trudgill ST, Cooke RU, Price CA, Crabtree RW, Pickles AM, Smith DI (1982) Weathering of the balustrade on St. Paul's Cathedral, London. Earth Surf Proc Land 7:387–389
Shushakova V, Fuller ER Jr, Siegesmund S (2011) Influence of shape fabric and crystal texture on marble degradation phenomena: simulations. Environ Earth Sci 63:1587–1601. doi:10.1007/s12665-010-0744-7
Siedel H (2009) Zur herkunft von salzen an bauwerken. In: Schwarz H-J, Steiger M (eds) Salzschäden an kulturgütern. Ri-Con, Hanover, pp 22–29
Siedel H, von Plehwe-Leisen E, Leisen H (2008) Salt load and deterioration of sandstone at the temple of Angkor Wat, Cambodia. Proceedings of the 11th international congress on deterioration and conservation of stone. Nicolaus Copernicus University Press, Torun, pp 267–274
Siegesmund S, Weiss T, Vollbrecht A, Ullemeyer K (1999) Marble as a natural building show: rock fabrics, physical and mechanical properties. Z Dt Geol Ges 150:237–257
Siegesmund S, Ullemeyer K, Weiss T, Tschegg EK (2000) Physical weathering of marbles. Int J Earth Sci 89:170–182
Siegesmund S, Ruedrich J, Weiss T (2004) Marble deterioration. In: Prikryl R (ed) Dimension Stone 2004. Taylor and Francis Group, London, pp 211–217
Siegesmund S, Mosch S, Scheffchük C, Nikolayev DI (2008a) The bowing potential of granitic rocks: rock fabric, thermal properties and residual strain. Environ Geol 55:1437–1448
Siegesmund S, Ruedrich J, Koch A (2008b) Marble bowing: comparative studies of three different public building facades. Environ Geol 56:473–494
Simon S, Drdácky M (eds) (2006) Problems of salts in masonry-SALTeXPERT. European research on cultural heritage. State-of-art studies, vol 5. Institute of Theoretical and Applied Mechanics, Academy of Sciences, Prague
Sippel J, Siegesmund S, Weiss T, Nitsch KH, Korsen M (2007) Decay of natural stones caused by fire damage. In: Prikryl R and Smith BJ (eds) Building stone decay: from diagnosis to conservation. geological society special publication 271. The Geological Society, London, pp 139–151
Smith BJ, Magee RW, Whalley WB (1994) Breakdown patterns of quartz sandstone in a polluted urban environment, Belfast, Northern Ireland. In: Robinson DA, Williams RBG (eds) Rock Weathering and landform evolution. Wiley, Chichester, pp 131–150, 139–151
Snethlage R (1984) Steinkonservierung 1979–1983. Arbeitsheft 22. Bayerisches Landesamt für Denkmalpflege, Munich
Snethlage R, Wendler E (1997) Moisture cycles and sandstone degradation. In: Baer NS, Snethlage R (eds) Saving our architectural heritage: conservation of historic stone structures. Wiley, Chichester, pp 7–24
Steiger M (1996) Distribution of salt mixtures in a sandstone monument: Sources, transport and crystallization properties. In: Zezza F (ed) Origin, mechanisms and effects of salts on degradation of monuments in marine and continental environments. Protection and conservation of the European cultural heritage research report no. 4, pp 241–246

Steiger M (2003) Salts and crusts. In: Brimblecombe P (ed) Air pollution reviews, vol 2. The effects of air pollution on the built environment. Imperial College Press, London, pp 133–181
Steiger M (2004) Influence of salts on the freezing temperature of water: implications on frost damage to porous materials. In: Kwiatkowski D, Löfvendahl R (eds) Proceedings of the 10th international congress on deterioration and conservation of stone. ICOMOS, Stockholm, pp 179–186
Steiger M (2005a) Crystal growth in porous materials—I: the crystallization pressure of large crystals. J Cryst Growth 282:455–469
Steiger M (2005b) Crystal growth in porous materials—II: influence of crystal size on the crystallization pressure. J Cryst Growth 282:470–481
Steiger M (2005c) Salts in porous materials: thermodynamics of phase transitions, modeling and preventive conservation. Restor Build Monum 11:419–432
Steiger M (2006a) Crystal Growth in porous materials: influence of supersaturation and crystal size. In: Fort R, Alvarez de Buergo M, Gomez-Heras M, Vazquez-Calvo C (eds) Heritage, weathering and conservation, vol 1. Taylor and Francis, London, pp 245–251
Steiger M (2006b) Freezing of salt solutions in small pores. In: Konsta-Gdoutos MS (ed) Measuring, monitoring and modeling concrete properties. Springer, Dordrecht, pp 661–668
Steiger M, Asmussen S (2008) Crystallization of sodium sulfate phases in porous materials: the phase diagram Na_2SO_4–H_2O and the generation of stress. Geochim Cosmochim Acta 72:4291–4306
Steiger M, Dannecker W (1994) Determination of wet and dry deposition af atmospheric pollutants on building stones by field exposure experiments. In: Zezza F, Ott H, Fassina V (eds) Conservation of monuments in the Mediterranean Basin. Proceedings of the 3rd international symposium, Venice, pp 171–178
Steiger M, Dannecker W (1995) Hygroskopische eigenschaften und kristallisationsverhalten von salzgemischen. In: Snethlage R (ed) Jahresberichte aus dem forschungsprogramm steinzerfall—steinkonservierung. Band 5–1993. Verlag Ernst and Sohn, Berlin, pp 115–128
Steiger M, Zeunert A (1996) Crystallization properties of salt mixtures—comparison of experimental results and model calculations. In: Riederer J (ed) International congress on deterioration and conservation of stone—proceedings. Möller Druck und Verlag GmbH, Berlin, pp 535–544
Steiger M, Wolf F, Dannecker W (1993) Deposition and enrichment of atmospheric pollutants on building stones as determined by field exposure experiments. In: Thiel M-J (ed) Conservation of stone and other materials. E&FN SPON, London, pp 35–42
Steiger M, Behlen A, Neumann H-H, Willers U, Wittenburg C (1997) Sea salt in historic buildings: deposition, transport and accumulation. In: Moropoulou A, Zezza F, Kollias E, Papachristodoulou I (eds) Proceedings of the 4th international symposium on the conservation of monuments in the mediterranean, vol 1. Rhodes, pp 325–335
Steiger M, Neumann HH, Grodten T, Wittenburg C, Dannecker W (1998) Salze in natursteinmauerwerk—probenahme, messung und interpretation. In: Snethlage R (ed) Handbuch Naturwissenschaft und Denkmalpflege: Natursteinkonservierung II. Fraunhofer IRB Verlag, Stuttgart, pp 61–91
Steiger M, Kiekbusch J, Nicolai A (2008a) An improved model incorporating Pitzer's equations for calculation of thermodynamic properties of pore solutions implemented into an efficient program code. Constr Build Mater 22:1841–1850
Steiger M, Linnow K, Juling H, Gülker G, El Jarad A, Brüggerhoff S, Kirchner D (2008b) Hydration of $MgSO_4 \cdot H_2O$ and generation of stress in porous materials. Cryst Growth Des 8:336–343
Steiger M, Linnow K, Ehrhardt D, Rohde M (2011) Decomposition reactions of magnesium sulfate hydrates and phase equilibria in the $MgSO_4$–H_2O and Na^+–Mg^{2+}–Cl^-–SO_4^{2-}–H_2O systems with implications for Mars. Geochim Cosmochim Acta 75:3600–3626
Sterflinger K (2000) Fungi as geologic agents. Geomicrobiol J 17:97–124

Sterflinger K (2005) Black yeasts and meristematic fungi: ecology, diversity and identification. In: Rosa C, Gabor P (eds) Yeast handbook, vol 1. Biodiversity and ecophysiology of yeasts. Springer, New York

Stockhausen N (1981) Die dilatation hochporöser festkörper bei wasseraufnahme und eisbildung, thesis. Technical University, Munich

Stumm W, Wollast R (1990) Coordination chemistry of weathering: kinetics of the surface controlled dissolution of oxide minerals. Rev Geophys 28:53–69

Taber S (1916) The growth of crystals under external pressure. Am J Sci 41:532–556

Taber S (1929) Frost heaving. J Geol 37:428–461

Taber S (1930) The mechanics of frost heaving. J Geol 38:303–317

Tang IN (1997) Thermodynamic and optical properties of mixed-salt aerosols of atmospheric importance. J Geophys Res 102:1883–1893

Theoulakis P, Moropoulou T (1988) Mechanisms of deterioration of the sandstone of the medieval city of Rhodes. In: Ciabach J (ed) Proceedings of the 6th international congress on deterioration and conservation OF Stone. Nicholas Copernicus University, Torun, pp 86–96

Török A, Hajpál M (2005) Effect of temperature changes on the mineralogy and physical properties of sandstones. A laboratory study. Rest Build Mon 11:211–218

Trudgill ST, Viles HA, Inkpen RJ, Cooke RU (1989) Remeasurement of weathering rates, St. Paul's Cathedral, London. Earth Surf Proc Land 14:175–196

Tsui N, Flatt RJ, Scherer GW (2003) Crystallization damage by sodium sulfate. J Cult Heritage 4:109–115

Turkington AV, Smith BJ, Basheer PAM (2002) The effect of block retreat on subsurface temperature and moisture conditions in sandstone. In: Přikryl R, Viles H (eds) Understanding and managing stone decay. The Karolinum Press, Prague, pp 113–126

UNI 11182 (2006) Beni culturali. materiali lapidei naturali ed artificiali. Descrizione della forma di alterazione—termini e definizioni. UNI, Milano

Hees RPJ Van, Brendle S, Nijland TG, Haas GJLM De, Tolboom HJ (2004) Decay of Rhenish tuff in Dutch monuments. In: Kwiatkowski D, Löfvendahl (eds) Proceedings of the 10th international congress on deterioration and conservation of stone. ICOMOS Sweden, Stockholm, pp 91–98

Van TT, Beck K, Al'Mukhtar M (2007) Accelerated weathering tests on two highly porous limestones. Env Geol 52:282–292

Vergès-Belmin V (1994) Pseudomorphism of gypsum after calcite, a new textural feature accounting for the marble sulphation mechanism. Atmos Environ 28:295–304

Vergès-Belmin V (ed) (2008) Illustrated glossary on stone deterioration patterns. Monuments and Sites XV. ICOMOS, Paris

Von Konow T (2002) Test results. In: von Konow T (ed) The study of salt deterioration mechanisms. Decay of brick walls influenced by interior climate changes. Suomenlinnan Hoitokunta, Helsinki, pp 57–79

Walder JS, Hallet B (1986) The physical basis of frost weathering: toward a more fundamental and unified perspective. Arct Alp Res 18:27–32

Wang A, Freeman JJ, Jolliff BL (2009) Phase transition pathways of the hydrates of magnesium sulfate in the temperature range 50–5 C: implications for sulfates on Mars. J Geophys Res 114:E04010

Wangler T, Scherer GW (2008) Clay swelling mechanism in clay-bearing sandstones. Env Geol 56:529–534

Warscheid T, Braams J (2000) Biodeterioration of stone: a review. Int Biodeterior Biodegr 46:343–368

Watchman AL (1991) Age and composition of oxalate-rich crusts in the northern territory, Australia. Stud Conserv 36:24–32

Weber J (1985) Natural and artificial weathering of Austrian building stones due to air pollution. In: Félix G (ed) Proceedings of the 5th international congress on deterioration and conservation of stone. Presses Polytechniques Romandes, Lausanne, pp 527–535

Weber J, Burszán R (2008) Salt-induced decay of interior walls and climate control. The case study of Virgil's chapel. In: Salt weathering on buildings and stone sculptures. Technical University of Denmark, Lyngby, pp 257–267
Weimann MB (2001) Hygrische eigenschaften von polymerbeton im vergleich zu porösen mineralischen werkstoffen im bauwesen, thesis. Technical University, Zurich, p 149
Weiss T, Leiss B, Oppermann H, Siegesmund S (1999) Microfabric of fresh and weathered marbles: implications and consequences for the reconstruction of the Marmorpalais Potsdam. Z Dt geol Ges 150:313–332
Weiss T, Rasolofosaon PNJ, Siegesmund S (2002a) Ultrasonic wave velocities as a diagnostic tool for the quality assessment of marble. In: Siegesmund S, Weiss T, Vollbrecht A (eds) Natural stones, weathering phenomena, conservation strategies, and case studies, Special Publication 205. Geological Society, London, pp 149–164
Weiss T, Siegesmund S, Fuller ER (2002b) Thermal stresses via finite element modeling. In: Siegesmund S, Weiss T, Vollbrecht A (eds) Natural stones, weathering phenomena, conservation strategies, and case studies, Special Publication 205. Geological Society, London, pp 89–102
Weiss T, Siegesmund S, Fuller E (2003) Thermal degradation of marbles: indications from finite element modelling. Build Environ 38:1251–1260
Weiss T, Siegesmund S, Kirchner D, Sippel J (2004a) Insolation weathering and hygric dilatation: two competitive factors in stone degradation. Environ Geol 46:402–413
Weiss T, Strohmeyer D, Kirchner D, Sippel J, Siegesmund S (2004b) Weathering of stones caused by thermal expansion, hygric properties and freeze-thaw cycles. In: Kwiatkowski D, Löfvendahl (eds) Proceedings of the 10th international congress on deterioration and conservation of stone. ICOMOS Sweden, Stockholm, pp 83–90
Wendler E, Rückert-Thümling R (1993) Gefügezerstörendes verformungsverhalten bei salzbefrachteten sandsteinen unter hygrischer wechselbeantspruchung. In: Witmann FH (ed) Werkstoffwissenchaften und bausanierung, kontakt und studium 420, vol 3. Expert Verlag, Ehningen bei Böblingen, pp 11818–11830
Whalley B, Smith B, Magee R (1992) Effects of particulate air pollutants on materials: Investigation of surface crust formation. In: Webster RGM (ed) Stone cleaning and the nature, soiling and decay mechanisms of stone: proceedings of the international conference held in Edinburg. Donhead, London, pp 227–234
Widhalm C, Tschegg E, Eppensteiner W (1996) Anisotropic thermal expansion causes deformation of marble cladding. Perf Constr Facil ASCE 10:5–10
Williams RBG, Robinson DA (1981) Weathering of sandstone by the combined action of frost and salt. Earth Surf Proc Land 6:1–9
Williams RBG, Robinson DA (2001) Experimental frost weathering of sandstone by various combinations of salts. Earth Surf Proc Land 26:811–818
Winkler EM (1987) Weathering and weathering rates of natural stone. Environ Geol Water Sci 9:85–92
Winkler EM (1994) Stone in architecture, 3rd edn. Springer, Berlin
Winkler EM (1996) Technical note: properties of marble as building veneer. Int J Rock Mech 32:215–218
Winkler EM, Wilhelm EJ (1970) Salt burst by hydration pressures in architectural stone in urban atmosphere. Geol Soc Am Bull 81:567–572
Winkler EM, Singer PC (1972) Crystallization pressure of salts in stone and concrete. Bull Geol Soc Am 83:3509–3514
Wright JS (2002) Geomorphology and stone conservation: sandstone decay in Stoke-on-Trent. Struct Surv 20:50–61
Zappia G, Sabbioni C, Gobbi G (1989) Weathering layers on stone monuments in maritime localities of northern and central Italy. In: Zezza F (ed) The conservation of monuments in the mediterranean Basin. Grafo, Brescia, pp 79–82
Zehnder K (1982) Verwitterung von molassesandsteinen an bauwerken und in naturaufschlüssen. Beitr Geol Schweiz, Geotechn Ser 61. Kümmerly and Frey, Bern

Zehnder K, Arnold A (1989) Crystal growth in salt efflorescence. J Crystal Growth 97:513–521
Zehnder K, Schoch O (2009) Efflorescence of mirabilite, epsomite and gypsum traced by automated monitoring on-site. J Cult Heritage 10:319–330
Zeisig A, Siegesmund S, Weiss T (2002) Thermal expansion and its control on the durability of marbles. In: Siegesmund S, Weiss, T, Vollbrecht A (eds) Natural stone, weathering phenomena, conservation strategies and case studies. Geological society special publication No. 205. The Geological Society, London, pp 65–80
Zezza F, Macrì F (1995) Marine aerosol and stone decay. Sci Total Environ 167:123–143
Zezza F, Pascua NG, Macrí F (1995) Rising damp and soluble salts in the weathering processes of biocalcarenites. Case study of cathedrals, churches and buildings of Leccese baroque. In: Preservation and restoration of cultural heritage, Proceedings of the 1995 LCP congress. Montreux, pp 161–176